



Norwegian University of  
Science and Technology

# Fatigue loads on large diameter offshore wind monopile foundations in non-operational situations

**Alexandra Bøhn**

Marine Technology

Submission date: August 2016

Supervisor: Jørgen Ranum Krokstad, IMT

Norwegian University of Science and Technology  
Department of Marine Technology







NTNU Trondheim

Norwegian University of Science and Technology

*Department of Marine Technology*

## **MASTER THESIS SPRING 2016**

**Stud. tech. Alexandra Bøhn**

### **Fatigue loads on large diameter offshore wind monopile foundations in non-operational situations**

The background for this project is related to the development of offshore wind turbine parks at Doggerbank outside of England. Good wind conditions and shallow water depth makes this a well suited site for offshore wind industry. One of the main issues of design of offshore wind turbines is the fatigue life of the structure. The design loads, that are used for both the fatigue life analysis and extreme response analysis, are also very important for the total cost of the project. Balanced approach towards a sufficient conservatism is strived for. The industry want to reduce the cost without compromising on safety. A large diameter monopile foundation is more likely to induce large over predictions of fatigue loads. This will have a large impact on the total cost. The size of wind turbines for offshore use increases on a general basis, which results in also increasing foundations. This means that diffraction will become increasingly important. The diffraction decreases the mass force of Morisons equation on the structure. Experience from oil and gas structures shows reduction of fatigue in short crested waves. The effect of short-crested waves will need to be investigated for shallower water, to see the effect it may have on offshore wind turbines. The non-operational situations may be design drivers. During the non-operational situations, the wind turbine is idling or parked and the system loses its aerodynamic damping. This means the structure is subjected to larger fatigue loads in these situations.

The project will use data from metocean data to do analysis on the fatigue life of offshore bottom fixed wind turbines.

- Review and describe the current design practice of offshore wind turbines based on monopile or mono bucket foundation types.
- Investigate the effect of turbine non-operational situations on fatigue loads including both below cut-in wind velocities and other sources of turbine idling conditions.
- Perform assessment of damping contributions when turbine is idling.

The candidate shall perform numerical analysis in the terms of fatigue simulations of a large monopile type of foundation in unavailability situations applied on Doggerbank metocean conditions.

The following test cases shall be investigated:

- Shortcrested seas versus longcrested
- MacCamy and Fuchs versus Morisons equation to observe the effect of diffraction compared with  $C_m=2$

- Separation of wind driven and swell driven seas versus combined seas
- Damping sensitivity

The numerical calculation shall utilize FEM based time simulations presented as fatigue equivalent loads at critical intersections and hot spots on the monopile- or mono bucket structure.

The work scope may prove to be more extensive than initially anticipated. Subject to approval from the supervisor, topics may be left out from the list above or reduced in extent.

In the thesis the candidate shall present his personal contribution to the resolution of problems within the scope of the thesis work. Theories and conclusions should be based on mathematical derivations and/or logic reasoning identifying the various steps in the deduction. The candidate should utilize the existing possibilities for obtaining relevant literature.

The thesis should be organized in a rational manner to give a clear exposition of results, assessments and conclusions, and the text should be brief and to the point. Telegraphic language should be avoided. The following elements must be included: A text defining the work scope, preface, summary, list of contents, list of symbols and acronyms, main body, conclusions with recommendations for further work, references and (optional) appendices. All figures, tables and equations shall be numerated.

The original contribution of the candidate and material taken from other sources shall be clearly defined. Work from other sources shall be properly referenced using an acknowledged referencing system.

The report shall be submitted in two copies in bound volumes, signed by the candidate. If needed, additional material shall be delivered in a separate folder.

According to the present rules NTNU has the ownership of the thesis. Any use of it has to be approved by NTNU (or an external partner when this applies). The department has the right to use the thesis as if an NTNU employee carried out the work, if nothing else has been agreed in advance.

Deadline: August 09, 2016

Jørgen R. Krokstad/prof II

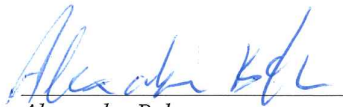
*Supervisor*

## Preface

I would like to thank my supervisor, Professor II Jørgen R. Krokstad for all support and help during the work with this thesis, and thank for all the good discussions and supervising with respect to the thesis. Furthermore, I would like to thank Lene Eliassen for the help with the software, FEDEM Windtechnology, and I would also like to thank PhD student Sebastian Schafhirt, who provided me with a model to use in the analysis, and who also provided support and help with the software. Lastly, I would like to thank my fellow students at NTNU for moral support, interesting discussions and for help with proofreading this thesis.

The thesis is written for someone with an educational background like myself, and with an interest in Offshore wind.

Trondheim, August 9, 2016



Alexandra Bøhn

## Abstract

The objective of this master thesis is to perform fatigue analysis on a large diameter offshore wind turbine with monopile foundation in non-operational situations. Offshore wind turbines are fatigue dominated structures, and the results from the fatigue analysis are therefore of great importance.

Offshore wind turbine projects are very expensive, and reducing the cost is always a priority. The foundation is one of the main cost-drivers. This thesis will investigate if performing more accurate wave load calculations and modeling of the sea state will reduce the calculated total fatigue damage on the monopile.

The offshore wind turbine is exposed to the variable stochastic environmental loadings from wind and waves. In non-operational situations the rotors are not rotating, which results in a negligible aerodynamic damping. The aerodynamic damping is the biggest contributor to the total damping during operation, and therefore the damping is significantly lower in non-operational situations. Low damping causes large dynamic responses, which leads to the non-operational situations being important for the fatigue analysis of offshore wind turbines. This thesis will focus on the three non-operational situations where the wind speed is below cut in, above cut out and the non-availability situations where the wind speed is within the operational range.

Load cases are chosen based on recommendations from DNV GL and the metocean report from the chosen site, Doggerbank. A wind speed with a corresponding sea state, is chosen for each load case. The chosen sea states have high probability of occurring along with the chosen wind speeds.

Simulations are run with the software FEDEM Wind Technology. The model of the offshore wind turbine is made according to the NREL 5MW reference wind turbine, with a monopile foundation according to the OC3 project.

The simulations were run with different considerations given to the modeling of the sea state and the wave load calculations to make them more accurate. This was to investigate if any of them would reduce the total fatigue damage.

In the first four methods, the analysis were done using short and long crested waves. Both of these were analyzed with the wave load according to Morison's and according to MacCamy and

Fuchs equation. JONSWAP spectrum was applied in all four methods.

In the fifth and sixth method, the wind driven and swell sea were separated by modeling the sea state with Torsethaugen spectrum instead of JONSWAP. Long crested waves were used. The difference between the two methods is the wave load calculation.

The calculated wave load on the monopile was reduced when the wave load calculation were done according to MacCamy and Fuchs equation instead of Morison's, especially in the sea states with low peak period. This is because MacCamy and Fuchs equation includes the effect of diffraction of waves with wavelength shorter than five times the diameter of the monopile in the wave load calculation.

Two hypothesis are tested in this thesis. The first one is that the short crested waves will reduce the calculated total fatigue damage on the monopile, compared with long crested waves. The second hypothesis is that the calculated total fatigue damage is reduced when the swell and wind driven sea is separated, compared with total sea.

The main result investigated is the total fatigue damage accumulated over the design life of 20 years. The analysis methods that calculated the wave load according to MacCamy and Fuchs always resulted in less total fatigue damage than the methods that calculated the wave load according to Morison's equation. Based on this, MacCamy and Fuchs equation should be used to calculate the wave load on a large diameter offshore wind turbine with monopile foundation.

The short crested waves reduced the total fatigue damage, compared with long crested waves, for both wave load calculation methods. The reduction of the total fatigue damage, due to the short crested waves, was greater when the wave load was calculated according to MacCamy and Fuchs than Morison's. The short crested waves, based on JONSWAP spectrum with wave load calculated according to MacCamy and Fuchs resulted in the lowest calculated total fatigue damage. The confidence in these results are acceptable. This shows that, based on the results here, the first hypothesis seems valid. The short crested waves did reduce the calculated total fatigue damage.

To apply Torsethaugen spectrum with the wave load calculated according to Morison's equation, increased the total fatigue damage compared to when JONSWAP spectrum was used. When Torsethaugen spectrum was applied with the wave load calculated according to MacCamy and Fuchs equation, the calculated total fatigue damage was reduced, compared with when JON-



SWAP spectrum was applied. This method, Torsethaugen with wave load according to MacCamy and Fuchs, resulted in the second lowest calculated total fatigue damage. The confidence in these results are low, due to the simulation length and number of seeds. However, the results indicate that the second hypothesis is valid as well, as long as the wave load is calculated according to MacCamy and Fuchs.

The goal of the thesis have been reached, since the results show that by modeling the sea state more accurately the calculated total fatigue damage is reduced.

Further simulations are needed to ascertain a higher confidence in the results, and to further investigate the effect of short crested waves and separated swell and wind driven sea on the fatigue damage.

A damping sensitivity study and availability sensitivity study have been run as well. The total fatigue damage is highly dependent on both of these variables. Increased damping and increased availability both decrease the calculated fatigue damage.

## Sammendrag

Formålet med denne masteroppgaven er å utføre utmattelses analyser på en stor-diameter offshore vindturbin med monopæl fundament i ikke-driftssituasjoner. Offshore vindturbiner er utmattelses dominerte strukturer, og resultatene fra utmattelses analysen er derfor av stor betydning.

Offshore vindturbin prosjekter er svært dyre, og å redusere kostnadene er alltid en prioritet. Fundamentet er en av de viktigste og største kostnadsdriverne ved prosjektene. Denne oppgaven undersøker om det å utføre mer nøyaktige bølgelastberegninger og modellering av sjøtilstanden, vil redusere utmattelsesskadene.

Offshore vindturbiner blir utsatt for de to variable stokastiske miljøbelastningene, vind og bølger. I ikke-driftssituasjonene roterer ikke rotorene noe som resulterer i en neglisjerbar aerodynamisk demping. Aerodynamiske demping er det største bidraget til den totale dempingen under drift. Dempingen er dermed betydelig lavere i ikke-driftssituasjoner. Lav demping fører til stor dynamisk respons av strukturen, noe som fører til at ikke-driftssituasjonene er viktige for utmattelsesanalysen av offshore vindturbiner. Denne oppgaven vil fokusere på de tre ikke-driftssituasjonene med vindhastighet under minimumsgrensen, vindhastighet over maximumsgrensen og utilgjengelighets situasjonene der vindhastigheten er innenfor driftsområdet, men turbinen likevel ikke er i drift.

De forskjellige lasttilfellene er valgt basert på anbefalinger fra DNV GL og metocean rapporten fra det valgte området, Doggerbank. En vindhastighet med en tilhørende sjøtilstand er valgt for hvert lasttilfelle. De er valgt slik at sannsynligheten er høy for at disse inntreffer samtidig.

Analysene kjøres i programvaren FEDEM Wind Technology. Modellen av vindturbinen er basert på NREL's 5MW referanse vindturbin, og monopælen er basert på OC3 prosjektet.

For hver analyse ble ulike hensyn tatt til beskrivelsen av sjøtilstanden og bølgelastberegningene, for å gjøre dem mer nøyaktig. Dette var for å undersøke om noen av disse hensynene vil redusere den totale utmattelsesskaden.

I de fire første metodene, ble analysen utført ved hjelp av å beskrive sjøtilstanden med kort- og langkammete bølger. Begge disse ble analysert med bølgelasten beregnet i henhold til Mori-

son's og i henhold til MacCamy og Fuchs ligning. JONSWAP spektrum ble brukt i alle fire metodene.

Den femte og sjette metoden separerer sjøen i vinddrevne bølger og dønninger, dette ble gjort ved å modellere sjøtilstanden med Torsethaugen spektrum istedenfor JONSWAP. Langkammete bølger ble brukt til disse analysene. Forskjellen mellom de to metodene er beregningen av bølgelasten.

Den beregnede bølgebelasten på monopælen ble betydelig redusert når bølgelasten ble beregnet i henhold til MacCamy og Fuchs ligning i stedet for Morison's. Dette er fordi MacCamy og Fuchs likning inkluderer effekten av diffraksjon av bølger med bølgelengde kortere enn fem ganger diameteren av monopælen, ved beregningen av bølgelasten.

To hypoteser er testet i denne avhandlingen. Den første er at de kortekammete bølgene vil redusere den totale beregnede utmattelseskaden på monopælen, sammenlignet med langkammete bølger. Den andre hypotese er at den beregnede totale utmattingskaden reduseres når sjøen modelleres som separert dønning og vinddreven sjø, sammenlignet med total sjø.

Hovedresultatet som er undersøkt er den totale utmattingskaden over levetiden på 20 år. De analysemetodene som beregnet bølgelasten i henhold til MacCamy og Fuchs likning, resulterer alltid i en mindre total utmattelseskade, enn de metodene som beregnet bølgelasten i henhold til Morison's likning. På bakgrunn av dette, bør MacCamy og Fuchs ligning benyttes for å beregne bølgelasten på en stor diameter offshore vindturbin med monopæl fundament.

De kortkammete bølgene reduserte den totale utmattelseskaden sammenlignet med langkammete bølger, når begge bølgelastene ble brukt. Reduksjonen av den totale utmattingskaden, på grunn av de kortkammete bølgene, var større når bølgelasten var beregnet i henhold til MacCamy og Fuchs enn Morison's. De kortkammete bølgene, basert på JONSWAP spektrum med bølgelast beregningen i henhold til MacCamy og Fuchs, resulterte i den laveste beregnede totale utmattingskade. Den statistiske konfidens til disse resultatene er akseptabel. Dette viser at, basert på resultatene, den første hypotesen er gyldig. De kortkammete bølgene reduserer den beregnede totale utmattelse skade sammenlignet med langkammete bølger.

Å anvende Torsethaugen spekteret med bølgelasten beregnet i henhold til Morison's likning, øker den totale utmattingskade, sammenlignet med da JONSWAP spektrum ble anvendt. Når Torsethaugen spektrum ble anvendt med bølgelasten beregnet i henhold til MacCamy og Fuchs

ligning, ble den beregnede totale utmattingskaden redusert, sammenlignet med når JONSWAP spektrum ble anvendt. Denne metoden, Torsethaugen med bølgelasten beregnet i henhold til MacCamy og Fuchs, resulterte i den nest laveste beregnede totale utmattingskaden. Den statistiske konfidensen til disse resultatene er lav, på grunn av lengden av simuleringen og antall frøtall. Resultatene viser at den andre hypotesen også virker gyldig, så lenge bølgelasten blir beregnet i henhold til MacCamy og Fuchs

Målet for oppgaven ble nådd, siden resultatene viste at ved å modellere sjøtilstanden mer nøyaktig ble den totale utmattelsesskaden redusert.

Ytterligere simuleringer bør kjøres for å sikre en høyere konfidens til resultatene, og for ytterligere å undersøke effekten av kortkammete bølger og separert vindreven og dønning sjø på den totale utmattelsesskaden.

Følsomhetsstudier av både dempingen og tilgjengelighet har blitt kjørt. Resultatene viser at den totale utmattelsesskaden er svært avhengig av begge disse variablene. Ved økt demping og tilgjengelighet, vil utmattelsesskaden reduseres.

# Contents

Abstract . . . . .	iv
<b>1 Introduction</b>	<b>1</b>
1.1 Problem Formulation . . . . .	3
1.2 Literature Review . . . . .	4
1.3 What Remains to be Done? . . . . .	6
1.3.1 Objectives . . . . .	6
1.4 Limitations . . . . .	7
1.5 Approach . . . . .	8
1.6 Structure of the Report . . . . .	9
<b>2 Definitions and Terminology</b>	<b>10</b>
2.1 Terminology . . . . .	10
2.1.1 Model Specifications . . . . .	12
<b>3 Review of Design Practice</b>	<b>15</b>
3.1 Traditional Design Approach . . . . .	16
3.2 Parallel Design Approach . . . . .	18
3.3 Integrated Design Approach . . . . .	19
3.3.1 Design for RAMS . . . . .	21
3.4 Building Blocks of Design . . . . .	22
3.4.1 Project Description . . . . .	23
3.4.2 Environmental Conditions . . . . .	23
3.4.3 Critical Details . . . . .	25

3.4.4	Ultimate Limit State Check . . . . .	25
3.4.5	Fatigue Limit State Check . . . . .	26
<b>4</b>	<b>Background Theory</b>	<b>27</b>
4.1	Wave Theory . . . . .	27
4.1.1	Linear Wave Theory . . . . .	29
4.1.2	Statistical Description of Waves . . . . .	31
4.2	Wind Process . . . . .	40
4.3	Metocean Design . . . . .	41
4.4	Load Calculation . . . . .	42
4.4.1	Morison's Equation . . . . .	43
4.4.2	MacCamy and Fuchs Equation . . . . .	45
4.5	Response . . . . .	45
4.6	Fatigue Calculation . . . . .	46
4.7	Integrated Analysis . . . . .	49
4.8	Damping . . . . .	49
4.8.1	Aerodynamic Damping . . . . .	49
4.8.2	Hydrodynamic Damping . . . . .	50
4.8.3	Structural Damping . . . . .	51
4.8.4	Soil Damping . . . . .	52
4.9	Natural Frequencies . . . . .	52
4.10	Non-Operational Situations . . . . .	54
4.10.1	Wind Speed below Cut-In . . . . .	54
4.10.2	Wind Speed above Cut-Out . . . . .	55
4.10.3	Availability . . . . .	55
4.10.4	Availability Effects on Fatigue . . . . .	56
4.11	Software . . . . .	60
<b>5</b>	<b>DNV GL Load Cases</b>	<b>61</b>
5.1	Design Situation . . . . .	61
5.1.1	DLC 2.4 - Power Production plus Occurrence of Fault . . . . .	62

5.1.2	DLC 6.4 - Parked . . . . .	63
5.1.3	DLC 7.2 - Parked and Fault . . . . .	63
<b>6</b>	<b>Metoccean Design Basis</b>	<b>64</b>
<b>7</b>	<b>Approach and Modeling</b>	<b>68</b>
7.0.1	Rotor and Nacelle . . . . .	68
7.0.2	Tower . . . . .	69
7.0.3	Monopile . . . . .	70
7.0.4	Control System . . . . .	71
7.0.5	Environmental State . . . . .	72
7.1	Load Cases for Analysis . . . . .	73
7.2	The Analysis . . . . .	75
7.2.1	Morison . . . . .	76
7.2.2	MacCamy and Fuchs Correction for Diffraction . . . . .	76
7.2.3	Short-Crested Sea . . . . .	77
7.2.4	Separation of Wind Driven and Swell Sea . . . . .	77
7.2.5	Damping Sensitivity Analysis . . . . .	78
7.2.6	Availability Sensitivity Study . . . . .	79
7.3	Post-Processing . . . . .	80
<b>8</b>	<b>Results</b>	<b>82</b>
8.1	Eigenvalue Analysis . . . . .	82
8.2	Dynamic Analysis . . . . .	83
8.2.1	Total Fatigue Damage . . . . .	84
8.2.2	Comparison of Fatigue Damage . . . . .	87
8.3	Response Spectra . . . . .	97
8.3.1	Summary of Trends . . . . .	97
8.4	Damping Sensitivity . . . . .	100
8.5	Availability Sensitivity . . . . .	101

<b>9 Discussion</b>	<b>102</b>
9.1 Total Fatigue Damage . . . . .	102
9.2 Morison's Force versus MacCamy and Fuchs Force . . . . .	105
9.3 JONSWAP versus Torsethaugen Spectrum . . . . .	109
9.4 The Natural Periods Effect on the Fatigue . . . . .	112
9.5 Statistical Confidence of the Results . . . . .	113
<b>10 Conclusion</b>	<b>115</b>
<b>11 Further Work</b>	<b>118</b>
<b>Bibliography</b>	<b>120</b>
<b>A Appendix A - MATLAB CODE</b>	<b>A.1-1</b>
A.1 head.m . . . . .	A.1-1
A.1.1 spekter.m . . . . .	A.1-1
A.1.2 kinematics1.m . . . . .	A.1-1
A.1.3 kinematics.m . . . . .	A.2-2
A.1.4 McFm . . . . .	A.2-2
A.1.5 tot_Fm . . . . .	A.2-2
A.2 head_postproc2.m . . . . .	A.2-2
A.2.1 readresults.m . . . . .	A.2-2
A.2.2 calc_stress.m . . . . .	A.2-2
<b>B Appendix B - Fatigue Damage</b>	<b>B.1-3</b>
B.1 Morison Method . . . . .	B.1-3
B.2 MacCamy Method . . . . .	B.2-5
B.3 Short Morison Method . . . . .	B.3-6
B.4 Short MacCamy Method . . . . .	B.4-7
B.5 Torsethaugen Method . . . . .	B.5-8
B.6 Torsethaugen MacCamy Method . . . . .	B.6-9



<b>C Appendix C - Response Spectrum</b>	<b>C.0-10</b>
C.1 Load Case 1-1 . . . . .	C.1-11
C.2 Load Case 1-2 . . . . .	C.2-12
C.3 Load Case 1-3 . . . . .	C.3-13
C.4 Load Case 1-4 . . . . .	C.4-14
C.5 Load Case 1-5 . . . . .	C.5-15
C.6 Load Case 1-6 . . . . .	C.6-16
C.7 Load Case 1-7 . . . . .	C.7-17
C.8 Load Case 1-8 . . . . .	C.8-18
C.9 Load Case 1-9 . . . . .	C.9-19
C.10 Load Case 2-1 . . . . .	C.10-20
C.11 Load Case 2-2 . . . . .	C.11-21
C.12 Load Case 2-3 . . . . .	C.12-22
C.13 Load Case 2-4 . . . . .	C.13-23
C.14 Load Case 3-1 . . . . .	C.14-24
C.15 Load Case 3-2 . . . . .	C.15-25

# List of Figures

2.1 Terminology for the offshore wind turbine, which will be used here (Arshad, M. & O’Kelly, B.C. (2016)) . . . . .	10
2.2 Terminology for the offshore wind turbine, model from FEDEM . . . . .	11
2.3 Dimensions for the Offshore Wind Turbine . . . . .	12
3.1 The upscaling of offshore wind turbines, courtesy of Fichaux, N., Beurskens, J., Jensen, P.H., Wilkes, J., Frandsen, S., Sorensen, J.D. & Eecen, P. (2011) . . . . .	15
3.2 The effect of increased tower height on natural frequency of wind turbine (Krokstad, J. R. (2015)) . . . . .	16
3.3 The sub systems of an OWECs (Kühn, M. (2001)) . . . . .	17
3.4 Control of the traditional design approach (Kühn, M. (2001)) . . . . .	17
3.5 Control of the parallel design approach (Kühn, M. (2001)) . . . . .	18
3.6 Control of the integrated design approach (Kühn, M. (2001)) . . . . .	20
3.7 Building blocks of design (Van der Tempel, J. (2006)) . . . . .	22
4.1 The Applicability of Wave Theories . . . . .	28
4.2 The velocity distribution under wave crest and wave trough according to linear wave theory (Faltinsen, O.M. (1990)) . . . . .	30
4.3 Irregular short-crested waves, as a sum of regular long crested waves(Myrhaug, D. & Lian, W. (2014)) . . . . .	33
4.4 The directional spreading function $D(\theta)$ according to eq 4.19 and eq 4.20 (Myrhaug, D. & Lian, W. (2014)) . . . . .	34

4.5	JONSWAP spectrum and Torsethaugen spectrum for a sea state with $H_s=1$ m and $T_p=6$ for the total sea . . . . .	36
4.6	Classification of the wave loads (Faltinsen, O.M. (1990)) . . . . .	43
4.7	Locations where maximum fatigue damage is expected. Waves main propagation is in x-direction, courtesy of Horn, J.T.H. (2015) . . . . .	47
4.8	Wave spectrum with natural frequency, 1P and 3P . . . . .	53
4.9	Theoretical and actual availability (Van Bussel, G.J.W. & Zaayer, M.B. (2001)) . . . . .	56
4.10	The three test wind turbines for the case study . . . . .	57
4.11	The resulting graph from case study . . . . .	58
6.1	The probability of occurrence for the different wind speed bins . . . . .	65
6.2	Scatter Diagram for Wind Speed bin 8-10 m/s . . . . .	67
7.1	The model in FEDEM, with the tower indicated as the visualized structure . . . . .	69
7.2	The model in FEDEM. The monopile is indicated as the visualized structure . . . . .	71
7.3	A sketch of the cross-section of the monopile with points where the fatigue damage is calculated . . . . .	81
8.1	The circumference of the monopile, with the $0^\circ$ point circled . . . . .	88
8.2	The fatigue damage from the 10 minutes simulations of each of the load case for the six methods, at the $0^\circ$ point . . . . .	89
8.3	The circumference of the monopile, with the $30^\circ$ point circled . . . . .	91
8.4	The fatigue damage from the 10 minutes simulations of each of the load case for the six methods, at the $30^\circ$ point . . . . .	92
8.5	The circumference of the monopile, with the $60^\circ$ point circled . . . . .	93
8.6	The fatigue damage from the 10 minutes simulations of each of the load case for the six methods, at the $60^\circ$ point . . . . .	94
8.7	The circumference of the monopile, with the $90^\circ$ point circled . . . . .	95
8.8	The fatigue damage from the 10 minutes simulations of each of the load case for the six methods, at the $90^\circ$ point . . . . .	96
8.9	Response spectra of the moments from load case 3-1 . . . . .	99

9.1 Graph comparing the wave load calculated at z=0 according to Morison inertia force and MacCamy & Fuchs, for Hs=0.5m, and Tp=4s . . . . . 105

9.2 Graph comparing the wave load calculated at z=-10 according to Morison inertia force and MacCamy & Fuchs, for Hs=0.5m, and Tp=4s . . . . . 105

9.3 Graph comparing the wave load calculated at z=0 according to Morisons inertia force and MacCamy & Fuchs, for Hs=6m, and Tp=17s . . . . . 106

9.4 Graph comparing the wave load calculated at z=10 according to Morison inertia force and MacCamy & Fuchs, for Hs=6m and Tp=17s . . . . . 106

9.5 Figure showing that the asymptotic value of MacCamy and Fuchs wave load is equal to the wave load according to Morison's with  $C_M = 2$ (Greco, M. (2014)) . . . . 108

9.6 Figure showing the wave load of a long wave according to both Morison's and MacCamy and Fuchs equation . . . . . 108

9.7 Graph comparing the wave spectra defined by Torsethaugen and JONSWAP for four sea states, frequency along x-axis . . . . . 109

9.8 Graph of the spectrum of the smallest sea state and of the largest sea state, with the first natural frequency . . . . . 112

C.1 Graph of responding moments from load case 1-1, in frequency domain . . . . . C.1-11

C.2 Graph of responding moments from load case 1-2, in frequency domain . . . . . C.2-12

C.3 Graph of responding moments from load case 1-3, in frequency domain . . . . . C.3-13

C.4 Graph of responding moments from load case 1-4, in frequency domain . . . . . C.4-14

C.5 Graph of responding moments from load case 1-5, in frequency domain . . . . . C.5-15

C.6 Graph of responding moments from load case 1-6, in frequency domain . . . . . C.6-16

C.7 Graph of responding moments from load case 1-7, in frequency domain . . . . . C.7-17

C.8 Graph of responding moments from load case 1-8, in frequency domain . . . . . C.8-18

C.9 Graph of responding moments from load case 1-9, in frequency domain . . . . . C.9-19

C.10 Graph of responding moments from load case 2-1, in frequency domain . . . . . C.10-20

C.11 Graph of responding moments from load case 2-2, in frequency domain . . . . . C.11-21

C.12 Graph of responding moments from load case 2-3, in frequency domain . . . . . C.12-22

C.13 Graph of responding moments from load case 2-4, in frequency domain . . . . . C.13-23

C.14 Graph of responding moments from load case 3-1, in frequency domain . . . . . C.14-24  
C.15 Graph of responding moments from load case 3-2, in frequency domain . . . . . C.15-25

# List of Tables

2.1	NREL 5MW wind turbine, gross properties(Jonkman, J., Butterfield, S., Musial, W. & Scott, G. (2009)) . . . . .	13
2.2	Material properties: Steel(Jonkman, J., Butterfield, S., Musial, W. & Scott, G. (2009))	13
2.3	Dimensions of the Support Structure, Monopile (Jonkman, J. & Musial, W. (2010)) .	14
5.1	Load cases for FLS, from table 4-5 in DNV GL (2014) . . . . .	62
7.1	Load cases for the 10 minutes fatigue analysis . . . . .	74
7.2	Load cases for the 1 hour fatigue analysis . . . . .	74
7.3	Load cases for the damping sensitivity study . . . . .	79
7.4	Load cases for the damping sensitivity study . . . . .	79
7.5	Parameters for S-N-curve . . . . .	80
8.1	Natural period for the Offshore Wind Turbine . . . . .	83
8.2	Total fatigue damage over 20 years for each method, from the 10 minutes simulations. . . . .	84
8.3	Total fatigue damage for each method, from the 1 hour simulations. . . . .	86
8.4	Fatigue damage from the damping sensitivity study for four load cases . . . . .	100
8.5	Total fatigue damage from the non-availability sensitivity study . . . . .	101
9.1	Percentage change for the total fatigue damage for the method compared with the MacCamy method which applied long crested waves based on JONSWAP spectrum, from the 10 minutes simulations . . . . .	103

B.1 Fatigue damage for each load case after 10 minute simulation. Load calculations done with Morison,  $C_m=2.0$   $C_d=1.0$  . . . . . B.1-4

B.2 Fatigue damage for each load case after 1 hour simulation. Load calculations done with Morison,  $C_m=2.0$   $C_d=1.0$  . . . . . B.1-4

B.3 Fatigue damage for each load case for 10 minute simulation. Wave load according to MacCamy and Fuchs . . . . . B.2-5

B.4 Fatigue damage for each load case after 1 hour simulation. Load calculations done with MacCamy and Fuchs . . . . . B.2-5

B.5 Fatigue damage for each load case for short crested 10 min analysis. Wave load calculated according to Morison equation . . . . . B.3-6

B.6 Fatigue damage for each load case for short crested 10 min analysis. Wave load according to MacCamy and Fuchs equation . . . . . B.4-7

B.7 Fatigue damage for each load case after 1 hour simulation. Load calculations according to MacCamy and Fuchs . . . . . B.4-7

B.8 Fatigue damage for each load case from the 10 minute simulation. Torsethaugen applied as wave spectrum . . . . . B.5-8

B.9 Fatigue damage for each load case from the 10 minute simulation. Torsethaugen applied as wave spectrum and wave load calculation according to MacCamy and Fuchs . . . . . B.6-9

## Nomenclature

### Roman Letters

a - fluid acceleration

$C_D$  - Drag Coefficient

$C_M$  - Mass Coefficient

D - Monopile Diameter

$D_i$  - Damage

$D_{tot}$  - total fatigue damage

f - Frequency

f<sub>p</sub> - Peak Frequency

f( $\theta$ ) - directional spectrum

F - Applied Force

$F_D$  - Drag Force (from Morisons Equation)

$F_M$  - Mass Force (from Morisons equation)

g - Acceleration of Gravity

h - Water Depth

H - Wave Height

H<sub>s</sub> - Significant Wave Height

k - Wave Number

KC - Keuligan Carpenter's number

M<sub>x</sub> - moment about x, fore-aft moment

M<sub>y</sub> - Moment about y, side-side moment

S - Spectral Density

t - Time

T - Period

T<sub>p</sub> - Peak Period

u - fluid velocity

$U_{10}$  - mean wind speed at 10 meters height



$U_{hub}$  - mean wind speed at hub height

## Greek letters

$\gamma$  - Peakedness Factor in JONSWAP Spectrum

$\epsilon$  - random phase angle

$\zeta$  - wave elevation

$\theta_k$  - angle of propagation for wave component

$\lambda$  - wave length

$\rho$  - Density

$\sigma$  - stress

$\Phi$  - velocity potential

$\omega$  - Wave Frequency in Radians per second

$\omega_p$  - Peak Wave Frequency

## Abbreviations

DFE - Design Fatigue Factor

FFT - Fast Fourier Transform

FLS - Fatigue Limit State

JONSWAP - Joint North Sea Wave Project

MSL - Mean Sea Level

NREL - National Renewable Energy Laboratory

OWECS - Offshore Wind Energy Conversion Systems

OWT - Offshore Wind Turbine

ULS - Ultimate Limit State

# Chapter 1

## Introduction

There is an increasing need for energy in the world, and there is an increasing need for this energy to be renewable. Wind energy is one of the renewable energy sources that is being warged the most. Available power for a wind turbine is proportional to the wind speed cubed, and with the disc area(Hansen, M. O. L. (2008)).

Wind energy is mostly produced in large onshore wind turbine parks today. Onshore wind turbine parks require a lot of space, which is one problem for them(Hansen, M. O. L. (2008)). To solve this, the parks can be built offshore instead. However, new problems arise with this amendment. For example, it is more expensive to install turbines offshore, more planning is needed, new loads arise and corrosion emerges. An additional reason for moving the wind turbines offshore is that the wind conditions are usually better, in the sense that the wind is usually stronger and has a better wind profile due to fewer obstacles. This increases the available power. Moving the wind parks offshore reduces the discomforts the onshore parks cause people who live close to them.

The cost of offshore wind turbine projects needs to be reduced to be able to compete with fossil fuel energy sources(Van Der Meulen, M. B., Ashuri, T., Van Bussel, G. J.W. & Molenaar, D. P. (2012)). The support structure is one of the main cost-drivers for an offshore wind turbine, and cost-reduction of this is therefore required. One possible way of reducing the cost, is to reduce the uncertainty in the wave load calculations(Van Der Meulen, M. B., Ashuri, T., Van Bussel, G. J.W. & Molenaar, D. P. (2012)), because today the wave load calculations are too conservative.

There are different types of support structures for an offshore wind turbine, for example the

monopile, jacket, jack-up, gravity based and floating. The bottom-fixed monopile foundation is the most commonly built foundation type for offshore wind turbines today. The different support structures have different limits to the water depth, with the monopile for shallow water, and the floating for deep water.

The wind turbines are trending towards larger diameters, because this increases the available power. The effect of larger foundations needs to be further researched. The wave loads will for example be increased, and the effect of diffraction of short waves relative to the monopile diameter will become increasingly important.

Fatigue analysis is needed on every structure that is subjected to cyclic loading of moderate size. The wave and wind loads are cyclic loads. The limit state for the structure is either Fatigue Limit State, FLS, or Ultimate Limit State, ULS. Wind turbines are usually FLS structures, which means the design of offshore wind turbines are dominated by fatigue loads.

The wind turbine is operational, producing power, while the wind speed is above cut-in and below cut-out wind speed. In the non-operational situations the turbine is parked or idling, which means the blades are not moving or barely moving. These situations include non-availability and when the wind speed is below cut-in and above cut-out. The non-availability situations are when the turbine is not operating as it should. Non-availability situations represent the amount of time the turbine is non-operational while the wind is within the operational range.

Damping is an important parameter for a fatigue analysis. Aerodynamic damping is the largest contributor to the total damping of an offshore wind turbine in operation. In a non-operational situation there is none to very little aerodynamic damping. This means the whole system has very little damping, which affects the magnitude of the responses of the structure. This leads to non-operational situations being important for the fatigue calculations for an offshore wind turbine.

## 1.1 Problem Formulation

Fatigue analysis will be performed on a large monopile foundation offshore wind turbine in non-operational situations applied on Doggerbank metocean conditions with the software FEDEM Wind Technology. MATLAB will be used for post-processing of results, wave load calculation according to MacCamy and Fuchs equation and for calculation of the Torsethaugen spectrum.

Currently, the standard practice for calculating the fatigue loads on offshore wind turbines is to use Airy linear wave theory in combination with long crested waves based on JONSWAP spectrum and with the wave load calculated according to Morison's equation with a modified mass coefficient corrected for diffraction (Krokstad, J. R. (2016) and Veldkamp (2005)). 10 minute simulations, with one to three seed numbers for the sea state, are usually run to calculate the fatigue damage(Krokstad, J. R. (2016)).

This thesis will investigate the fatigue damage in non-operational situations. The wave loads will be calculated according to Morison's equation and MacCamy and Fuchs equation. The simulations will be run when the waves are modeled as long-crested and short crested waves. The effect of separating the wind driven sea and the swell sea will be investigated. The effect these different approaches have on the fatigue damage in non-operational conditions will be investigated.

The goal of the thesis is to reduce the calculated fatigue loads by taking different considerations to the modeling of the sea and to the wave load calculations, in an effort to do it more accurately. The wave loads are calculated according to Morison's equation and MacCamy and Fuchs equation to investigate the effect of diffraction in the sea states. The diffraction at wave length shorter than five diameters, is known to reduce the fatigue damage, and it is included in fatigue analysis today in a simplified way by including a diffraction corrected mass coefficient. Two hypothesis will be investigated related to the modeling of the waves. The first hypothesis is that short crested waves will reduce the calculated wave loads and fatigue damage on the structure. The second hypothesis is that the calculated wave loads and fatigue damage will be reduced when the swell and wind driven sea is separated.

## 1.2 Literature Review

There has been done a significant amount of research on offshore wind turbines, and a few of those relevant for this thesis will be reviewed here. Articles on offshore wind, other offshore structures, wave load calculations and application of wave spectra will be reviewed.

Fischer and Kühn investigated the loading on offshore wind turbines on monopile structures in non-availability cases. They showed that it is important to include non-availability cases in the fatigue calculations (Fischer, T. & Kühn, M. (2010)) and that they are important to include in the design phase. They also found that the non-availability cases are more important for structures in deeper waters because the hydrodynamic loading is larger here.

MacCamy and Fuchs calculated an equation for the wave force on a large diameter cylinder extending from the seabed and up through the sea surface which includes the effect of diffraction of short waves compared with the cylinder diameter (MacCamy, R.C. & Fuchs, R.A. (1954)). The diffraction reduces the wave force on the cylinder, by reducing the inertia force. A correction for the inertia coefficient in Morisons equation can be created from the MacCamy and Fuchs equation. The diffraction effect is important when the cylinder diameter is large compared with the wave length, the limit being  $\frac{\lambda}{D} = 5$  (Faltinsen, O.M. (1990)). MacCamy and Fuchs equation should be used for calculation of the wave force in the diffraction regime. Experiments have been conducted and the results compared to MacCamy and Fuchs equation and found to be in good agreement, for example by Neelamani, S., Sundar, V. & Vendhan, C.P. (1989).

Horn, J.T.H. (2015) investigated hydro-elastic contributions to total fatigue damage on a large monopile. He used USFOS as analysis program for the fatigue analysis, which applies a MacCamy and Fuchs correction for the mass coefficient for the first order waves. Horn did do analysis with different wave theories and compared the baseline moments and fatigue. He found that for small sea states the first order diffraction theory corresponded well with higher order wave loads(Horn, J.T.H. (2015)).

The use of long-crested waves in analysis is known, from the offshore oil industry, to give conservative results in wave load calculations(Leira, B.J. & Olufsen, A. (1987)). The wave loads are reduced when short-crested sea is used instead for offshore structures in deep waters. Leira and Olufsen have investigated the effect of using short crested sea on the fatigue damage on

offshore risers. They showed that to use short crested seas instead of long crested seas decreased the expected fatigue damage on the risers. Their calculations were done on 300 meters water depth, and with extreme sea states. The effect of using short crested waves tends to be more pronounced for moderate sea states than for extreme sea states (Leira, B.J. & Olufsen, A. (1987)). This means that using short crested waves is especially important when calculating the fatigue damage.

Zhu, S. & Moule, G. (1994) investigated the forces induced by short-crested waves on vertical cylinders with arbitrary cross-sections, which included the circular cross-section. They performed the calculations on a vertical circular cylinder with radius of 10 meters in water depth of 50 meters. When calculating the wave forces from the short crested waves, they included diffraction. They found that, for a circular cylinder, the largest wave-induced forces from short-crested waves are still smaller than the wave forces induced by the long-crested waves with equal total wave number.

Diffraction for short-crested waves have also been researched by Zhu, S. (1993). The wave loads on the cylinder was found to increase as the incident waves became less short-crested (Zhu, S. (1993)). The results show that the total force on the cylinder in the direction of the wave propagation is smaller for the short-crested waves compared to the total force on the same cylinder in the direction of wave propagation for long-crested waves with the same wave number. The total wave load was also found to increase as the wave number in the direction perpendicular to the main direction of the wave propagation increased, meaning as the incident waves became shorter. These results show that if the wave loading is calculated with plane incident waves, they will be over-estimated if the incident waves actually are short-crested. Diffraction was included in all these calculations.

The two most important wave parameters are the significant wave height and the mean wave period. However, it is important to notice that two wave fields with the same wave characteristics may be very different (Semedo, A., Sušelj, K., Rutgersson, A. & Sterl, A. (2011)); one may be a mixed sea state with both wind and swell seas, while the other may have larger wind sea and no swell. To distinguish between these conditions additional information about the wave characteristics and propagating directions are needed of the wind driven sea and the swell sea separately. To distinguish between these two may be important for scientific and practical rea-

sons, for example during design of offshore structures.

In this thesis the fatigue life of the offshore wind turbine will be estimated, and the effect on the fatigue damage from different aspects of the waves will be investigated. The effect on the fatigue damage of applying short crested waves, the effect of separating the wind driven and swell seas and the effect of including diffraction of short waves will be investigated.

## 1.3 What Remains to be Done?

What remains to be done is summarized in the objectives below.

### 1.3.1 Objectives

The main objectives of this master thesis are

1. Review and describe the current design practice of offshore wind turbines based on monopile or mono bucket foundation types.
2. Investigate the effect of turbine non-availability situations on fatigue loads including both below cut-in wind velocities and other sources of turbine idling conditions.
3. Perform assessment of damping contributions when turbine is idling.

Numerical analysis in terms of fatigue simulations are also to be performed. The fatigue simulations are done on a large diameter monopile foundation in non-availability situations applied on Doggerbank metocean conditions, in FEDEM. MATLAB is applied for post-processing of the results. The following test cases will be investigated:

1. Short-crested seas versus long-crested.
2. MacCamy and Fuchs versus Morison
3. Separation of wind driven and swell driven seas versus combined seas.
4. Damping sensitivity.

## 1.4 Limitations

There are limitations related to the analysis and the computer program used for the analysis. Simplifications are made when the model of the offshore wind turbine is made, and assumptions are made for the waves and the sea conditions. The sea state is determined based on metocean report from the site, and there are uncertainties related to this.

Current and tidal variations are present at the site, but they will not be taken into account in the analysis. Neglecting the current loads is as recommended by DNV GL for fatigue analysis (DNV GL (2014)).

A large number of analysis is required to determine the fatigue damage from all wind and sea states present. Therefore, a few load cases are chosen to simulate the environment on the site. A full fatigue analysis of the structure is not performed, but rather an investigation on how the fatigue from the chosen sea states are affected by the different analysis methods that are performed here. The total fatigue damage is calculated based on those chosen load cases, which means it is not the actual total fatigue damage that is expected on the site. Since this thesis is investigating the damage in non-operational conditions, the chosen environmental states will have wind speed within the operational range, as well as below and above cut in and cut out wind speed.

Higher order loading terms are not included in the load calculations performed here.

In FEDEM, Wheeler stretching is included to calculate the wave kinematics more accurately. Wheeler stretching have not been included in the wave load calculations performed in MATLAB, which means they are less accurate than the ones calculated by FEDEM.

Ultimate Limit State, ULS, checks are not performed in this thesis. This means that extreme wind and sea states are not considered, and neither are occurrence of slamming or braking waves.

The simulations in this thesis are run as 10 minutes simulations for all the analysis, instead of the recommended 1 hour simulation. This was done because the wind is optimally only assumed constant over a 10 minutes interval, and because 10 minutes simulations are used in the offshore wind industry today. However, since the results from an 1 hour simulation will have a greater confidence related to them, simulations, for a few load cases, were run for this as well.



Multiple realizations of each sea state should have been run for all the analysis. However, there was not enough time for this. The different seed numbers should be run to establish some statistical confidence in the results.

The structural damping in the model is set very low for the analysis. This was due to an error in interpretation and calculation early on in the work on the thesis. The error was found and corrected, however all the analysis had already been run, and therefore the results were kept as they were. The low damping level causes large dynamic effects on the structure, which leads to large responses and large fatigue damages. This means that the fatigue damages obtained in these analyzes are larger than what would be found for a more realistic wind turbine.

A wind speed was applied to the wind turbine in all the load cases, even though the turbine is not operating, this is believed to add some extra damping.

## **1.5 Approach**

Numerical analysis in terms of fatigue analysis is performed. The software FEDEM Windpower R7.1.4, is chosen to perform the analysis. MATLAB is chosen for calculation of the wave loads according to MacCamy and Fuchs, calculation of the Torsethaugen spectrum and for the post-processing of the results from FEDEM. A model of a 5MW monopile foundation wind turbine was given by PhD student Sebastian Schafhirt for the use in this thesis.

The analysis is run with a number of load cases in FEDEM, and the fatigue damage is calculated in MATLAB. The fatigue damage is calculated for the point along the monopile where maximum moment occurs, which is at the mudline of the monopile. The fatigue damage from the different analysis are compared.

## 1.6 Structure of the Report

The rest of the report is organized as follows: Chapter 2 will review some of the terminology that will be used in the thesis, as well as the model specifications. Chapter 3 reviews current design practices for offshore wind turbines, and Chapter 4 will go through some relevant background theory for the work on this thesis.

In Chapter 5 the recommended load cases from DNV GL will be reviewed. The metocean report will be reviewed in Chapter 6.

Chapter 7 will go through the approach for the modeling of the offshore wind turbine, choose the load cases for analysis and the approach for the fatigue analysis. The results from the analysis are presented in Chapter 8 and discussed in Chapter 9. Chapter 10 presents the conclusion of the work, and Chapter 11 gives recommendations for further work.

# Chapter 2

## Definitions and Terminology

### 2.1 Terminology

An offshore wind turbine is a structure consisting of multiple components. The terminology applied here will now be clarified, in two figures.

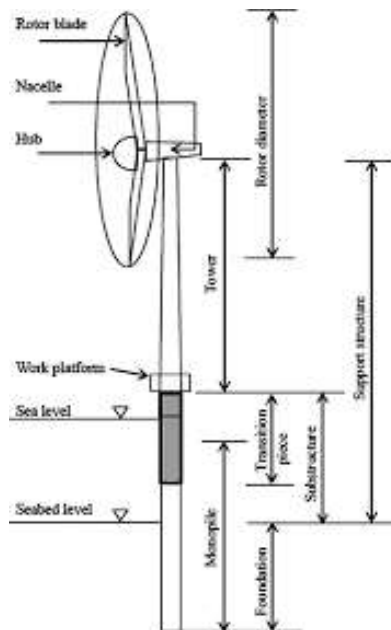


Figure 2.1: Terminology for the offshore wind turbine, which will be used here (Arshad, M. & O’Kelly, B.C. (2016))

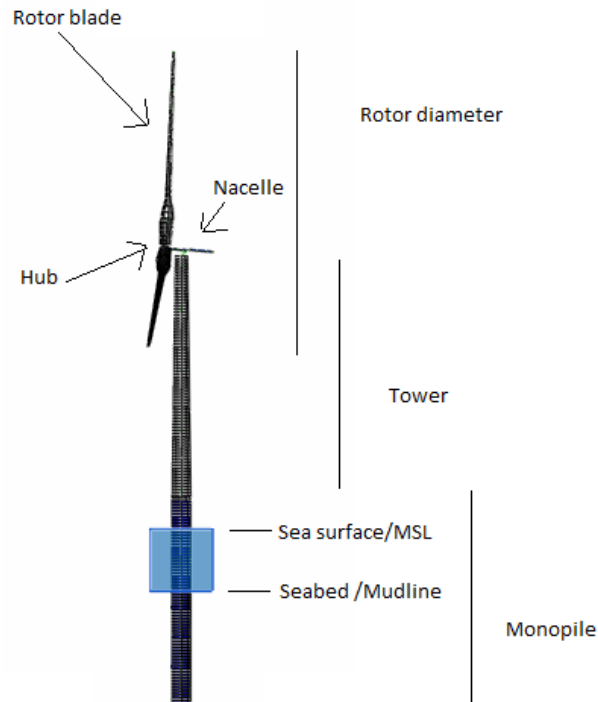


Figure 2.2: Terminology for the offshore wind turbine, model from FEDEM

Figure 2.1 shows a monopile wind turbine with the names of the different components of a wind turbine. The monopile is piled down into the seabed, and the transition piece attaches the monopile to the tower. The transition piece is present to ensure that the tower is vertical, and to help transfer the forces down into the seabed. The rotor is attached to the nacelle which is attached to the top of the tower.

Figure 2.2 shows the model of the offshore monopile foundation wind turbine that will be used in the analysis in this thesis. The figure visualizes the names for different components present in the model. As can be seen, this model does not have a transition piece. The function of the transition piece is to connect the tower and monopile and to transfer forces, this can be modeled with the connection, between the tower and monopile. If the forces on the transition piece was going to be investigated, further modeling of the transition piece would have been needed. In figure 2.2 the sea surface is identified as the mean sea level (MSL).

A fatigue analysis will be performed in this thesis. The structure will be excited and there will be responding motions, forces and moments. To describe the motions of the wind turbine it is common to use the terminology fore-aft and side-side motion. The fore-aft motion refers

to motion in the same direction as the wind flow direction, while the side-side motion refers to the motion across the wind flow direction. For the analysis performed in this thesis, the wind flow direction is defined to be along the x-axis, and so fore-aft motion is motion in x-direction and side-side motion is motion in y-direction. The responding moments will be referred to as the moment in x- and y-direction.

### 2.1.1 Model Specifications

The 5 MW wind turbine is well defined and well tested. A 5 MW reference wind turbine will be used in this thesis.

The specifications of the wind turbine have been taken from a representative utility-scale multimegawatt wind turbine known as the “NREL offshore 5-MW baseline wind turbine” (Jonkman, J., Butterfield, S., Musial, W. & Scott, G. (2009)). This is a well established reference wind turbine.

Figure 2.3 shows the model from FEDEM with some of the dimensions of the wind turbine shown as defined in NREL (Jonkman, J., Butterfield, S., Musial, W. & Scott, G. (2009)).

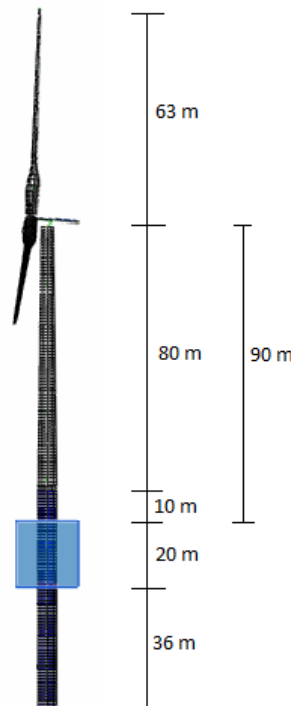


Figure 2.3: Dimensions for the Offshore Wind Turbine

Table 2.1: NREL 5MW wind turbine, gross properties(Jonkman, J., Butterfield, S., Musial, W. &amp; Scott, G. (2009))

Rating	5 MW
Rotor Orientation, Configuration	Upwind, 3 Blades
Control	Variable Speed, Collective Pitch
Drivetrain	High-Speed, Multiple-Stage Gearbox
Rotor, Hub Diameter	126 [m], 3 [m]
Hub Height	90 [m]
Tower Height	87.6 [m]
Tower Base Diameter, Top Diameter	6 [m], 3.87 [m]
Tower Bas Thickness, Top Thickness	0.027 [m], 0.019 [m]
Cut-In, Rated, Cut-Out Wind Speed	3 [m/s], 11.4 [m/s], 25 [m/s]
Cut-In, Rated Rotor Speed	6.9 [rpm], 12.1 [rpm]
Rated Tip Speed	80 [m/s]
Overhang, Shaft Tilt, Precone	5 [m], 5 °, 2.5 °
Rotor Mass	110,000 [kg]
Nacelle Mass	240,000 [kg]
Tower Mass	347,460 [kg]
Coordinate Location of Overall $C_M$	-0.2 [m], 0.0 [m], 64.0 [m]

A collection of the specifications from NREL's definition are presented in table 2.1. There is more information on the properties of the wind turbine in the Technical Report (Jonkman, J., Butterfield, S., Musial, W. & Scott, G. (2009)) this have been collected from, for example more data on the blades, the nacelle and hub, the drivetrain and the baseline control system.

The material used for the structure is steel. Table 2.2 presents the material properties of the steel used in the model in FEDEM, which was presented in NREL(Jonkman, J., Butterfield, S., Musial, W. & Scott, G. (2009)).

Table 2.2: Material properties: Steel(Jonkman, J., Butterfield, S., Musial, W. &amp; Scott, G. (2009))

Density	8,500 [kg/m <sup>3</sup> ]
Youngs Modulus	210 [GPa]
Shear Modulus	80.8 [GPa]

As can be seen, the material used for the model has a density of 8,500 [kg/m<sup>3</sup>], in stead of the typical density of steel of 7,850 [kg/m<sup>3</sup>]. This is to account for paint, bolts, welds and flanges(Jonkman, J., Butterfield, S., Musial, W. & Scott, G. (2009)) that exist on the structure but are not present in the model.

From tower base to tower top, the diameter and thickness of the tower is assumed linearly

tapered.

A structural damping ratio of 1 % of critical is assumed in all modes for the isolated tower (Jonkman, J., Butterfield, S., Musial, W. & Scott, G. (2009)).

The monopile is taken as in the OC3 project (Jonkman, J. & Musial, W. (2010)), who like in this thesis have used the NREL 5 MW reference wind turbine on top of the support structure. The monopile dimensions are described in table 2.3 and the dimensions can also be observed in figure 2.3.

Table 2.3: Dimensions of the Support Structure, Monopile (Jonkman, J. & Musial, W. (2010))

Total length	66 [m]
Length below mudline	36 [m]
Length Above MSL	10 [m]
Water depth	20 [m]
Monopile diameter	6 [m]
Monopile thickness	0.06 [m]

The material used in the monopile is the same steel as for the tower. The reason for using a higher density steel is the same for the monopile as for the tower.

The structural damping level is also here assumed to be 1 % of critical in all modes for the isolated structure (Jonkman, J. & Musial, W. (2010)).

# Chapter 3

## Review of Design Practice

This chapter will give an introduction to the design practice of offshore wind farms. A few different design approaches will be reviewed. The wind turbine technology has gone through a rapid development and has improved significantly in just a few years (Corbetta, G. & Mbistrova, A. (2014)). The wind turbines have increased in size and average rating, from being 15 meters and producing 0.05MW in 1985 to being over 160 meters and producing up to 10MW in 2010, as seen in figure 3.1. The cost per installed capacity and per produced energy unit have decreased significantly during this time as well. An optimum design of an offshore wind farm will provide energy in the most cost-efficient and reliable way over its lifetime.

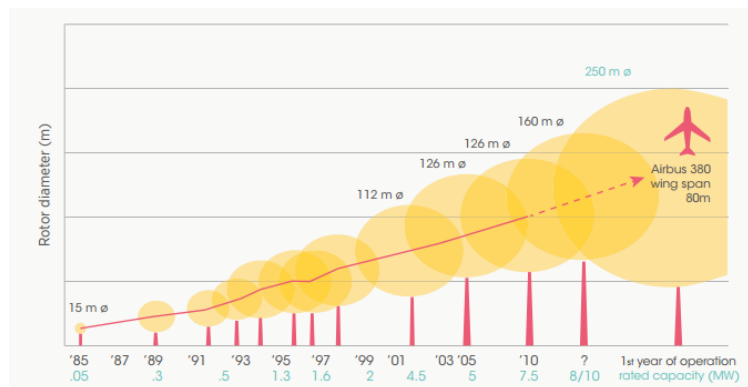


Figure 3.1: The upscaling of offshore wind turbines, courtesy of Fichaux, N., Beurskens, J., Jensen, P.H., Wilkes, J., Frandsen, S., Sorensen, J.D. & Eecen, P. (2011)

The energy available for a wind turbine is proportional to the wind speed cubed and with the swept area (Gao, Z. (2015)). The swept area is defined by the rotors as they rotate. A larger



rotor disc area increases the rating and is done by increasing the length of the rotor blades. The increased length of the blades will cause the tower height to increase. Another reason for increasing the tower height is that the wind higher up is generally stronger and better. The increase in turbine height and in the rotor disc area have improved the rating of the wind turbines, along with improved knowledge of the technology.

The increasing dimensions of the turbines leads to lower rotations per minute. This again decreases the natural frequency of the system (Krokstad, J. R. (2015)). This means that as the turbines increase in size, the natural frequency decreases and moves closer to the high energy wave frequencies, this effect can be seen on figure 3.2. The increased size of the wind turbines increases the dynamics of the system. New and safe design solutions are needed for these larger wind turbines to ensure safe operation of the turbine.

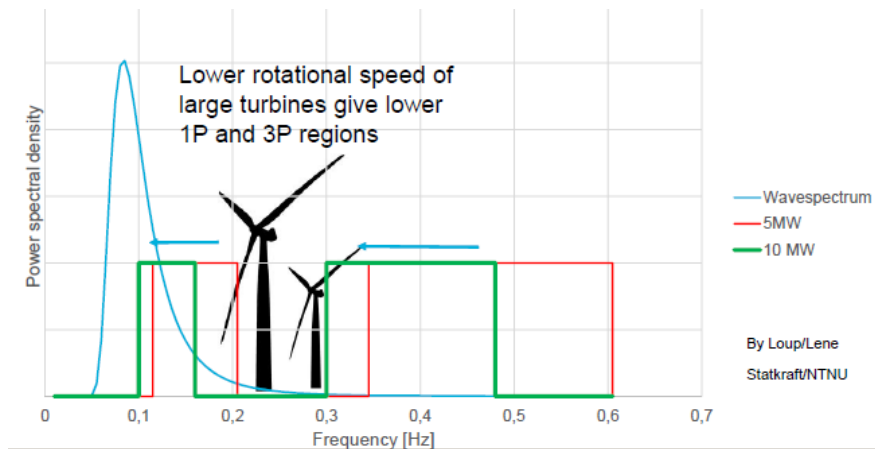


Figure 3.2: The effect of increased tower height on natural frequency of wind turbine (Krokstad, J. R. (2015))

The different subsystems and the aspects of an offshore wind energy conversion system is shown in figure 3.3. The design approach needs to address every subsystem to reach the design solution. Three design approaches will be reviewed below, and they have different approaches of dealing with the subsystems.

### 3.1 Traditional Design Approach

The design approach that has been used for the design of offshore wind turbines in the earlier years is here called the traditional design approach. It applies an onshore design approach to

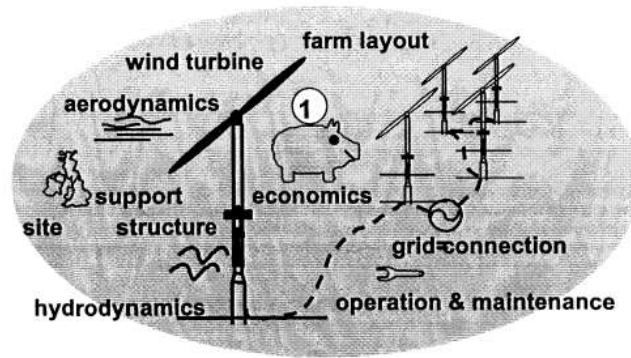


Figure 3.3: The sub systems of an OWECS (Kühn, M. (2001))

the offshore environment(Kühn, M. (2001)). This approach is suitable for prototype projects but is not suitable for large scale offshore wind farms. A good example of this approach is the second Danish offshore wind farm at Tunø Knob(1995)(Kühn, M. (2001)).

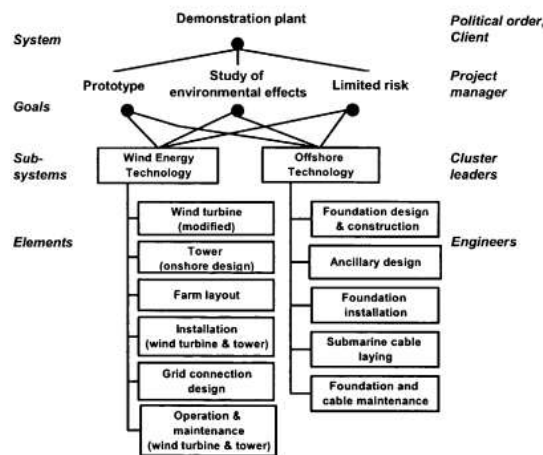


Figure 3.4: Control of the traditional design approach (Kühn, M. (2001))

The main objective of this approach was to investigate and demonstrate the environmental effects on the structure(Kühn, M. (2001)). Standard and well tested onshore wind turbines were used in the approach. To protect against environmental loads stiff gravity caissons were used to counter the ice loads(Kühn, M. (2001)), and because the structure was moved to a marine envi-

ronment the structure was improved by applying corrosion protection, built-in lifting facilities and an air-tight nacelle. All of this was to help reduce the operation and maintenance cost of the project.

This design approach is organized in two main clusters, the offshore and the wind turbine technology. Foundation, subsea cables and marine operations were dealt with by the offshore technology, while the wind turbine, tower, farm layout and grid connections were dealt with by the onshore technology(Kühn, M. (2001)). A schematic drawing of the control of the traditional design approach is shown in figure 3.4.

The two technologies treat the overall performance, and the operation and maintenance separately as elements in sub-systems rather than as separate sub-systems. The subsystems are as defined in figure 3.3. The overall performance and the operation and maintenance are therefore never treated for the entire system as a whole.

### 3.2 Parallel Design Approach

The parallel design approach considers the design requirements separately for the main sub-systems of the offshore wind farm(Kühn, M. (2001)). The main sub-systems are the wind turbine, support structure, operation and maintenance, and the grid connections.

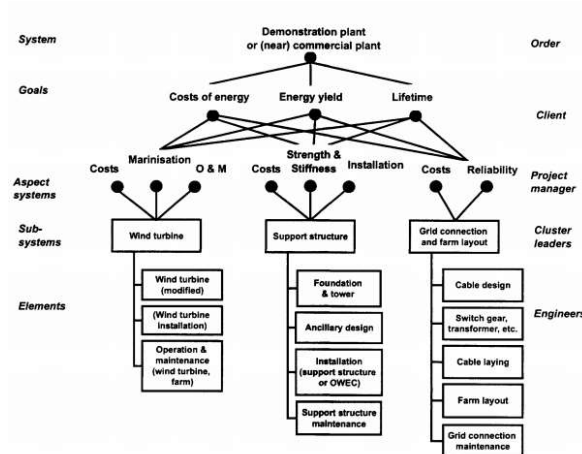


Figure 3.5: Control of the parallel design approach (Kühn, M. (2001))

The design requirements of the systems are decomposed and different aspects are valid for

the different sub-systems(Kühn, M. (2001)). However, design requirements are not controlled for the system level. For example cost is an important design requirement for every sub-system, but the cost is not controlled for the system as a whole. This means that the total cost is controlled by the summation of the cost of every sub-system, and is not optimized for the system as a whole.

As for the traditional design approach, the installation and the operation and maintenance are only considered on the sub-system level. Figure 3.5 shows the controls of the parallel design approach.

This design approach is typical for demonstration projects, but also for the first commercial plants. Examples of where this approach have been used is the Dutch pilot project Lely, the Swedish Nogersund onshore wind energy converter and the Danish Middelgrunden wind farm(Kühn, M. (2001)).

Certification of this design approach and the previous one, may be done with respect to both the wind turbine standard and the standard for offshore structures(Kühn, M. (2001)and Krokstad, J. R. (2016)). This means they risk to have to be certified for both, which may result in stricter requirements than necessary.

### **3.3 Integrated Design Approach**

The integrated design approach is an approach that treats the offshore wind farm as an entire system, the Offshore Wind Energy Conversion System, OWECS(Kühn, M. (2001)). The integrated design approach is meant to account for the dynamic dependency between the rotor and nacelle, and the support structure(Fischer, T., Vries, W., Rainey, P., Schmidt, B., Argyriadis, K. & Kühn, M. (2012)). This approach considers interactions between the sub-systems. This means that the design is governed by the overall criteria, which may for example be levelised production costs, dynamics of the entire system and availability(Kühn, M. (2001)). Figure 3.6 shows the controls of the integrated design approach.

This design approach may easily result in a novel design due to the evolutionary nature of technical progress(Kühn, M. (2001)). The commercial risks in innovative solutions must be kept in mind. For example it is not smart to apply an unproven wind turbine design to the harsh

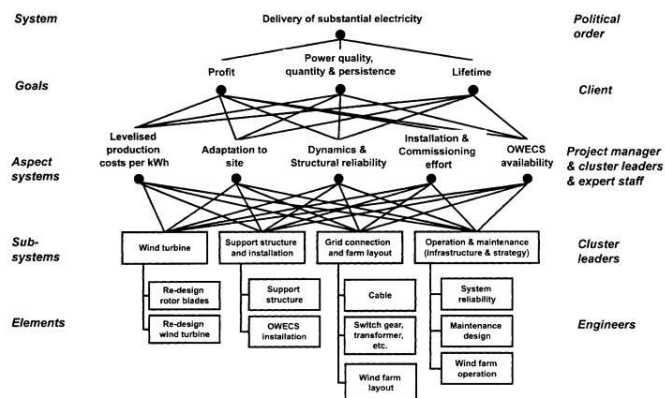


Figure 3.6: Control of the integrated design approach (Kühn, M. (2001))

offshore conditions.

The success of the design process is dominated by the organization of the design team (Kühn, M. (2001)). This is because the process and organization cannot be separated for the integrated design approach. A good organization of the design team may reduce the number of design conflicts and increase the flexibility of the design team.

With this approach, specific offshore wind energy standards are used and the certification is done with respect to the particular site conditions (Kühn, M. (2001)). The design standards that will be used in the design process needs to be identified at an early stage.

It is important to design the offshore wind turbine as an integrated system to be able to reach an optimal and cost-effective design (Van der Tempel, J. (2006)). The sub-systems should all be taken into account while simultaneously optimizing the entire system as a whole. However, this is not an easy task. Steps that can be treated in a separate manner within the integrated process should be identified.

Integrated analysis as done today is not yet fully integrated (Krokstad, J. R. (2014)). The turbine contractor performs integrated analysis with the aerodynamic loads and calculates the global load responses for tower and foundation, with the controller included in these calculations. The foundation contractor then performs independent calculations based on input from the turbine contractor for their foundation. This is not a fully integrated approach, but it is the established practice for the industry and is caused by the lack of access to the controller for the

foundation contractor.

Turbine information, given by the turbine supplier, is critical for the integrated approach(Krokstad, J. R. (2014)). However, the maximum aerodynamic fault load is typically given without detailed background information(Krokstad, J. R. (2014)), which means traceability is missing. The controller and aerodynamics are usually approximated. An open source turbine is typically used and very few developers have access to the real turbine loads including advanced controller. All these are severe limiting factors for a correct integrated design approach. A correct integrated approach is important for both risk reduction and cost optimization.

The design needs to be evaluated and checked(Kühn, M. (2001)), procedures for this is for example through overall cost models, simulation tools and codes for design calculations.

The load and response analysis during the integrated approach have been done as a superposition of the wind and wave loads and as a fully integrated analysis(Krokstad, J. R. (2014)). When superposition is used the response from the wind load analysis is added to the model for the wave load analysis and then the code check is performed. During a fully integrated approach a fully integrated design tool is used and the design is checked with both the wind and wave loads applied to the structure.

The design of offshore wind turbines is usually driven by fatigue. However, as the size of the wind turbines are increasing the design of the wind turbines are becoming ULS driven instead. For an ULS driven design, slamming loads, ringing loads and run up is important. The contour method is then used in the design to determine the environmental states. For a FLS driven design a complete metocean basis including misalignment is used. This metocean basis includes both the wind speeds and sea states, and it is important to include the coupling between wind speed and the sea state.

### **3.3.1 Design for RAMS**

Reliability, availability, maintainability and serviceability(RAMS) are very important for the design of offshore wind turbines(Van der Tempel, J. (2006)). Design targets for RAMS of an optimized offshore wind farm are best met with an integrated design approach. The RAMS design targets are connected, and specific design targets need to be established and controlled in all phases of the design process.

Design for reliability and availability means design for failure rates and states, while design for maintainability and serviceability means design for ratio, ease and cost of repair and regular service.

The design targets of price, quality, quantity and persistence of the delivered power (Van der Tempel, J. (2006)), guides the technical design and the design for RAMS.

The design of RAMS is important for the fatigue analysis, because the fatigue damage is dependent on the availability of the turbine. When the turbine is non-available, it is not operating, and the aerodynamic damping is negligible. The aerodynamic damping is the largest contributor to the damping of the system during operation. And so, in the non-operational conditions, there is very little damping present and therefore the fatigue damage accumulated in these situations may become large. The design of RAMS is important for the design target for cost, because while the turbine is non-operational the turbine does not produce electricity which reduces profit and therefore increases cost. This shows that both the design requirement for cost and fatigue, requires a high availability.

### 3.4 Building Blocks of Design

Figure 3.7 shows the building blocks of design (Van der Tempel, J. (2006)).

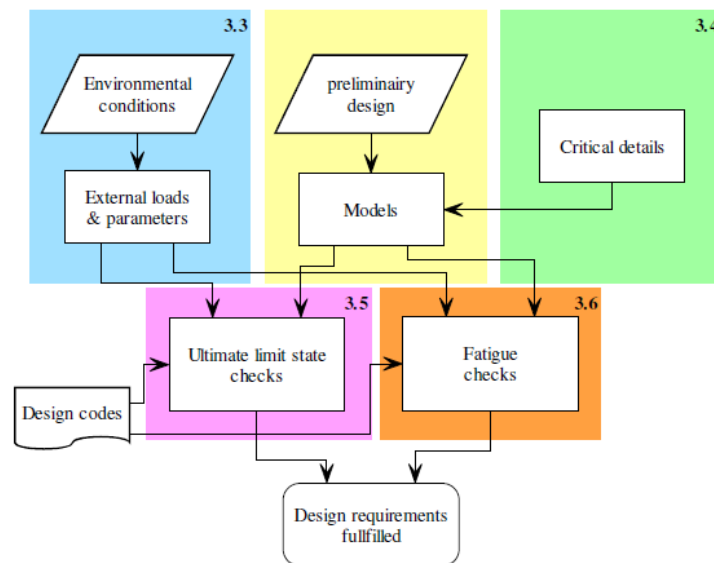


Figure 3.7: Building blocks of design (Van der Tempel, J. (2006))

To start the design process the project needs to be described and the location must be chosen along with other particulars (Van der Tempel, J. (2006)). The codes and standards that will be used for the design must be identified at this early stage. From the location of the wind turbine, the environmental conditions are described and the loads can be calculated. Critical design parameters, if there are any, needs to be identified and described.

The structure will then need to go through ULS checks and FLS checks. There will be a focus on FLS check in this thesis. The results from the analysis is controlled against the codes and standards and if necessary the design is altered and the ULS and FLS checks are performed again.

### **3.4.1 Project Description**

The location of the site and the type of turbine needs to be established early on (Sarkar, A. (2013)). The choice of the location determines the water depth, the dominant wind speeds and sea states. The type of turbine determines the turbine capacity, range of operating rpm, nacelle mass, rotor diameter and the hub height.

### **3.4.2 Environmental Conditions**

Offshore wind turbines are specially designed to catch as much wind as possible and to generate as much energy from that wind as possible. This criteria makes the design of them rather difficult. The impact of the wind on the structure and the economical aspect of the wind, should be separated (Van der Tempel, J. (2006)), because the economy is not related to the structural impact. The calculations of both the economy and the structural impact of the loads are critical for the design, and the projects success rely on those factors.

The environmental data is needed to determine the required work-platform and hub elevation for the structure (Arshad, M. & O'Kelly, B.C. (2016)). It is also needed for the first estimate of an initial geometry for the monopile. The initial estimate of the geometry leads to an estimate of the natural frequency of the structure, which is very important for further work and for the dynamic analysis. The natural frequency is a factor that will be checked again during the design, and when the geometry of the structure is changed so is the natural frequency.



## **Wind and Wave**

The wind and wave conditions are important for the design of offshore wind turbines. The chosen site needs to have good and steady wind conditions.

The wind and wave data can be obtained by measurements, satellite observations or by theoretical models of the wind and waves (Van der Tempel, J. (2006)). The use of metocean data and hindcasts are quite common. A hindcast have been created for the North Sea (Van der Tempel, J. (2006)). It is based on a mathematical model, which includes the land-masses and wind-wave interactions, and is then fed with meteorological data. The hindcast was validated with wind and wave measurements from different offshore platforms in the North Sea.

Scatter diagrams are created from the hindcast data, which may for example include wind speed and direction, significant wave height, peak period and direction for the total sea, swell sea and wind-driven sea. It is possible to create scatter diagrams for the sea state conditioned on the wind speed, for total sea, wind-driven sea and swell sea. A directional scatter is also often created, it represents the misalignment between wind and waves. Directional spectra will not be further discussed here. Scatter diagrams and hindcasts are used for FLS analysis.

The wind data from the hindcast is the wind speed and direction, given at a height over MSL. The reference wind speed is often referred to as the wind speed at 10 meters above MSL (Sarkar, A. (2013)). For wind turbines, another often applied reference height is the hub height.

The extreme waves, with direction, are needed for the ULS analysis, and are obtained from statistical data using for example contour method. The occurrence of slamming must be investigated since these can apply large loads on the structure (Sarkar, A. (2013)). Extreme waves, slamming and braking waves will be considered during an ULS analysis.

## **Currents, Tides and Storm Surges**

Tidal and current data, are a lot easier to collect than wind and wave data (Van der Tempel, J. (2006)). There is a relationship between large tidal differences and high current velocities. The current speed and direction, along with the return period are needed in the design process.

A storm surge is the elevated sea level due to a close-by storm system (Van der Tempel, J. (2006)). If site-specific data is available, a storm surge can be determined from long-term mea-

surements and extreme value analysis. If site-specific data is not available, then the storm surge needs to be estimated.

For a fatigue driven design these are not important, but they need to be included in the ULS checks.

### **Seabed**

The local bathymetry influence the wave and current patterns significantly, which is why it needs to be studied and determined (Van der Tempel, J. (2006)). The soil is an important factor when selecting the foundation type (Sarkar, A. (2013)), and geometry.

### **3.4.3 Critical Details**

The entire structure will be designed for the fatigue limit state and the ultimate limit state. However, there are some critical details that need to be assessed and determined before these checks. Some critical design details may for example be the transition piece, the access platform, the J-tube, the boat landing, vessel impact, scour, corrosion protection and marine growth.

### **3.4.4 Ultimate Limit State Check**

A limit state is a state for the structure in which it no longer fulfills the relevant design criteria (Eurocode (2001)). Design criteria describes for the limit the conditions that need to be fulfilled. Design conditions represents real conditions occurring during a time interval, and the design will have to demonstrate that the relevant limit states are not exceeded in the design conditions. The design conditions are created specially for each limit state check.

The ULS is related to structural collapse and other forms of structural failure (Eurocode (2001)). ULS checks are performed to check whether the structure, or structural design, can withstand the maximum design loads (Van der Tempel, J. (2006)). To test this, the relevant load cases need to be identified along with the relevant external loads. Then check to see if the structure meets the ULS requirements. If the structure fails during the test, then the structure needs to be re-designed.

### 3.4.5 Fatigue Limit State Check

FLS is related to the failure of the structure due to the cumulative damage effect of cyclic loading(DNV GL (2014)). The methods for doing fatigue checks varies from project to project for offshore wind turbines(Van der Tempel, J. (2006)). There is a large variety of fatigue calculation methods available. One reason for this is that the responsibility of the design is still divided in two, the offshore contractor is responsible for the foundation pile and transition piece while the wind turbine manufacturer is responsible for the tower and the rotor-nacelle assembly. However, the structure will behave dynamically from foundation pile to blade tip, and this needs to be accounted for in the fatigue analysis. An integrated design approach and integrated analysis is strived for.

To be able to do an integrated analysis, there should be some information sharing between the wind turbine manufacturer and the offshore contractor, so that a complete model and a proper fatigue analysis is achievable(Van der Tempel, J. (2006)). The turbine manufacturer is however, reluctant to share turbine details(Krokstad, J. R. (2014)). There is also the problem that if the wind turbine manufacturer shared the turbine details to the offshore contractor, then the offshore contractor may not have the required expertise to be able to use it correctly in a fatigue analysis. This is based on the same problem as discussed in chapter 3.3.

A solution may be to do the fatigue assessment in frequency domain. This would enable the offshore contractor to use his traditional methods, software and experience for the analysis(Van der Tempel, J. (2006)). The frequency domain method also provides the offshore contractor with clear information on environmental and structural properties. This method would help the contractor to optimize the design and to speed-up the design process. However, the wind turbine simulation programs are in time domain today.

Operational and idling situations are the two most important contributors to the fatigue, however, both start-up and stopping will also contribute and needs to be accounted for in a full FLS. The operational situation is the situation the wind turbine is in the most during its lifetime, and is of course important, and in the idling situations, which is the non-operational situations, the damping is very low and therefore large dynamic amplification may occur.

# Chapter 4

## Background Theory

### 4.1 Wave Theory

A kinematic description of the waves needs to be developed. To do this three assumptions is made for the fluid (Greco, M. (2014)):

- Inviscid
- Irrotational
- Incompressible

From those three assumptions potential flow theory can be used, this means that only the velocity potential,  $\phi$ , needs to be found to solve for velocity and pressure.

The governing equation, also called the Laplace equation, resulting from those three assumptions is:

$$\nabla^2 \phi = 0 \quad (4.1)$$

Because the velocity vector,  $V$ , is:

$$V = \nabla \phi \quad (4.2)$$

The pressure can be obtained from the Bernoulli equation:

$$p - p_a = -\rho g z - \rho \frac{\partial \phi}{\partial t} - \frac{1}{2} \rho (\nabla \phi)^2 \quad (4.3)$$

To find the velocity potential, the Laplace equation needs to be solved, with relevant boundary conditions.

The boundary conditions are expressed in their mathematical form here(Faltinsen, O.M. (1990)).

Kinematic conditions

$$\frac{d\phi}{dz} = 0, \text{ on } z = -h \tag{4.4}$$

$$\frac{\partial\phi}{\partial z} = \frac{\partial\zeta}{\partial t} + \frac{\partial\phi}{\partial x} \frac{\partial\zeta}{\partial x} + \frac{\partial\phi}{\partial y} \frac{\partial\zeta}{\partial y}, \text{ on } z = \zeta(x, y, t) \tag{4.5}$$

Dynamic condition

$$g\zeta + \frac{\partial\phi}{\partial t} + \frac{1}{2}(\nabla\phi)^2 = 0, \text{ on } z = \zeta(x, y, t) \tag{4.6}$$

Where  $h$  is the depth,  $\zeta$  is the surface elevation and  $\phi$  is the velocity potential.

Based on the Laplace equation and the boundary conditions, different wave theories have been created. The different wave theories are based on different sets of assumptions and are therefore applicable in different cases. They range from simple linear wave theory to theories that include non-linearities.

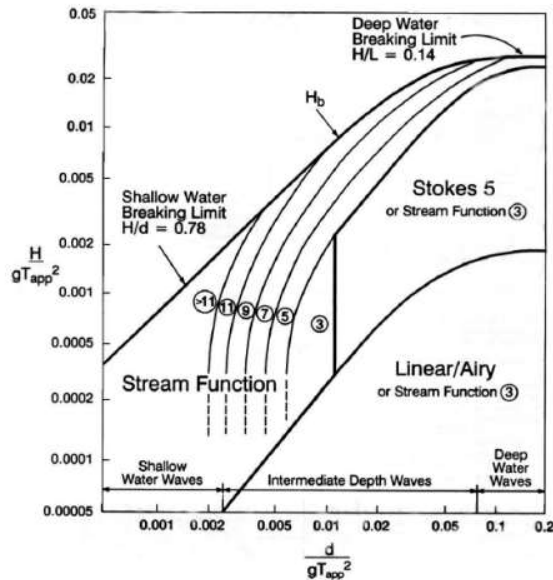


Figure 4.1: The Applicability of Wave Theories

Figure 4.1 shows when different wave theories are applicable. The breaking wave limit is shown along with the applicability ranges for Linear/Airy wave theory, Stokes fifth and the stream function. Linear/Airy wave theory is applicable in intermediate and deep water waves, with a wave height limit. Linear wave theory will be applied in this thesis.

### 4.1.1 Linear Wave Theory

Linear, or Airy, wave theory is obtained by neglecting the non-linear terms in the boundary conditions, while still obtaining sufficient information in most cases (Faltinsen, O.M. (1990)).

The linear wave theory is a good approximation of the wave characteristics as long as the wave amplitude is small relative to the characteristic wavelength and body dimensions. The new boundary conditions, obtained by neglecting the non-linear terms, are:

Kinematic condition

$$\frac{\partial \phi}{\partial z} = \frac{\partial \zeta}{\partial t}, \text{ on } z = 0 \quad (4.7)$$

Dynamic condition

$$g\zeta + \frac{\partial \phi}{\partial t} = 0, \text{ on } z = 0 \quad (4.8)$$

Equations 4.7 and 4.8 can be combined to:

$$\frac{\partial \phi}{\partial t^2} + g \frac{\partial \phi}{\partial z} = 0, \text{ on } z = 0 \quad (4.9)$$

When the velocity potential,  $\phi$ , oscillates harmonically in time with frequency  $\omega$ , equation 4.9 becomes

$$-\omega^2 \phi + g \frac{\partial \phi}{\partial z} = 0, \text{ on } z = 0 \quad (4.10)$$

The velocity potential, wave profile, velocity and acceleration can be calculated according to linear wave theory.

The velocity potential in finite water depth, is ((Faltinsen, O.M. (1990))):

$$\phi = \frac{g\zeta_a}{\omega} \frac{\cosh k(z+h)}{\cosh kh} \cos(\omega t - kx) \quad (4.11)$$

The corresponding wave elevation becomes:

$$\zeta = \zeta_a \sin(\omega t - kx) \quad (4.12)$$

$\zeta_a$  is the wave amplitude,  $k$  is the wave number,  $h$  is the water depth and  $\omega$  is the wave frequency. The dispersion relation for finite water depth is:

$$\omega^2 = kg \tanh(kh) \quad (4.13)$$

Where the wave number  $k$  is defined as:

$$k = \frac{2\pi}{\lambda} \quad (4.14)$$

Where  $\lambda$  is the wave length.

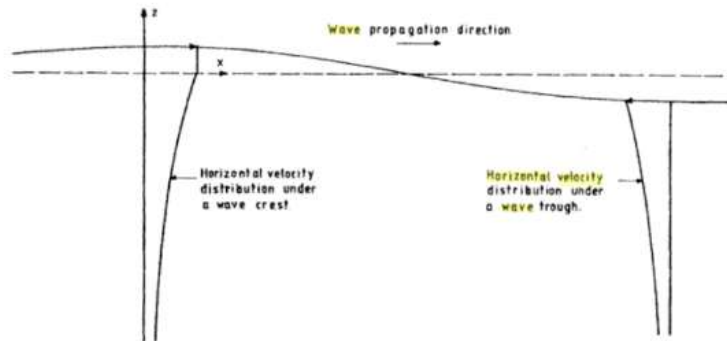


Figure 4.2: The velocity distribution under wave crest and wave trough according to linear wave theory (Faltinsen, O.M. (1990))

In linear wave theory, the velocity and acceleration is only defined up to the mean sea surface,  $z = 0$ . Linear theory assumes that the velocity potential and fluid velocity is constant from the mean sea surface,  $z = 0$ , and up to the free surface,  $z = \zeta$  (Faltinsen, O.M. (1990)). The distribution of the horizontal velocity shown in figure 4.2 is consistent with linear wave theory. This

is a source of conservatism(Haver, S. (2016)) for the linear wave theory.

The mass force is proportional to the acceleration. The mass force is sufficiently accurately estimated using linear wave theory because the maximum acceleration occurs when the wave is at  $z = 0$ . The drag force is proportional to the velocity squared. This causes the maximum drag force to be underestimated using only linear wave theory(Haver, S. (2016)).

If the structure is mass dominated it might be accurate enough to use linear theory, but if the drag force is of a concern or any importance, another wave theory or a correction of the linear wave theory should be used. Wheeler stretching is an example of a correction for the velocity distribution in linear wave theory.

Other wave theories are for example Stokes, stream function and Schwartz(Faltinsen, O.M. (1990)). These are non-linear solutions to the Laplace equation satisfying the boundary conditions.

### 4.1.2 Statistical Description of Waves

Linear wave theory is used to describe the wave kinematics. It is used to simulate an irregular sea state, as that is what is actually seen out in real life.

A regular wave is a wave with a constant amplitude and frequency. Irregular waves are mathematically made by superposition of multiple different regular waves. This means that the irregular waves consist of a sum of a large number of different wave components, and each wave component has different amplitude and frequency(Myrhaug, D. & Lian, W. (2014)).

A sea state is assumed to be a stationary random process, but only for a small amount of time. It is often assumed that a sea state is stationary for a 3-hour period(Myrhaug, D. & Lian, W. (2014)). The description of a 3-hour stationary wave process is the short-term description of waves. This 3-hour sea state is either described in the time domain as a time history, or in the frequency domain as a wave spectrum. A Fast Fourier Transform, FFT, can be used to transform between time domain and frequency domain. The wave spectrum is identified by the peak period and significant wave height, and these identifiers are assumed constant over a three hour period. A wave spectrum is directly related to the energy in the wave. The total energy in the sea state is equal to the area under the spectrum.



### Long-Crested Waves

Long-crested waves are waves with a clear direction, and when they are seen from above long wave crests can be seen.

So, the equation for a long-crested irregular sea propagating along positive x-axis becomes (Myrhaug, D. & Lian, W. (2014)):

$$\zeta(x, t) = \sum_{j=1}^N \zeta_{Aj} \sin(\omega_j t - k_j x + \epsilon_j) \quad (4.15)$$

Here  $\zeta_{Aj}$ ,  $\omega_j$ ,  $k_j$  and  $\epsilon_j$  are the amplitude, frequency, wave number and random phase angle of wave component j. The random phase angle is uniformly distributed between 0 and  $2\pi$ .

The energy in the waves is proportional to the wave amplitude squared. The wave spectrum describes how the wave energy is distributed between the various frequencies. And so the wave spectrum and amplitude is related by (Myrhaug, D. & Lian, W. (2014))

$$\zeta_{Aj} = \sqrt{2S(\omega_j)\Delta\omega} \quad (4.16)$$

This shows a relationship between the wave amplitude and the wave spectrum.  $\Delta\omega$  is the difference between two successive frequencies. This is the absolute value of the wave amplitude. The wave amplitude may be described as a complex number, by including the random phase angle in the wave amplitude instead.

### Short-Crested Waves

Irregular short-crested waves are a summation of different wave components with different amplitudes, frequencies, wave numbers, phase angles and wave directions (Myrhaug, D. & Lian, W. (2014)). Figure 4.3 shows how irregular short crested waves are created from regular long crested waves.

The equation for the surface elevation of short crested waves is shown here (Myrhaug, D. & Lian, W. (2014)):

$$\zeta(x, y, t) = \sum_{j=1}^N \sum_{k=1}^K \zeta_{Aj k} \sin(\omega_j t - k_j x \cos\theta_k - k_j y \sin\theta_k + \epsilon_{jk}) \quad (4.17)$$

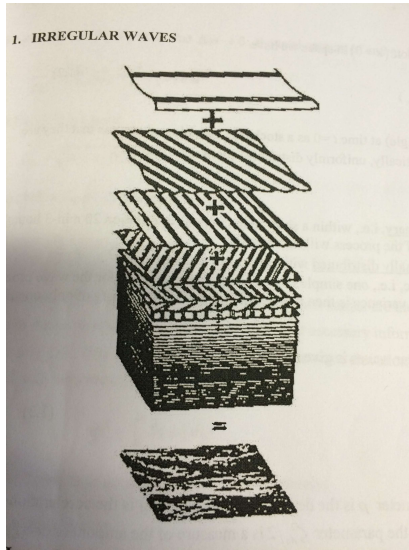


Figure 4.3: Irregular short-crested waves, as a sum of regular long crested waves(Myrhaug, D. & Lian, W. (2014))

where  $\zeta_{Ajk}$  is the wave amplitude and  $\theta_k$  is the angle with the direction of the main propagation of the waves.

The wave spectrum for short crested waves is dependent on how the energy is distributed over the direction, as well as the frequencies. Meaning the complete wave spectrum is the long-crested wave spectrum times a directional spectrum. The directional wave spectrum is dependent on the wave frequency, however, it is quite common to simplify it by assuming that the directional spectrum is independent of wave frequency(Myrhaug, D. & Lian, W. (2014)). That way the equation for the wave spectrum becomes:

$$S(\omega, \theta) = S(\omega) f(\theta) \quad (4.18)$$

There are a couple of established expressions for  $f(\theta)$ , and the most common one is(Myrhaug, D. & Lian, W. (2014))

$$f(\theta) = \begin{cases} K_n \cos^n(\theta - \theta_0) & \text{for } -\frac{\pi}{2} < \theta - \theta_0 < \frac{\pi}{2} \\ 0 & \text{else} \end{cases} \quad (4.19)$$

Where the main direction of the waves is  $\theta = \theta_0$ , and n normally is a number,  $n = 2s$ .

Since the integration of  $f(\theta)$  across every direction is 1, then a solution for  $K_n$  is (Myrhaug, D. & Lian, W. (2014)):

$$K_n = \frac{1}{\int_{-\frac{\pi}{2}}^{\frac{\pi}{2}} \cos^n \theta d\theta} = \frac{2^{n-1} \Gamma\left(\frac{n}{2}\right) \Gamma\left(\frac{n}{2} + 1\right)}{\pi \Gamma(n)} \quad (4.20)$$

Where  $\Gamma$  is the gamma-function. The effect of  $n$ , when  $n = 2s$ , on the directional spectrum can be seen in figure 4.4.

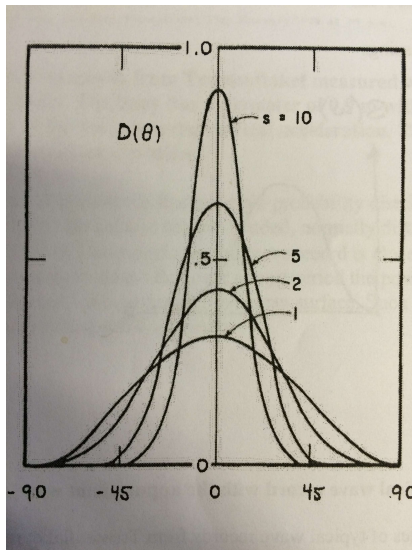


Figure 4.4: The directional spreading function  $D(\theta)$  according to eq 4.19 and eq 4.20 (Myrhaug, D. & Lian, W. (2014))

The wave amplitude can, like for long-crested waves, be calculated from the wave spectrum.

$$\zeta_{Ajk} = \sqrt{2S(\omega_j, \theta_k) \Delta\omega_j \Delta\theta_k} \quad (4.21)$$

The wave amplitude can be expressed as a complex number here as well, by including the random phase.

### JONSWAP Spectrum

The most commonly used wave spectrum for the North sea is the JONSWAP spectrum, which is a spectrum for a developing sea state with limited fetch (DNV GL (2007)).

The equation for the JONSWAP spectrum is(DNV GL (2007)):

$$S(\omega) = A_\gamma \frac{5}{16} H_s^2 \omega_p^4 \omega^{-5} \exp\left(-\frac{5}{4}\left(\frac{\omega}{\omega_p}\right)^{-4}\right) \gamma \exp\left(-0.5\left(\frac{\omega-\omega_p}{\sigma\omega_p}\right)^2\right) \quad (4.22)$$

Where

$\omega$  - angular wave frequency,  $\omega = \frac{2\pi}{T}$

T - wave period

$\omega_p$  - angular peak frequency,  $\omega_p = \frac{2\pi}{T_p}$

$T_p$  - peak period

g - acceleration of gravity

$\sigma$  - spectral width parameter

$\gamma$  - non dimensional peak shape parameter

$A_\gamma = 1 - 0.287 \ln(\gamma)$  - a normalizing factor

$\sigma$  is given as:

$$\sigma = \begin{cases} \sigma_a & \text{for } \omega \leq \omega_p \\ \sigma_b & \text{for } \omega > \omega_p \end{cases}$$

Average values are  $\sigma_a = 0.07$  and  $\sigma_b = 0.09$ , from DNV GL (2007).

and  $\gamma$  is given as:

$$\gamma = \begin{cases} 5 & \text{for } \frac{T_p}{\sqrt{H_s}} \leq 3.6 \\ \exp\left(5.75 - 1.15 \frac{T_p}{\sqrt{H_s}}\right) & \text{for } 3.6 < \frac{T_p}{\sqrt{H_s}} \leq 5 \\ 1 & \text{for } 5 < \frac{T_p}{\sqrt{H_s}} \end{cases}$$

Average value, from DNV GL (2007), is  $\gamma = 3.3$ .

### Torsethaugen Spectrum

If the sea elevation process has a significant swell and wind component, a two peaked spectrum like Torsethaugen may fit better with the process. Torsethaugen spectrum combines the sea state of the swell and wind driven sea. It assumes that the swell and wind driven component propagates in the same direction.

Figure 4.5 shows a JONSWAP spectrum and a Torsethaugen spectrum for the same sea state. As can be seen Torsethaugen has two peaks while JONSWAP only has one.

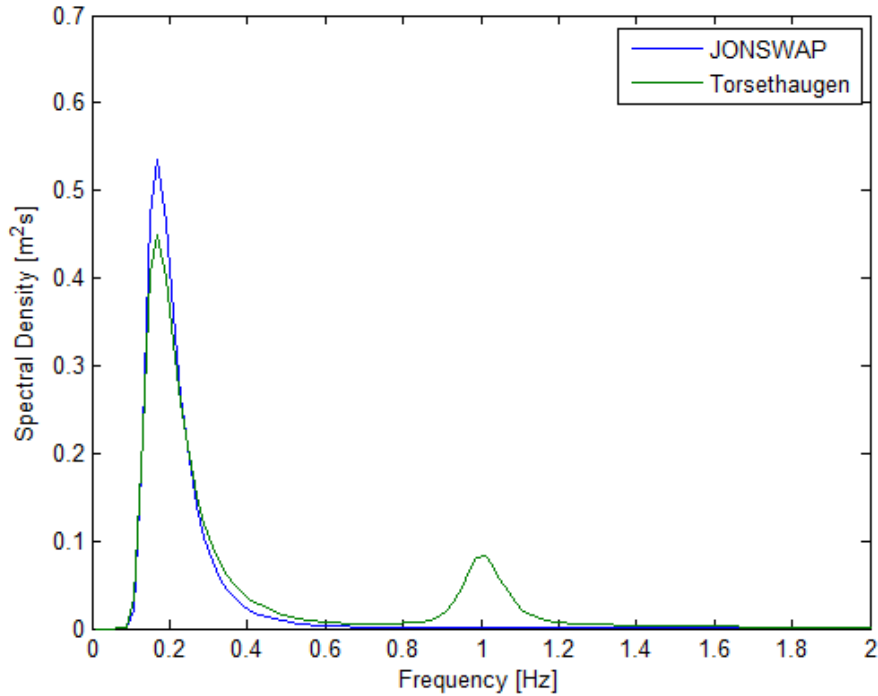


Figure 4.5: JONSWAP spectrum and Torsethaugen spectrum for a sea state with  $H_s=1$  m and  $T_p=6$  for the total sea

The Torsethaugen is defined in appendix A in DNV GL (2007). First a fetch of 370 km is assumed (DNV GL (2007)). The spectrum is defined as the sum of swell and wind sea. The sea state is either wind dominated or swell dominated.

$$S(f) = \sum_{j=1}^2 E_j S_{nj}(f_{nj}) \quad (4.23)$$

where  $j = 1$  for the primary system, the dominating sea state, and  $j = 2$  for the secondary system.  $E_j$ ,  $S_{nj}$  and  $f_{nj}$  is defined as

$$f_{nj} = f * T_{Pj} \quad (4.24)$$

$$E_j = \frac{1}{16} H_{Sj}^2 T_{Pj} \quad (4.25)$$

$$S_{nj}(j) = G_0 A_{ij} \Gamma_{Sj} \gamma_{Fj} \quad (4.26)$$

A general form for the equations defining the spectrum are in DNV GL (2007). However, a simplified form may be used. The simplified form is used for the design because some of the parameters of the general form will only have an effect for the low sea states and are of small importance for the design.

The simplified form for the Torsethaugen spectrum is, as defined in DNV GL (2007):

$$\Gamma_{Sj} = f_{nj}^{-4} \exp(-f_{nj}^{-4}) \quad (4.27)$$

$$G_0 = 3.26 \quad (4.28)$$

$$\gamma_{F1} = \gamma^{\exp\left(-\frac{1}{2\sigma^2}(f_{n1}-1)^2\right)} \quad (4.29)$$

$$\gamma_{F2} = 1 \quad (4.30)$$

$$\sigma = \begin{cases} 0.07 & \text{for } f_{nj} < 1 \\ 0.09 & \text{for } f_{nj} \geq 1 \end{cases}$$

$$A_{\gamma 1} = \frac{\left(1 + 1.1(\ln(\gamma))^{1.19}\right)}{\gamma} \quad (4.31)$$

$$A_{\gamma 2} = 1 \quad (4.32)$$

The primary and secondary peak is defined differently, depending on which sea state, swell or wind driven, is dominating. There is defined a check for this, which uses the parameter  $T_f$ , and for the simplified form, this check is defined as(DNV GL (2007)):

$$T_f = 6.6H_S^{1/3} \quad (4.33)$$

The sea is wind dominated when  $T_P < T_f$  and is swell dominated when  $T_P > T_f$ .

The equations for the Torsethaugen spectrum when the sea is wind dominated is presented here.

For the primary peak:

$$H_{S1} = H_{Sw} = r_{pw}H_S \quad (4.34)$$

$$T_{P1} = T_{Pw} = T_P \quad (4.35)$$

$$\gamma = 35 \left( \frac{2\pi}{g} \frac{H_{Sw}}{T_P^2} \right)^0 .857 \quad (4.36)$$

For the secondary peak:

$$H_{S2} = H_{Ssw} = \sqrt{1 - r_{pw}^2} H_S \quad (4.37)$$

$$T_{P2} = T_{Psw} = T_f + 2 \quad (4.38)$$

$$\gamma = 1 \quad (4.39)$$

The parameter  $r_{pw}$  is defined as

$$r_{pw} = 0.7 + 0.3 \exp \left( -2 \frac{T_f - T_P}{T_f - 2\sqrt{H_S}} \right)^2 \quad (4.40)$$

The equations for the Torsethaugen spectrum when the sea is swell dominated is presented here.

For the primary peak:

$$H_{S1} = H_{Ssw} = r_{ps}H_S \quad (4.41)$$

$$T_{P1} = T_{Psw} = T_p \quad (4.42)$$

$$\gamma = 35 \left( \frac{2\pi}{g} \frac{H_S}{T_f^2} \right)^0 .857 \left( 1 + 6 \frac{T_p - T_f}{25 - T_f} \right) \quad (4.43)$$

For the secondary peak:

$$H_{S2} = H_{Sw} = \sqrt{1 - r_{ps}^2} H_S \quad (4.44)$$

$$T_{P2} = T_{Pw} = 6.6H_{Sw}^{1/3} \quad (4.45)$$

$$\gamma = 1 \quad (4.46)$$

The parameter  $r_{ps}$  is defined as

$$r_{ps} = 0.6 + 0.4 \exp\left(-2 \frac{T_p - T_f}{0.3(25 - T_f)}\right)^2 \quad (4.47)$$

### Long Term Probability

The long term probability distribution of  $H_s$  and  $T_p$  can be represented in generic distributions or scatter diagrams. A Weibull distribution of the  $H_s$  along with a lognormal distribution of  $T_p$  conditional on  $H_s$  is a typical generic distributions used for representing the long term probability. A scatter diagram is another method which easily gives the frequency of occurrence of pairs of  $H_s$  and  $T_p$  in a given discrepancy of the  $H_s$  and  $T_p$  space.

When a metocean report is available, with  $H_s$  and  $T_p$  for every three hours for a sufficient length of time, a scatter diagram can be made and used for the longterm distribution for fatigue calculations. For ULS, the countour method is often used for the long term distribution.

### Nyquist Frequency

The Nyquist frequency is an important parameter when calculating between the time history and the spectrum. It is the maximum frequency that can be taken into account from the spectrum, and it gives the number of datapoints needed to describe the time history.

$$f_N = \frac{1}{2(\Delta t)} \quad (4.48)$$

Here  $f_N$  is the Nyquist frequency and  $\Delta t$  is the time increment in the time history.

The Nyquist frequency is used to avoid aliasing.



## 4.2 Wind Process

The wind process is a stochastic process. It can be assumed to be stationary over a short period of time, usually in 10 minute intervals. It is the mean wind speed that is assumed constant over this time period.

The wind speed is measured at a height over MSL. The short term wind speed is represented by a slowly varying mean wind speed and a fluctuating term which represents the turbulence, as shown in equation below.

$$U(t) = U_m(t) + U_t(t) \quad (4.49)$$

A wind profile shows how the mean wind speed varies with the height over sea level. The wind profile is due to wind shear. The wind profile can be represented by a logarithmic wind profile(DNV GL (2007)):

$$U(z) = \frac{u^*}{k_a} \ln \frac{z}{z_0} \quad (4.50)$$

Here  $k_a$  is von Karman's constant,  $k_a = 0.4$ ,  $z$  is the height,  $z_0$  is a terrain roughness parameter and  $u^*$  is the friction velocity defined as(DNV GL (2007)):

$$u^* = \sqrt{\kappa} U_{10} \quad (4.51)$$

where  $\kappa$  is a surface friction coefficient and  $U_{10}$  is the mean wind speed at 10 m over sea level. For offshore locations, the terrain roughness,  $z_0$ , depends on the wind speed, the upstream distance to land, the water depth and the wave field(DNV GL (2007)). For open sea with waves, the DNV GL recommended roughness parameter,  $z_0$ , is 0.0001-0.01, where  $z_0 = 0.0001$  represents the roughness at open sea without waves.

It is also possible to use an alternative form to the logarithmic wind profile, and this is shown here(DNV GL (2007)):

$$U(z) = U(h) \left( \frac{z}{h} \right)^\alpha \quad (4.52)$$

where  $\alpha$  depends on the terrain roughness. DNV GL recommends an  $\alpha = 0.12$  for open sea

with waves.  $U(h)$  is the mean wind speed at height  $h$ .

The short term stationary wind conditions can be described by a wind spectrum. The spectral density of the wind may be represented by a model spectrum, when the wind data available is insufficient to establish site-specific spectral densities(DNV GL (2014)). There are multiple spectra available, however most are calibrated to wind data obtained over land. Unless data indicates otherwise, the Kaimal spectrum should be used(DNV GL (2014)).

$$S_U(f) = \sigma_U^2 \frac{4 \frac{L_k}{U_{10}}}{\left(1 + 6 \frac{f L_k}{U_{10}}\right)^{\frac{5}{3}}} \quad (4.53)$$

Where  $f$  is the frequency and  $L_k$  is an integral scale parameter, and should be taken as:

$$L_k = \begin{cases} 5.67z, & \text{for } z < 60m \\ 340.2m, & \text{for } z \geq 60m \end{cases} \quad (4.54)$$

### 4.3 Metocean Design

To perform analysis on a structure, environmental data from the site is needed. The environmental loads are estimated based on the environmental data. It is therefore important that the data is representative for the geographical site where the structure will be situated(DNV GL (2007)).

The most optimal is to have measurements from the site over a sufficiently long time span. However, in most cases such measurements are not available. Sufficient time span for the wind measurements are especially difficult. When enough measurements from the site is not available, hindcast databases are used to provide the metocean data.

Environmental data, like the wind and waves, are presented in the metocean report. Geotechnical data also needs to be provided from the site when the wind turbine is going to be bottom-fixed.

The wave data given in the metocean data, is usually given in 3h intervals, because it is normal to assume stationary wave conditions with constant  $H_s$  and  $T_p$  over a 3-hour period(DNV GL (2014)). The sea states are therefore given in the metocean data as 3-hour sea states with constant  $H_s$ ,  $T_p$  and wave direction.

In the metocean data the wind data is represented as a mean wind speed, and direction, at a certain height over MSL. The height over MSL must be specified for the wind data. The mean wind speed is optimally measured at 10-minute intervals, because it is normal to assume stationary wind conditions over a 10 minute interval.

The wind and wave processes are correlated. The wind causes the waves. For an offshore wind turbine both environmental conditions, wind and waves, are present and will need to be applied to the structure. The differences in the periods for stationarity may cause problems when they are applied to the system.

## 4.4 Load Calculation

The calculation of forces on a structure in the sea can be difficult. However, a lot of research and work have previously been done on bottom-fixed cylinders. Morison's equation can be used to find the forces on such a cylinder. This equation simply sums up the contribution from the mass force and the drag force. A structure may be mass force dominated or drag force dominated. Strip theory is used to calculate the forces on the cylinder. The forces are calculated at the midpoint of the cylinder, as if the cylinder is not there.

When the diameter of the cylinder becomes large enough, the presence of the cylinder will start to change the wave pattern. The presence of the cylinder can no longer be ignored. The cylinder causes there to be an additional effect that takes energy away from the system. This is a diffraction effect.

Figure 4.6 shows the classification of wave loads with respect to the structure (Faltinsen, O.M. (1990)), with the wave braking limit. The structure is drag dominated for a wave height over diameter ratio of approximately 10 and higher waves. For smaller waves the structure is mass dominated. However, a diffraction effect becomes important when the wave length over diameter is approximately 5 or less. These relationships are important when calculating the loads on a cylinder, because it shows what part of the Morison's equation is the most important one for that case, or if MacCamy and Fuchs equation should be used.

From previous work (Boehn, A. (2015)), the structure was found to be mass force dominated, and the cylinder diameter will be large enough for diffraction to be important in some sea states.

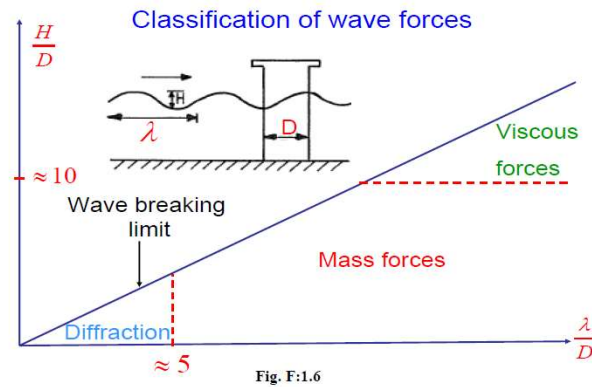


Figure 4.6: Classification of the wave loads (Faltinsen, O.M. (1990))

#### 4.4.1 Morison's Equation

Morison's equation can be used to calculate the wave forces on a bottom-fixed cylinder. The Morison's equation consist of the mass force and the drag force. The mass force is the force that is proportional to the undisturbed fluid acceleration. The mass force in Morison's equation can be derived based on potential theory.

The wave exciting forces on the cylinder is the forces on the cylinder when there are incident waves and the cylinder is restrained from oscillating(Faltinsen, O.M. (1990)). The force on the cylinder can be divided into two forces. First there is a force due to the undisturbed pressure field induced by the undisturbed waves, called Froude-Kriloff force. Secondly, there is a force on the structure because its presence changes this pressure field. This is called a diffraction force. This diffraction effect will further be referred to as long wave diffraction.

Morison's equation is defined as(Faltinsen, O.M. (1990))

$$dF = \rho \frac{\pi D^2}{4} C_M a dz + \frac{\rho}{2} C_D D |u| u dz \quad (4.55)$$

where

$C_M$  - the mass coefficient

$C_D$  - the drag coefficient

$u$  - the fluid velocity

$a$  - the fluid acceleration

$D$  - cylinder diameter

$\rho$  - density

The equation gives the force on a small strip,  $dz$ , of the cylinder. The part containing  $C_M$  is the mass force and the part containing  $C_D$  is the drag force. The  $C_M$  and  $C_D$  are for example dependent on Keuligan-Carpenters(KC) number, Reynolds number and the surface roughness. For a mass dominated structure the drag force will be very small compared to the mass force. This means that to apply a realistic  $C_M$  value is very important for mass dominated structures.

Potential theory results in a  $C_M = 2$  for a circular cylinder, where half of the contribution is from Froude-Kriloff force and the other half is from the long wave diffraction force.  $C_M$  will differ from 2 if viscous effects are accounted for. Applying Morison's equation with  $C_M = 2$  is conservative.

For Morison's equation the wavelength was assumed to be long compared with the cylinder diameter. For a wavelength less than 5 times the diameter of the cylinder there will be an additional diffraction of these short waves, which reduces the  $C_M$  to a value between 1 and 2.

### **Keuligan Carpenters Number (KC)**

The mass and drag coefficient depends on the KC number, Reynolds number and the roughness. KC is a number that describes the distance a fluid particle of a free stream travels relative to the body diameter(Faltinsen, O.M. (1990)). KC for a harmonically oscillating flow around a fixed circular cylinder with diameter,  $D$ , is (Faltinsen, O.M. (1990)):

$$KC = \frac{\pi H}{D} \quad (4.56)$$

Where  $H$  is the wave height far away from the body.

For  $KC < 3$ , the added mass coefficient is assumed independent of KC, and taken as 1.0. For  $KC > 3$ , the added mass coefficient varies with KC number, with asymptotic values of 1.0 and 0.6 for smooth cylinder and 1.0 and 0.2 for rough cylinder. A graph, and equation, showing the added mass variation with KC number is in DNV-RP-C205 (DNV GL (2007)).

### 4.4.2 MacCamy and Fuchs Equation

For arbitrary wavelength the analytical solution by MacCamy and Fuchs may be used to calculate the mass wave force on the cylinder (Faltinsen, O.M. (1990)). MacCamy and Fuchs investigated a large diameter bottom-fixed cylinder, and looked at the loads from the on-coming waves (MacCamy, R.C. & Fuchs, R.A. (1954)). They investigated the effect of diffraction at wavelength shorter than five times the diameter of the cylinder, and resulted in an equation for the mass force that includes diffraction of short waves. This diffraction effect will further be referred to as short wave diffraction.

$$dF = \frac{2\rho g H \cosh(k(h+z))}{k \cosh(kh)} \left( \sqrt{(J_1'(kr))^2 + (Y_1'(kr))^2} \right)^{-1} \cos\left(\omega t - \tan^{-1}\left(\frac{J_1'(kr)}{Y_1'(kr)}\right)\right) \quad (4.57)$$

The  $J_1'(kr)$  and  $Y_1'(kr)$  are the derivatives of the Bessel functions and  $r$  is the radius of the cylinder. The MacCamy and Fuchs equation is only an equation for the mass force. To find the total force per strip, the drag force from Morison's should be added to MacCamy and Fuchs mass force.

The diffraction, at wavelength shorter than five times the diameter of the cylinder, takes energy out of the system, and therefore, by including it, the total force is reduced compared to when it was not included. This diffraction reduces the mass force and is therefore dependent on the acceleration. The acceleration reduces with depth below MSL. This means that this diffraction will have largest effect on the mass force close to the surface.

## 4.5 Response

The response from the applied loads is calculated by simply solving the equation of motions:

$$\mathbf{m}a(t) + \mathbf{c}u(t) + \mathbf{k}x(t) = \mathbf{F}(t) \quad (4.58)$$

where  $\mathbf{m}$  is mass matrix,  $\mathbf{c}$  is damping matrix and  $\mathbf{k}$  is stiffness matrix.  $\mathbf{F}$  is the excitation load, while  $a$ ,  $u$  and  $x$  is the acceleration, velocity and displacement of the structure, respectively.

The solution to the equation of motions is:

$$x(t) = \mathbf{h}(t)\mathbf{F}(t) \quad (4.59)$$

Where  $\mathbf{h}(t)$  contains all the structural information from the equation of motion.  $\mathbf{h}(t)$  is equal to the ratio of the amplitude of the response and the amplitude of the load.

Since the loads on an offshore wind turbine vary in time, so does the response. The response can be viewed in time domain or frequency domain.

A response spectra, which is the response in frequency domain, will show the characteristic responses of the structure. The response spectrum can be found by doing the analysis in frequency domain or by Fourier Transforming the time history response. The response,  $x(t)$ , Fourier Transformed to  $X(\omega)$  is shown below(Newland, D.E. (1993)):

$$X(\omega) = \frac{1}{2\pi} \int_{-\infty}^{\infty} x(t)e^{-i\omega t} dt \quad (4.60)$$

It is useful to evaluate the response in frequency domain because the spectrum shows which frequencies are most dominant. It is also useful to compare the response spectrum with the excitation spectrum, because it may reveal if the structure is excited at resonance or if a certain loading will lead to responses at other frequencies. Resonance will be seen as spectral peaks in the response spectrum that do not have a linear relationship with the excitation. At resonance the response is amplified.

Notice that the spectrum only provides information on which frequencies contain energy and the magnitude of this energy.

## 4.6 Fatigue Calculation

Fatigue damage is caused by cyclic loading. The environmental loadings from the wind and waves are cyclic, and contribute to the fatigue damage. The fatigue damage is calculated from the responding stresses, and it is the stress range that is of importance for the fatigue damage. The stress is calculated from the moments. The location with maximum stress will be the most critical for the fatigue damage. Maximum stress occurs where maximum moment occur, which

is at the mudline of the monopile.

The stress in the cross-section is calculated according to the equation below.

$$\sigma = \frac{N_x}{A} + \frac{M_y}{I_y}x + \frac{M_x}{I_x}y \quad (4.61)$$

Where  $M_x$  and  $M_y$  are the moments about x and y,  $I_x$ , and  $I_y$  are the moment of inertia,  $N_x$  is the axial force and A is the cross-sectional area.

For waves with main propagation in positive x-direction, the stress calculation for a point anywhere around the circumference is simplified to:

$$\sigma = \frac{M_y}{I_y}x + \frac{M_x}{I_x}y = \frac{M_y}{I_y}r\cos(\theta) + \frac{M_x}{I_x}r\sin(\theta) \quad (4.62)$$

Where x and y are the position for the stress calculation around the circumference, and  $\theta$  is the angle. The stress at the two points at the x-axis are only dependent on the moment about y, while the two points at the y-axis are only dependent on the moment about x. The stress in every other point is dependent on a combination of the two.

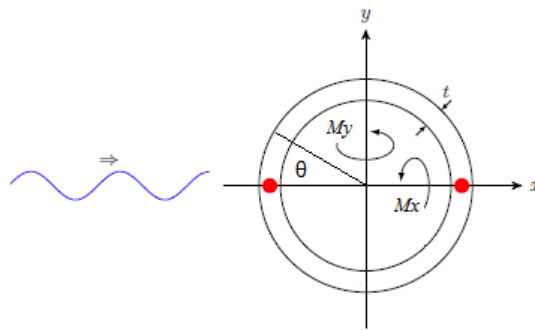


Figure 4.7: Locations where maximum fatigue damage is expected. Waves main propagation is in x-direction, courtesy of Horn, J.T.H. (2015)

Figure 4.7 is a slightly modified figure from Horn, J.T.H. (2015), to show the directions of the two moments and where the expected maximum stress around the circumference will occur. A positive angle  $\theta$  is also shown.

After the stress time series have been calculated, a rainflow count is performed on the responding stress time series, which means that the number of times a certain stress range occurs



is counted.

The S-N-curve is then used to determine the number of cycles,  $N$ , the structure is capable of enduring of a certain stress range,  $\Delta\sigma$ , before failure. The S-N curve is given as(DNV GL (2014)):

$$\log N = \log a - m \log \left( \Delta\sigma \left( \frac{t}{t_{ref}} \right)^k \right) \quad (4.63)$$

Where  $t$  is the thickness,  $t_{ref}$  is a reference thickness,  $\Delta\sigma$  is the stress range,  $m$  is the negative slope,  $\log a$  is the intercept of  $\log N$  axis and  $k$  is the thickness exponent. The parameters  $\log a$ ,  $m$  and  $k$  is based on the material chosen for the structure, for example welded steel in seawater with cathodic protection, which is curve D in table 2-2 in DNV GL(DNV GL (2010)).

Predictions of the fatigue damage is based on calculations of the cumulative fatigue damage, which can be calculated according to Miner-Palmgren sum(DNV GL (2014)). The Miner-Palmgren sum is defined as:

$$D = \sum_{i=1}^I \frac{n_i}{N_i} \quad (4.64)$$

Here  $D$  is the fatigue damage,  $I$  is the number of stress ranges,  $n_i$  is the number of cycles occurring of stress range  $i$ , and  $N_i$  is the number of cycles of stress range  $i$  the structure can endure. If the  $D \geq 1$ , failure due to fatigue damage will occur for the given stress history.

To find the total damage over the design life of the structure, the contribution to the total damage from each stress history during the design life needs to be summed up. This means that the total fatigue damage becomes

$$D_{tot} = \sum_{i=1}^N D_i P_i \quad (4.65)$$

$D_i$  is the damage from a certain stress history while  $P_i$  is the probability of occurrence for that stress history, and  $N$  is the number of stress histories.

From DNV GL(DNV GL (2014)), the design damage is obtained by multiplying the calculated damage with a design fatigue factor, DFF, which is a safety factor for the fatigue design. The application of DFF is given as:

$$D_{design} = DFF \cdot D \quad (4.66)$$

## 4.7 Integrated Analysis

To perform dynamic analysis on an offshore wind turbine, an integrated analysis should be run. The integrated analysis takes into account the structural properties, the environmental loading and systems that may affect the environmental loadings (Schl er (2014)), and then it calculates the coupled responses from the aero- and hydrodynamic loading, the dynamics of the system and control system. This is to ensure realistic and accurate results.

During an integrated analysis the loads from wind and waves are calculated simultaneously, and so a more correct loading is obtained. The coupled responses are then calculated, instead of the response from the separate excitation loads. Integrated analysis may give a more cost efficient design, since the responses to the loading is predicted more accurately.

## 4.8 Damping

Damping is the structures ability to dissipate kinetic energy (Langen, I. & Sigbj rnsson, R. (1979)). For an offshore wind turbine there are different types of damping present, for example aerodynamic, hydrodynamic, structural and soil damping. It is difficult to model the damping correctly, so simplified models are used to estimate the different damping contributions.

The damping level is usually given in percentage of critical damping, called the damping ratio, given as:

$$\lambda = \frac{c}{c_{cr}} = \frac{c}{2m\omega_0} \quad (4.67)$$

Where  $c$  is the damping,  $m$  is the mass and  $\omega_0$  is the natural frequency of the system.

Damping is velocity dependent. The different damping contributions to an offshore wind turbine mentioned above, is described below.

### 4.8.1 Aerodynamic Damping

Aerodynamic damping is the largest contribution to the total damping of the offshore wind turbine during operation. The effect is called aerodynamic damping because it decreases the motions of the top of the wind turbine and is caused by aerodynamic loads.

Aerodynamic damping can be illustrated by considering a tower top in motion. The tower top is moving forward, which gives the blades the experience of an increase in wind speed, and it will respond aerodynamically (Salzmann, D. & Van der Tempel, J. (2005)). The extra aerodynamic force will counteract the tower top motion. When the tower top moves backward the aerodynamic force is decreased, which again reduces the tower top motion. This effect is clearly linked to the velocity term of the equation of motion and is considered a type of damping.

The aerodynamic damping depends on the direction of the wind. It decreases the motion and velocity of the top of the wind turbine in the same direction as the wind flows. This means that misalignment between wind and waves are situations worth looking into, when considering the aerodynamic damping. When the wind and waves are misaligned the aerodynamic damping might not, depending on the degree of misalignment, be able to damp much of the motions due to the waves. The effect of this misalignment have been researched by for example Trøen (2014), and the effect can be considerable. However, the misalignment between wind and waves will not be taken into account in this thesis.

Aerodynamic damping is negligible during non-operation. The non-operational situations are therefore important for the fatigue analysis.

## 4.8.2 Hydrodynamic Damping

This is the damping due to the hydrodynamic effects on the wind turbine's motion.

As a structure vibrates in a fluid, some of the pressure on the structure from the fluid will be in-phase with the velocity of the structure (Langen, I. & Sigbjørnsson, R. (1979)). This pressure results in the hydrodynamic damping. This damping can be said to consist of two parts. First there is the geometrical damping. This damping is caused by some of the kinetic energy being transported away from the system in the form of propagating waves (Langen, I. & Sigbjørnsson, R. (1979)). The vibrations of the structure generate waves that travels away from the system. The second part is the drag damping. This part is due to vortices being shed and viscous effects of the water (Langen, I. & Sigbjørnsson, R. (1979)). The geometric damping is proportional to the velocity, and can be described by a linear viscous damping model, while the drag damping is proportional to the relative velocity squared and is therefore a nonlinear term.

In this thesis a large diameter monopile is used and so the drag damping will be of little

importance, while the linear geometric damping dominates.

This damping depends on the geometry of the structure, but also the frequency of the vibrations, the mode shape, Reynolds number, the roughness etc.

The hydrodynamic damping can for example be estimated by means of potential theory.

### 4.8.3 Structural Damping

Structural damping is the damping in a material related to the internal friction of the material (Langen, I. & Sigbjørnsson, R. (1979)).

The structural damping will be represented by Rayleigh damping (Carswell, W., Johansson, J., Løvholt, E, Arwade, S.R., Madshus, C., DeGroot, D.J. & Myers, A.T. (2015)). The Rayleigh damping, or proportional damping, is a coupling of a damping force proportional to the mass velocity and a damping force proportional to the stiffness of the structure. This means the Rayleigh damping consists of two contributions. The equation for the Rayleigh damping is presented below (Langen, I. & Sigbjørnsson, R. (1979)):

$$\mathbf{C} = \alpha_1 \mathbf{M} + \alpha_2 \mathbf{K} \quad (4.68)$$

where  $\mathbf{M}$  is the mass matrix,  $\mathbf{K}$  is the stiffness matrix and  $\alpha_1$  and  $\alpha_2$  is the proportionality constants for the mass and the stiffness correspondingly.  $\mathbf{M}$  and  $\mathbf{K}$ , and therefore  $\mathbf{C}$ , have orthogonality properties, which results in the equation presented below

$$\bar{c}_i = \alpha_1 \bar{m}_i + \alpha_2 \bar{k}_i \quad (4.69)$$

Where  $\bar{c}_i$  is the modal damping coefficient,  $\bar{m}_i$  the modal mass coefficient and  $\bar{k}_i$  is the modal stiffness coefficient. The damping ratio, for Rayleigh damping, can now be written as

$$\lambda_i = \frac{\bar{c}_i}{2\bar{m}_i\omega_i} = \frac{1}{2} \left( \frac{\alpha_1}{\omega_i} + \alpha_2\omega_i \right) \quad (4.70)$$

Where  $\omega_i$  is the natural frequency of mode  $i$ , and  $\lambda_i$  is the damping ratio for that mode.

When:  $\alpha_1 = 0$ , then  $\lambda_i$  is proportional to  $\omega_i$ , and when  $\alpha_2 = 0$ , then  $\lambda_i$  is inversely proportional to  $\omega_i$ .

This means that  $\alpha_1$ , the mass proportionality, damps out the lower mode shapes, and  $\alpha_2$ , the stiffness proportionality, damps out the higher mode shapes.

#### 4.8.4 Soil Damping

The soil damping can give a significant contribution to the total damping for a bottom-fixed structure. It works beneath the foundation of the structure. The soil damping is distinguished between two types of damping; the geometrical damping and the internal damping(Langen, I. & Sigbjørnsson, R. (1979)).

Geometrical damping is due to wave energy propagating away from the fundament, and is linked to the frequency of vibrations. Internal damping is due to the material and can be approximated as part of the structural damping.

The soil damping is commonly included as Rayleigh damping, which was described in the previous subsection.

For structures in the North Sea, a damping ratio for the soil damping, can be estimated to lie in the range of 2-5 % of critical.

The soil damping may be significant, or insignificant, depending on the displacement and vibrations of the foundation in the surrounding soil.

### 4.9 Natural Frequencies

The natural frequency is very important for the structure, and for the dynamic effects the structure will experience during its lifetime. There are multiple different eigenmodes and for each eigenmode there is a corresponding eigenfrequency, or natural frequency. The structure behaves according to which eigenmodes are activated. The most important eigenfrequency is typically the first one, with the largest eigenfrequency. The equation for the natural frequency,  $\omega_n$ , is:

$$\omega_n = \sqrt{\frac{k}{m}} \quad (4.71)$$

Where  $k$  is the stiffness and  $m$  is the mass.

The natural frequency of the structure is an important parameter and can help ensure that

resonance is avoided. The natural frequency should be outside the frequency range of any significant wave excitations. The natural frequency also needs to avoid being within the frequency range corresponding to the rotational speed of the blades, 1P, and the blade passing frequency, 3P. Although, while in non-operational situations the 1P and 3P frequencies are not important since the blades are not rotating.

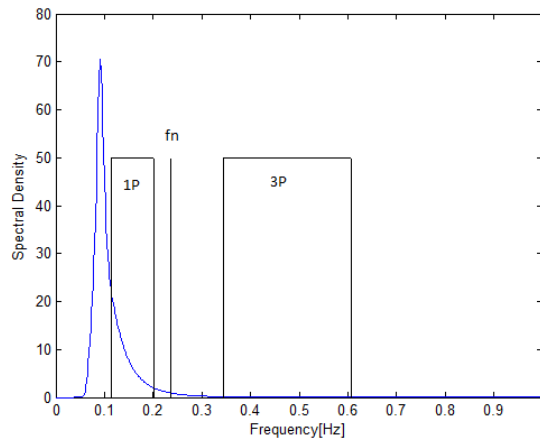


Figure 4.8: Wave spectrum with natural frequency, 1P and 3P

The natural frequency of the wind turbine is typically located between 1P and 3P, to avoid resonance, because the peak frequency of the linear wave excitation is located below 1P, as seen on figure 4.8. The natural frequency will however, still be excited by the waves. The location of the peak frequency and bandwidth of the wave spectrum can be altered between sea states, this will change the degree of excitation of the natural frequency. This means that depending on the sea state, the natural frequency is excited in varying degree for different sea states. An increase in spectral value at the natural frequency leads to larger excitations of the natural frequency in that sea state.

It is important to notice that the dynamic amplification does not only occur at the natural frequency but at a range of frequencies close to the natural frequency. This means there is a bandwidth of load frequencies that will cause significant dynamic amplification due to the natural frequency. Large dynamic amplification leads to a significant increase in accumulated fatigue damage. Dynamic amplification should be avoided.

The damping is an important factor when considering dynamic amplification, because it has an effect on both the amplitude and bandwidth of the dynamic amplification. A small damping

causes a small bandwidth and high amplitude, while large damping does the opposite, large bandwidth and small amplitude for the dynamic amplification.

As the wind turbine size increases, the natural frequency as well as the rotational frequencies are decreasing and so the natural frequency, 1P and 3P move closer to the wave excitation frequencies. This leads to a risk of larger dynamic amplifications for these larger wind turbines. Figure 3.2 illustrated this.

## 4.10 Non-Operational Situations

When the wind turbine is operating, it is generating power. However, there are situations where the wind turbine is not operating.

The wind turbine have defined a cut-in and a cut-out wind speed. These are the limits for when the wind turbine is operating. So the wind turbine is not operating when the wind speed is below cut-in or above cut-out wind speed.

There are also situations where the turbine cannot operate while the wind speed is within its operational limits. These situations are described as non-availability situations, and they include when the structure needs maintenance or repair work and when the turbine has faults.

To summarize, the wind turbine is non-operational when:

- Wind speed less than cut-in speed
- Non-availability situations
- Wind speed larger than cut-out speed

A short description of each situation is given in the following subsection.

### 4.10.1 Wind Speed below Cut-In

When the wind speed is below cut-in wind speed, the wind exerts insufficient torque on the blades, and they do not rotate. As cut-in wind speed is reached the blades will start to rotate.

Since the wind speed is low, the corresponding sea state will be small.

### 4.10.2 Wind Speed above Cut-Out

Wind speed above cut-out means that the wind speed is so large so that it is not safe to continue producing power. Cut-out wind speed is usually quite large, and does not happen as often as below cut-in.

As cut-out wind speed is reached, the forces on the wind turbine are getting so large that there is a risk of damage to the rotor. A braking system is used to bring the rotor to a standstill, or idling position, when the cut-out wind speed has been reached.

Today, the wind turbine is made so that the wind turbine is put in idling position slowly so as to not cause too large reacting forces from the idling process on the structure.

The corresponding sea state to these larger wind speeds are quite large.

### 4.10.3 Availability

Availability is important for this thesis because the non-availability situations are part of the non-operational situations. Availability is defined as the probability that the system is operating satisfactorily (Van Bussel, G.J.W. & Zaayer, M.B. (2001)), while the wind speed is below cut-out and above cut-in wind speed. Availability is closely related with reliability, maintenance and serviceability, RAMS, but also with accessibility.

The non-availability situations are the situations where the wind turbine is not operational even though the wind speed is within the operational range. These situations include maintenance and repair situations, when faults or failure occurs to the structure, and in fact every situation where the wind turbine is idling or parked while the wind is within the operational range.

The availability of onshore wind turbines is today very high, higher than 96 % (Fischer, T. & Kühn, M. (2010)). The availability of offshore wind turbines are much lower, especially for the first two years of operation. The accessibility of the site for maintenance and repair work, as well as maintenance strategy, is very important for the availability of offshore wind turbines. The availability of offshore wind turbines is typically at about 90 % (Tavner, P. (2012)).

The availability of offshore wind turbines depend on multiple factors. A theoretical availability can be defined, and it depends on the reliability (failures/year), maintainability and ser-



viceability (Van Bussel, G.J.W. & Zaayer, M.B. (2001)). The actual availability depends on the theoretical availability, accessibility of the site and the maintenance strategy, as shown in figure 4.9.

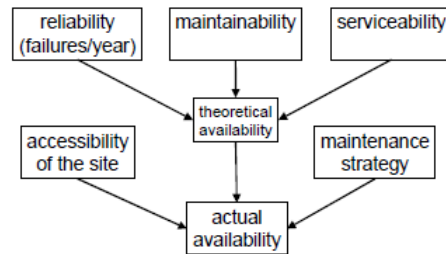


Figure 4.9: Theoretical and actual availability (Van Bussel, G.J.W. & Zaayer, M.B. (2001))

As stated, availability is related to RAMS. The reliability of the system is defined as the probability that the structure will perform its tasks (Van Bussel, G.J.W. & Zaayer, M.B. (2001)). It is related to the number of failures per year, or failure rates. Ensuring redundancy of some components will improve reliability. Maintainability is about the ease of repair issue for the wind turbine. Maintenance effort needs to be reduced as the wind turbines are moved offshore.

#### 4.10.4 Availability Effects on Fatigue

The availability is higher onshore than offshore, as expected since it is easier to do maintenance and repair work on an onshore structure. The availability of the wind turbine is more important for an offshore wind turbine than an onshore, partly because the offshore wind turbine is always exposed to the wave loads as opposed to the onshore wind turbine, and therefore is more dependent on the aerodynamic damping which is only present during operation.

For an offshore wind turbine a higher availability will increase the revenue, and can also lead to a decrease in fatigue damage for the support structure, since a higher availability will increase the time where aerodynamic damping is present. The aerodynamic damping damps, during operation, the responses from the hydrodynamic loads on the support structure, as well as the response from the aerodynamic loads.

As stated before, fatigue loading is a driving design factor in the design of most offshore wind turbines. The fatigue loading is a combination of the hydrodynamic and aerodynamic loading. However, depending on the support structure, turbine and site, either the hydrodynamic

or aerodynamic loading can be the dominant contributor to the fatigue loading. Depending on which is the dominant contributor, the fatigue damage can be either increased or decreased in the non-availability cases (Fischer, T. & Kühn, M. (2010)). This will be investigated now.

The top mass and the hub height of the turbine is a large contributor to the structure's natural frequency, which means that they help define the relationship between the natural frequency and the wave frequency. This relationship is very important when considering the loading effect of the waves. The softer the support structure is, the greater the loading effect from the waves (Fischer, T. & Kühn, M. (2010)).

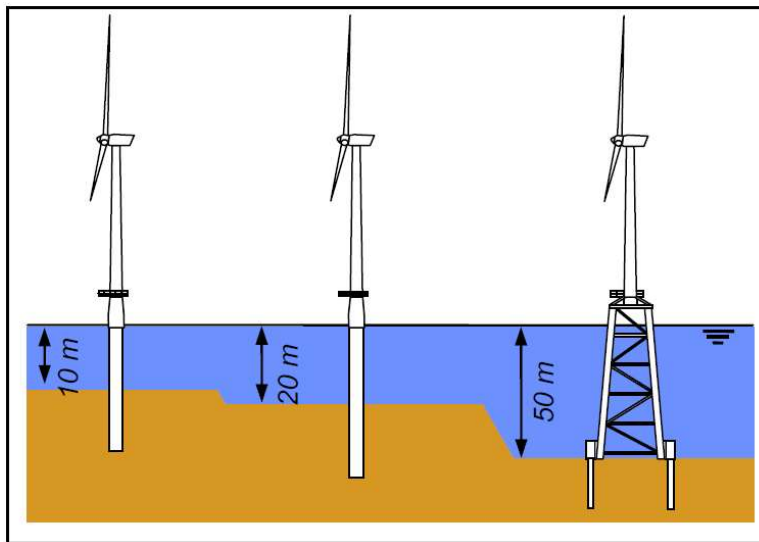


Figure 4.10: The three test wind turbines for the case study

The rotor design will give the amount of aerodynamic loading the system can capture from the wind, where a large rotor design results in large aerodynamic loading. A large rotor will also result in larger aerodynamic damping.

The hydrodynamic loading on the structure increases with a larger diameter monopile. A jacket will have even less hydrodynamic loading than a small diameter monopile, because the legs and braces of the jacket have very small diameters compared with the one monopile. Marine growth and corrosion will influence the hydrodynamic loading on the structure.

The site of the offshore wind farm will define how much fatigue load is present on location. A deep-water site generally has larger hydrodynamic loads present than at a shallower site. The

soil and its stability can again influence the eigenfrequency of the system.

So, if the wind turbine is installed in deep waters and has a soft support structure the hydrodynamic loading can be greater than the aerodynamic loading. It is in these cases that the availability of the wind turbine becomes important. When this structure is non-available and the turbine is idling, then there is non to a negligible amount of aerodynamic damping combined with a large hydrodynamic loading. This can cause large contributions to the fatigue damage on the structure and may be a driving design factor for the system. However, for the opposite case, a stiffer support structure installed in shallower water the hydrodynamic load contribution will be small. The non-availability situations will not be as important here, because when the aerodynamic damping is lost the aerodynamic loading will become small, while the hydrodynamic loading remains small, and so there is a reduction in overall loading.

A case study of this was done by Fischer, T. & Kühn, M. (2010) and it showed that a slender monopile installed in shallow water would decrease its damage as the availability decreased. For a large diameter monopile installed in deeper waters the damage increased with the decreasing availability. This shows that the non-availability situations are increasingly important for the fatigue analysis, as the diameter of the monopile increases and the wind turbine is moved to deeper waters.

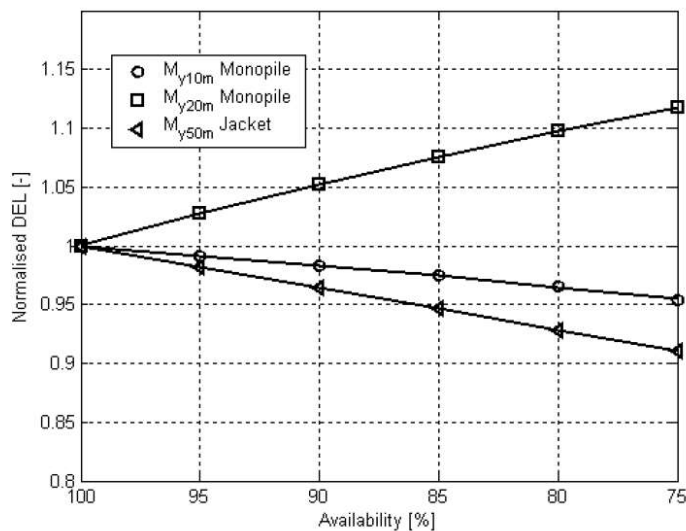


Figure 4.11: The resulting graph from case study

The results from the case study is shown in figures 4.10 and 4.11, where the first monopile (circle) has pile diameter 4.5 meters and installed in 10 meter water depth, the second monopile (square) is installed in 20 meters water depth and has a diameter of 5.5 meters. Lastly a jacket support structure is also shown which shows the same effect as the slender monopile, because it too experiences small hydrodynamic loading.

Offshore monopile foundations wind turbines are increasing in size and installed in deeper waters. Based on the results from this case study, the non-availability situations are increasingly more important for the fatigue analysis of these increasingly larger offshore wind turbines with monopile foundations.

## 4.11 Software

The integrated analysis will be performed in the software FEDEM Wind Technology.

There exists a few softwares that can perform the integrated analysis on offshore wind turbines, and FEDEM is one of them. FEDEM is a software that performs dynamic analysis for various mechanical structures and system. One of these structures is the offshore wind turbine.

The software is able to combine wind and wave loads, and to perform an integrated analysis on a model.

The software applies Morison's equation to calculate hydrodynamic loads on a slender beam structure. This also yields added mass and drag forces due to the motion of the turbine. Added mass and drag due to marine growth may also be accounted for in FEDEM.

JONSWAP spectrum is used to describe the irregular waves. The regular and irregular waves are based on linear Airy wave theory for both finite and infinite deep waters. 5th order Stokes theory and streamline functions are available to describe deterministic extreme waves.

The soil piles are modeled as beam structures with nonlinear springs at every FE node. This gives a discrete representation of the soil interaction.

# Chapter 5

## DNV GL Load Cases

For a proper fatigue analysis of an offshore wind turbine, a range of load cases needs to be analyzed to obtain the total fatigue damage. To perform analysis as the industry would do it, load cases and recommendations according to a class society must be used. For this thesis the DNV GL rules and recommendations are used.

Normally a fatigue analysis include load cases from all operational and non-operational states. However, this thesis is looking at fatigue while the wind turbine is non-operational and therefore are only load cases where the wind turbine is parked or idling included.

The offshore wind turbine model applied for the fatigue analysis in this thesis, has a 6 meter diameter monopile foundation and is located at 20 meter water depth. Based on the case study in chapter 4.10.4, the non-availability cases will have a large effect on the fatigue damage, and increased non-availability will increase the total fatigue damage.

### 5.1 Design Situation

The Design Load Cases, DLC, concerning the fatigue limit state in non-operational situations will be described here. The design situations involving start-up, shut-down and during operation is not considered in this thesis.

In the non-operational situations the turbine is parked or idling. The wind and wave conditions for the design load cases are described in DNV-OS-J101(DNV GL (2014)), and the relevant load cases are shown in table 5.1.

Table 5.1: Load cases for FLS, from table 4-5 in DNV GL (2014)

Design Situation	Load Case	Wind Condition	Wave Condition	Wind and Wave Directionality	Current	Water Level	Limit State
Power Production plus Occurrence of Fault	2.4	NTM $v_{in} < U_{10,hub} < v_{out}$	NSS $H_s = E\{H_s U_{10,hub}\}$	Codirectional in one direction	Can be ignored	Range between upper and lower 1-year water level	FLS
Parked (Standing still or Idling)	6.4	NTM $U_{10,hub} < 0.7U_{10,50yr}$	NSS Hs according to joint probability distribution of Hs, Tp and $U_{10,hub}$	Codirectional in multiple direction	Can be ignored	Range between upper and lower 1-year water level	FLS
Parked and Fault Condition	7.2	NTM $U_{10,hub} < 0.7U_{10,50yr}$	NSS Hs according to joint probability distribution of Hs, Tp and $U_{10,hub}$	Codirectional in multiple direction	Can be ignored	Range between upper and lower 1-year water level	FLS

NTM stands for the Normal Turbulence Model. It is a model that employs a characteristic standard deviation of the wind speed,  $\sigma_{U,c}$ , to represent the turbulence. This characteristic standard deviation is defined as the 90 % - quantile in the probability distribution for the standard deviation conditioned with the 10-minute mean wind speed at hub height.

NSS stands for Normal Sea State, and is characterized by an Hs, Tp and wave direction, along with a simultaneous mean wind speed. The Hs for a NSS is defined as the expected value for Hs conditioned on the simultaneous 10-minute mean wind speed. For fatigue analysis, calculations with a series of normal sea states needs to be considered. The series of normal sea states needs to be associated with different mean wind speeds. It is important that the numbers and resolution of these sea states are so that they are sufficient for the prediction of the fatigue damage associated with the full long term distribution. The range of Tp for each Hs also needs to be considered. The design calculations are based on the Tp that results in the highest loads or load effects on the structure.

### 5.1.1 DLC 2.4 - Power Production plus Occurrence of Fault

This design load case accounts for when fault occurs while the wind speed is within the operational range. The fault cases are dependent on the controller. The faults are control or protection system faults, including loss of electrical network.

This is the only design situation where the wind speed is within operational range but the wind turbine is parked or idling. This means that this design situation will account for the non-availability situations.

### **5.1.2 DLC 6.4 - Parked**

The design situation parked means that the wind turbine is either standing still or idling.

The design load case accounts for fatigue effects at large wind speeds, during idling. The design load case is to be executed in the same way as the load case for fatigue in power production DLC 1.2(DNV GL (2014)), just with idling and larger wind speeds. However, this design load case also accounts for the effects on fatigue during idling at lower wind speeds. These may even be more critical for the fatigue than the higher wind speeds. This is due to the fact that the waves may have frequencies closer to the natural frequency of the structure and because low wind speeds occur more often than high wind speeds.

In this design load case, the wind speeds below cut-in are included, which means that this design load case accounts for the load cases with wind speed below cut-in and above cut-out.

### **5.1.3 DLC 7.2 - Parked and Fault**

In this design situation there is fault on the wind turbine and it is parked. When something fails on the wind turbine, this may significantly contribute to the fatigue, especially when the turbine is parked. However, these events cannot be foreseen.

As can be seen in the table, this load case is also for the larger wind speeds, and there are not really any differences between this and DLC 6.4, except that in this one fault has occurred. There will not be any difference in execution of this DLC and DLC 6.4 during the fatigue analysis performed here, because the event of fault will not be included. This means that during the fatigue analysis only DLC 2.4 and DLC 6.4 is executed.



# Chapter 6

## Metocean Design Basis

The metocean data, applied in this thesis, is the hindcast data from the NORA10 database from 01.09.1957-31.12.2010. The site is Doggerbank, at latitude N54.87 °and longitude E1.79 °.

The metocean data, provides information on the environmental conditions at the site. It provides information on the wind speed and direction at different heights above sea level, as well as significant wave height, peak period and wave direction for the total sea state, and for the wind driven and swell sea separated.

Boehn, A. (2015), performed an evaluation of the environmental conditions based on the metocean report. The waves were found to be intermediate to deep water waves. The structure is inertia dominated. The KC number was calculated for the significant wave height of the sea states, according to equation 4.56. KC was found to be larger than three in only 0.0006% of the time for the total sea, in 0.0004% of the time for wind driven sea and never for the swell sea. According to DNV GL (2007) and DNV GL (2014), a  $KC < 3$  means that an added mass coefficient of 1.0 can be assumed, which corresponds to a mass coefficient of 2.0. A correction for the effect of short wave diffraction is not included when the mass coefficient equals 2.0.

Boehn, A. (2015), found that the sea states was in the diffraction area,  $\frac{\lambda}{D} < 5$ , for 9% of the time for the total sea. A fatigue analysis is performed here, which means these small sea states are important and therefore the effect of short wave diffraction should be included. Boehn, A. (2015), evaluated the need for separating swell and wind driven sea by investigating the importance of short wave diffraction for the sea states. She found that when swell and wind driven seas are looked at separately the percentage of wind driven sea states inside the diffraction area

is 45% while the percentage for swell sea is 5%. Based on this, short wave diffraction will be more important for separated swell and wind driven sea than for the total sea.

The wind speed 100 meters above MSL is used for the development of the scatter diagrams. This was chosen because the hub height of the wind turbine is 90 meters above MSL. However, in FEDEM the wind speed applied will correspond to the wind speed at hub height.

Figure 6.1 shows the probability of occurrence for the different wind speeds. The x-axis is the wind speed, while the y-axis is the probability of occurrence in percent. Each bar in the graph represents a wind speed bin of 2 m/s. As can be seen on the figure the highest occurring wind speeds are in the range of 6-12 m/s. Average wind speed on site over the past 50 years is 9.95 m/s. The rated wind speed for the turbine is among the highest occurring wind speeds, and the wind speed is frequently above rated.

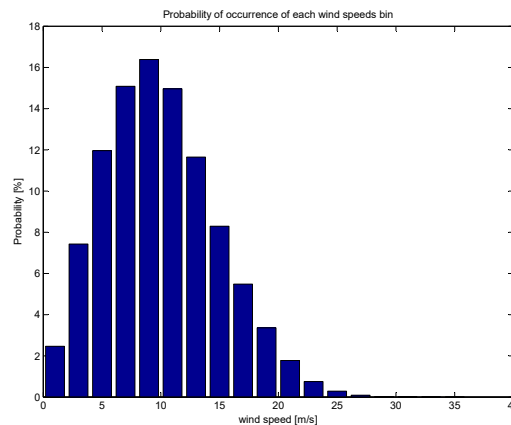


Figure 6.1: The probability of occurrence for the different wind speed bins

The metocean data is analyzed and ordered into scatter diagrams in order to find the probability of occurrence for the different environmental states, as well as providing a basis for determining which environmental cases to be applied in the different load cases for the investigation of the fatigue damage. The sea state is dependent on the wind speed. Therefore scatter diagrams are created for each wind speed bin. The wind speed is sorted into 2 m/s bins, the significant wave height in 0.5 meter bins, while the peak period is sorted into bins of 1 seconds. These chosen bin sizes are very common for scatter diagrams (Krokstad, J. R. (2016)), and was therefore recommended.

The scatter diagram will help to determine the environmental states that will be used in the different load cases in the analysis and give the probability of occurrence of these. The analysis will be run for a certain wind speed along with its corresponding most likely sea state.

This thesis will investigate the effect of separating wind driven and swell sea on the fatigue damage. Therefore, scatter diagrams are made for every wind speed bin for both the total sea and for the wind driven and swell sea separated.

As stated before, misalignment between wind and waves will not be considered in this thesis, so the wind and waves will be assumed to be in the same direction at all times.

The scatter diagram for the total sea for wind speed bin 8-10 m/s is shown in figure 6.2. Every scatter diagram for the total sea, wind driven sea and swell sea is included in a excel document handed in as an electronic file with the thesis.

The non-operational situations are investigated in this thesis, so the probability for the wind speed to be below cut in and above cut out is calculated. From this metocean report, and with a cut in wind speed of 3 m/s and a cut out wind speed of 25 m/s, the probability for the wind speed to be below cut in is 5.5571 %, and the probability for the wind speed to be above cut out is 0.2105 %. This shows that the wind speed is significantly more often below cut in than above cut out, and the low wind speed load cases will be of greater importance in the analysis. The wind turbine is assumed to be non-available for 10 % of the time, meaning that 10 % of the time the wind is within the operational range the wind turbine is parked and not producing power. These probabilities will be included in the fatigue damage calculations for the design life. The wind turbine is non-operational 15.7676% of the time.

Hs\Tp	1	2	3	4	5	6	7	8	9	10	11	12	13	14	15	16	17	18	19	20	21	Tot:	
0.5	0	0	0.018	0.0533	0.0468	0.0205	0.0205	0.0077	0.0051	0.0019	0.0019	0.0013	0.0039	0	0.0006	0	0	0	0	0	0	0	0.1815
1	0	0	0.025	0.9003	1.6806	0.659	0.2689	0.0963	0.0725	0.0533	0.0424	0.0257	0.0135	0.0058	0.0019	0	0.0013	0	0	0	0	0	3.8465
1.5	0	0	0	0.0404	1.2205	2.9082	1.524	0.3709	0.2535	0.2137	0.2015	0.1399	0.0687	0.025	0.0135	0	0.0013	0	0.0006	0	0	0	6.9817
2	0	0	0	0	0.0083	0.3587	1.5067	0.6141	0.4607	0.2907	0.1899	0.2156	0.1283	0.0347	0.0154	0	0.0064	0	0	0	0	0	3.8295
2.5	0	0	0	0	0	0.0019	0.0988	0.1469	0.2034	0.2451	0.1527	0.1168	0.0886	0.0526	0.0135	0	0.0039	0	0	0	0	0	1.1242
3	0	0	0	0	0	0	0.0019	0.0071	0.0225	0.0302	0.0886	0.0699	0.0622	0.0334	0.0128	0	0.0026	0	0.0013	0.0006	0	0	0.3331
3.5	0	0	0	0	0	0	0	0.0006	0.0013	0.0032	0.0019	0.0193	0.0167	0.0141	0.0167	0	0.0013	0	0	0	0	0	0.0751
4	0	0	0	0	0	0	0	0	0	0.0019	0.0006	0.0019	0.0013	0.0013	0.0026	0	0.0026	0	0	0	0	0	0.0122
4.5	0	0	0	0	0	0	0	0	0	0	0	0	0	0	0	0	0.0006	0	0	0	0	0	0.0006
5	0	0	0	0	0	0	0	0	0	0	0.0006	0	0	0	0	0	0	0	0	0	0	0	0.0006
5.5	0	0	0	0	0	0	0	0	0	0	0	0	0	0	0	0	0	0	0	0	0	0	0
6	0	0	0	0	0	0	0	0	0	0	0	0	0	0	0	0	0	0	0	0	0	0	0
6.5	0	0	0	0	0	0	0	0	0	0	0	0	0	0	0	0	0	0	0	0	0	0	0
7	0	0	0	0	0	0	0	0	0	0	0	0	0	0	0	0	0	0	0	0	0	0	0
7.5	0	0	0	0	0	0	0	0	0	0	0	0	0	0	0	0	0	0	0	0	0	0	0
8	0	0	0	0	0	0	0	0	0	0	0	0	0	0	0	0	0	0	0	0	0	0	0
8.5	0	0	0	0	0	0	0	0	0	0	0	0	0	0	0	0	0	0	0	0	0	0	0
9	0	0	0	0	0	0	0	0	0	0	0	0	0	0	0	0	0	0	0	0	0	0	0
9.5	0	0	0	0	0	0	0	0	0	0	0	0	0	0	0	0	0	0	0	0	0	0	0
10	0	0	0	0	0	0	0	0	0	0	0	0	0	0	0	0	0	0	0	0	0	0	0
10.5	0	0	0	0	0	0	0	0	0	0	0	0	0	0	0	0	0	0	0	0	0	0	0
11	0	0	0	0	0	0	0	0	0	0	0	0	0	0	0	0	0	0	0	0	0	0	0
<b>Tot:</b>	0	0	0.043	0.994	2.9562	3.9483	3.4208	1.2436	1.019	0.84	0.6801	0.5904	0.3832	0.1669	0.077	0	0.02	0	0.0019	0.0006	0	0	<b>16.385</b>

Figure 6.2: Scatter Diagram for Wind Speed bin 8-10 m/s

# Chapter 7

## Approach and Modeling

In this chapter, the approach for the analysis and modeling is reviewed.

The model used for the analysis in FEDEM Windpower was created by PhD student Sebastian Schafhirt, and is based on the NREL 5 MW reference wind turbine with a monopile foundation based on the OC3 project.

The model is created so that the main direction of the wind and waves are in the positive x-direction. This means that fore-aft motion is motion along x-axis, and side-side motion is motion along y-axis, as previously defined in chapter 2.1.

The offshore wind turbine is located at 20 meters deep water.

### 7.0.1 Rotor and Nacelle

A sample 5 MW wind turbine is provided by FEDEM when the software is downloaded. This has been used when the model was created. The sample turbine is based on the NREL 5 MW reference wind turbine. The main characteristics are listed in table 2.1 and a more detailed description can be found in the NREL Technical Report (Jonkman, J., Butterfield, S., Musial, W. & Scott, G. (2009)).

The nacelle contains in this model a gearbox, a generator and one bearing.

## 7.0.2 Tower

The hub height is set to 90 meters. The tower extends from 10 meters above sea level and up to the tower top, located at 87.6 meters above MSL, which means that the tower is 77.6 meters tall.

The tower is modeled by beams. The beam elements have a length of one meter, except the bottom beam, which is the one that is connected to the monopile and is 0.6 meters. The tower's diameter and thickness are decreasing with the height. The bottom of the tower has an outer diameter of 6 meters and inner diameter of 5.946 meters, while the top has an outer diameter of 3.87 meters and inner diameter of 3.832 meters.



Figure 7.1: The model in FEDEM, with the tower indicated as the visualized structure

Figure 7.1 shows the model of the wind turbine in FEDEM, where the tower is highlighted as a visualized structure.

The bottom part of the tower may, in extreme cases, be at risk for splashing. Hydrodynamic properties have, therefore, been defined for the first two meters of the tower. A drag coefficient of 1.0 and a mass coefficient of 2.0 have been defined.

The beam elements in the offshore wind turbine model have been given a structural damp-

ing, and it has been defined according to Rayleigh damping as,

$$C = 0 * M + 0.005 * K \quad (7.1)$$

As can be seen, there is only stiffness proportional damping defined for the structural damping of the tower. The mass proportional damping has not been included because it is most efficient at lower frequencies, and the stiffness proportional damping is assumed to be able to damp the natural frequency of the first mode sufficiently. This applied damping corresponds approximately to a structural damping of 0.37 %, which is well below the damping of 1% of critical specified in Jonkman, J., Butterfield, S., Musial, W. & Scott, G. (2009). This low damping have been specified as a limitation for the thesis in chapter 1.4. The low damping level causes there to be large dynamic amplification in the response.

Later, a damping sensitivity analysis was run, and then the effect of increasing the damping can be observed.

### 7.0.3 Monopile

The foundation which here is a monopile is modeled with beam elements. The monopile extends from 36 meters below the mudline and up 10 meters above the sea surface, which gives it a total length of 66 meters. It is modeled as two parts in the model, the substructure which reaches down to the sea bottom, and the pile foundation which is the part below the mudline. The entire monopile can be seen on figure 7.2.

The substructure is 30 meters long, from 10 meters above MSL and down to the mudline. The substructure has a constant diameter and thickness of 6 meters and 0.06 meters. The beam elements are all one meter long. This part of the structure is submerged in sea water or at risk of splashing, and so hydrodynamic properties are included and specified as a drag coefficient of 1.0, and a mass coefficient of 2.0.

The pile foundation is also modeled with beam elements, and it includes the soil-pile interactions which are modeled with translational spring functions. The pile extends 36 meters down below the seabed. No hydrodynamic properties are included for the pile foundation, because the pile is in the soil.



Figure 7.2: The model in FEDEM. The monopile is indicated as the visualized structure

#### 7.0.4 Control System

There is a control systems in a wind turbine. The control system is there to control the power production. It is done with two basic control systems, a full-span rotor-collective blade-pitch controller and a generator-torque controller (Jonkman, J., Butterfield, S., Musial, W. & Scott, G. (2009)). The purpose of the generator-torque controller is to maximize the power capture when the wind speed is below rated wind speed. The purpose of the blade-pitch controller is to control and regulate the generator speed when the wind speed is above the rated wind speed.

A control system was created for the model used in the analysis. This model of the control system does not know the cut-in or the cut-out wind speed, because it was not designed for non-power-production operations (Jonkman, J., Butterfield, S., Musial, W. & Scott, G. (2009)). This means that when analysis are run with wind speed outside the operational range, the controller needs to be modified. In the non-operational situations the pitch angle is set to be a constant of  $-\frac{\pi}{2}$  and the torque controller is set to zero. This means that the turbine is idling and not



producing power.

### 7.0.5 Environmental State

The environmental state consists of both the wind and the sea state, and they need to be defined in FEDEM.

The wind condition can be defined as either a constant or a turbulent wind. Turbulent wind is applied for every analysis here, since that will result in more accurate results. TurbSim generates the turbulent wind files. The turbulence intensity is set to the value of 0.11 for all generated turbulent wind files. One wind file is generated for each wind speed, with different seed numbers, i.e. only one set of wind data for each environmental condition. The aerodynamic loads are calculated by AeroDyn which is implemented in FEDEM. Even though the wind turbine is not operational, the applied wind will give a small aerodynamic damping and force to the system. This aerodynamic damping is possible to calculate, by performing decay tests for the wind turbine with strong wind applied and without. However, this have not been done in this thesis.

A linear wave model is used for the analysis. There are a limited number of wave theories available in FEDEM, and linear theory is chosen for the analysis in this thesis. Wheeler stretching is applied by default in FEDEM, to calculate the wave kinematics more accurately up to the free surface.

The waves can be generated as regular sinusoidal waves or as irregular waves modeled with the JONSWAP spectrum or with a user-defined spectrum. Irregular waves are used in these analyzes, as those are more realistic. The JONSWAP spectrum will be applied in every analysis except when the wind and swell sea is separated, which is when Torsethaugen spectrum will be used. The Torsethaugen spectrum will be applied as a user-defined spectrum. For every load case run, the random seed number for the waves are changed. Long crested or short crested waves can be chosen for the analysis. For the short crested waves, the number of wave directions need to be chosen.

For fatigue analysis, moderate sea states are used in the analysis. Realistic waves in moderate sea states are short crested. The degree of short crested waves will depend on the site. The swell and wind driven sea is separated in a real sea state, and they often have different direction. Parameters defining the separated swell and wind driven sea will also depend on the site.

This means that long crested waves and JONSWAP spectrum are conservative choices for the modeling of the sea state.

## 7.1 Load Cases for Analysis

The load cases for FLS for non-operational situations need to include wind below and above cut in and cut out, and load cases where the wind turbine is parked while the wind is within the operational range. In all the load cases, the wind turbine is parked. The environmental conditions for the load cases are chosen from the scatter diagrams.

The first design situation is the non-available design situation. This is the situations where the wind turbine is non-operational while the wind speed is within the operational range. These design situations will together result in the fatigue damage accumulated during 10% of the design life. However, all the load cases cannot be run, so a selected few are chosen for use in the analysis.

The second situation is when the wind turbine is parked or idling, because the wind speed is below cut in or above cut out. These load cases will include wind speeds up to 70% of the 50 year wind speed. The 50 year wind speed is assumed to be approximately 30-40 m/s(Krokstad, J. R. (2016)). This leads to a maximum wind speed of 28 m/s to be applied in the fatigue analysis.

The scatter diagrams are used to choose the environmental states for the analysis. First, the wind speed is chosen and then the sea state is chosen from the scatter diagram for the chosen wind speed.

The wind speed, significant wave height and peak period used in the analysis is the maximum of its bin.

10 minutes and 1 hour simulations will be run. The 10 minutes analysis was chosen because the wind speeds is optimally only assumed constant for 10 minutes, and because the 10 minute simulations is what is usually used by the offshore wind industry today(Krokstad, J. R. (2016)). The 1 hour simulations are recommended for fatigue analysis of offshore wind turbines, because it has lower statistical uncertainty connected with the results. 1 hour is an acceptable averaging time for both the wind and wave process, even though it is considered short for the waves. Table 7.1 shows the load cases run for the 10 minute simulation and table 7.2 shows the load cases run

for the 1 hour simulation.

For the probability of occurrence in tables 7.1 and 7.2, notice that the probabilities are for the environmental state. Since load case 1-1 to 1-9 is non-availability cases, the probability for the wind turbine to be non-available will need to be included in the calculations of the total fatigue damage over the design life.

Table 7.1: Load cases for the 10 minutes fatigue analysis

Load case	Wind Speed [m/s]	Hs [m]	Tp [s]	Probability[%]
1-1	4	1	7	0.3478
1-2	6	1	6	1.6915
1-3	8	1	5	1.9867
1-4	10	1.5	6	2.9082
1-5	12	2	7	2.6342
1-6	14	2.5	7	2.5783
1-7	18	3	7	1.4291
1-8	22	4.5	9	0.3613
1-9	24	6	10	0.016
2-1	2	1	7	0.3478
2-2		1	6	0.3234
2-3		0.5	5	0.2098
2-4		0.5	4	0.1399
3-1	26	5.5	10	0.0732
3-2	28	6	10	0.016

Table 7.2: Load cases for the 1 hour fatigue analysis

Load case	Wind Speed [m/s]	Hs [m]	Tp [s]	Probability[%]
1-4	10	1.5	6	2.9082
1-5	12	2	7	2.6342
1-7	18	3	7	1.4291
2-1	2	1	7	0.3478
3-2	28	6	10	0.016

## 7.2 The Analysis

The offshore wind industry perform fatigue analysis by doing 10 minute simulations. They apply Morison's equation with a diffraction corrected  $C_M$ . This correction is often a correction of the viscous effects, this is KC-dependent, or it is a wavelength dependent correction, often based on MacCamy and Fuchs. This correction reduces the mass coefficient from  $C_M = 2$ . To apply Morison's equation with  $C_M = 2$  is conservative. As stated, the diffraction effect included in Morison's equation from long waves, will here be referred to as long wave diffraction.

There are multiple different analysis that is run for this thesis. All the load cases are run for each analysis method, so that the results from the different analysis methods can be compared. The 10 minutes simulations are first run for all analysis, and then the 1 hour simulations are run for three of the analysis methods.

The responding moments and forces at specific nodes are taken out as results from the analysis. The stresses and corresponding fatigue damage is then calculated for points around the cross-section at the location of that node.

The maximum fatigue damage along the monopile is accumulated where the maximum moment occur. The maximum moment along a monopile occurs a little below the mudline of the monopile, and therefore the moments and forces are taken out for the node at the mudline. The fatigue damage is calculated for the cross-section at this location.

The results from the analysis of the different methods is compared. The goal is that by calculating the wave forces and modeling the sea state more accurately the calculated total fatigue damage will be reduced.

The method that is applied by the industry today have not been performed. However, the wave loads are calculated according to Morison's and MacCamy and Fuchs equation. As stated, the additional diffraction effect from short waves, included in MacCamy and Fuchs equation, will further be referred to as short wave diffraction. The effect of including the short wave diffraction, in MacCamy and Fuchs, on both the wave load and on the fatigue damage will be observed. Other considerations to the wave modeling will be made to try to model the waves more realistic and to reduce the calculated fatigue damage.

The different analysis methods are described below.

### 7.2.1 Morison

For this first analysis, the sea state is modeled with a long crested JONSWAP spectrum. The wave loads are calculated according to Morison's equation by FEDEM, with, as previously stated, a mass coefficient of 2.0 and a drag coefficient of 1.0. This means the wave loads calculated in this method are conservative.

This simulation method will further be referred to as the Morison method.

### 7.2.2 MacCamy and Fuchs Correction for Diffraction

For this analysis method, every load case is run with the mass wave load calculated according to MacCamy and Fuchs equation. This means that in this method the effect of diffraction of waves with wavelength less than five times the diameter is included. The total wave load is found by adding the drag load to the wave load calculated according to MacCamy and Fuchs.

The sea state is modeled with a long crested JONSWAP spectrum. The time history of the wave load is calculated in MATLAB, then transferred to FEDEM, and applied at the nodes of the monopile below the sea surface in the model.

To obtain the wave force, that is applied to the model, the wave force is integrated over a small distance  $dz$ , and then this force is applied at the midpoint of this distance in the model. There is a node every meter in the model, which means the wave force applied to a node have been integrated over a one meter distance,  $dz$ , so that the node is located in the midpoint of this distance. The force is applied at every node from MSL,  $z=0$ , and down to the mudline.

This method will result in some uncertainties since the force is applied in the nodes. There are also some uncertainties in the integration of the force, since the integration is done with the trapezoidal rule in MATLAB which is an approximation to integration. Another source of inaccuracies is that linear wave theory was applied, which means that the wave forces is only calculated up to MSL.

The MATLAB code that is run for the calculation of this is the "head.m", with functions that are called upon by the head file.

This simulation method will from now on be referred to as the MacCamy method.

### 7.2.3 Short-Crested Sea

Analysis will be run for all the load cases with the wave process modeled as short-crested. This means the waves are multi-directional. In FEDEM the number of wave directions need to be specified, from offshore oil and gas, 7 to 11 wave directions are usually chosen, and so 7 wave directions are chosen here (Eliassen, L. (2016)).

The hypothesis is that the short crested waves will reduce the calculated fatigue damage, as they do for the deeper sea structures in offshore oil and gas.

The analysis with short crested waves are run with the wave load calculated according to Morison's and according to MacCamy and Fuchs equation. In the first analysis, the wave loads are calculated according to Morison's equation in FEDEM, with  $C_M = 2$ .

In the second analysis, the wave loads are calculated according to MacCamy and Fuchs equation, which means it includes the effect of short wave diffraction. The wave loads according to MacCamy and Fuchs are, as before, calculated in MATLAB, and then applied to the model in FEDEM. The short crested waves are multi-directional, which means the wave load is multi-directional. The wave load is decomposed, and the load contributions in x and y-direction is added up and applied to the model.

These two simulation methods will be referred to as the short Morison and short MacCamy method.

### 7.2.4 Separation of Wind Driven and Swell Sea

The separation of wind driven and swell sea is obtained here by applying the Torsethaugen spectrum instead of a JONSWAP spectrum. The Torsethaugen spectrum is a two-peak spectrum which combines the spectra for the wind driven and swell sea. The Torsethaugen spectrum assumes that the swell and wind driven sea propagates in the same direction. However, as can be seen in the metocean report, the swell and wind driven sea often propagates in different directions. This means that Torsethaugen is a conservative way of describing the separated wind driven and swell sea.

It can be observed from the metocean data that, while the wind speed is low the total sea is dominated by the swell sea, and as the wind speed increases the wind driven sea contributes

increasingly until it dominates the total sea at high wind speeds.

From the metocean report the significant wave height and peak period for both the wind driven and swell sea is given. The wind driven and swell wave data was organized into separate scatter diagrams, given the wind speed. The swell and wind driven sea states applied in the construction of the Torsethaugen spectrum was chosen as the highest occurring sea states for the given wind speed.

The Torsethaugen spectrum was calculated in MATLAB, in the script called Torsethaugen.m. It was calculated according to the equations for the simplified Torsethaugen spectrum as found in DNV GL (2007). For the check to see if the sea state was swell or wind dominated, the significant wave height for the total sea was used. Other than that, the parameters used was as defined for the simplified form of the equation in DNV GL (2007). The calculated wave spectrum was applied as a user-defined spectrum in FEDEM.

Long crested waves are applied in the analysis. The wave load is first calculated according to Morison's equation, and then according to MacCamy and Fuchs. MATLAB is applied to calculate the wave loads according to MacCamy and Fuchs equation, and then the loads are applied to the model.

These two simulation methods will be referred to as the Torsethaugen and Torsethaugen MacCamy method.

### 7.2.5 Damping Sensitivity Analysis

A damping sensitivity analysis is also performed. A few load cases are run with different damping levels.

The chosen load cases to perform the damping sensitivity on is presented in table 7.3. Four load cases are chosen and a 10 minutes simulation are run for each.

The damping sensitivity is run with the sea state modeled as long crested waves based on JONSWAP spectrum and the wave load calculated according to MacCamy and Fuchs equation.

The load cases that the damping sensitivity study will be run on is presented in table 7.3.

Only the structural damping will be modified for this damping sensitivity study. The structural damping level is determined as Rayleigh damping, as determined in section 4.8.3, with  $\alpha_1$  as the mass proportional and  $\alpha_2$  as the stiffness proportional damping coefficient. In the origi-

Table 7.3: Load cases for the damping sensitivity study

Load case	Wind Speed [m/s]	Hs [m]	Tp [s]
1-3	8	1	5
1-4	10	1.5	6
1-6	14	2.5	7
1-7	18	3	7

nal model, a structural damping with 0.005 stiffness proportional damping was applied, which corresponded to a damping ratio of 0.37 % of critical.

The damping levels applied in this sensitivity study can be observed in table 7.4.

Table 7.4: Load cases for the damping sensitivity study

Case	$\alpha_1$	$\alpha_2$	$\lambda$ [%]
1	0	0.005	0.37
2	0	0.013	0.96
3	0	0.067	4.96
4	0.005	0.005	0.54

### 7.2.6 Availability Sensitivity Study

This thesis is considering the wind turbine in non-operational conditions, which consist of wind speed below cut in, above cut out and non-availability.

The percentage time that the wind speed is below or above cut in or cut out wind speed cannot be controlled or improved by engineering. However, the non-availability can be improved, or worsened. In this last part, the wind turbine's fatigue damage sensitivity to non-availability is investigated. Most of the time the wind turbine is non-operational is because it is non-available. It is expected that a change in non-availability will have a visible effect on the total fatigue damage of the wind turbine. Based on the results from the case study in chapter 4.10.4, it is expected that an increase in non-availability will increase the calculated total fatigue damage.

For the other analysis the non-availability was assumed to be 10 %. For this study, the total fatigue damage is calculated with 5%, 10% and 15% non-availability. The results from the simulation of the short MacCamy method is applied for this study. The simulation will not need to be run again for this study. To obtain the results for the availability study, the results from the



simulation are run through the MATLAB code that calculates the fatigue damage three times, with different percentage non-availability.

### 7.3 Post-Processing

The post-processing of the results from the analysis is done in MATLAB.

The fatigue damage is calculated at the mudline, because this is where the maximum moment occurs for the wind turbine, and therefore maximum stress and fatigue damage. The moments has its maximum there because this point is the furthest away from the point of attack of the applied forces. The MATLAB script calculates the fatigue damage from the time series of the responding moments at the mudline. The stress is first calculated from the moments, then the rainflow counting script from the WAFO toolbox in MATLAB is applied for the rainflow counting of the stress time series, and lastly the damage is calculated. The fatigue damage is calculated for each of the load cases, and the total fatigue damage is calculated for the full design life of 20 years. The probability for the load case to occur is included in the calculation of the total fatigue damage for the design life.

Table 7.5 shows the parameters used for the S-N curve in the calculation of the fatigue damage. The parameters have been collected from table 2-2 in DNV GL (2010), it is curve D which is for a structure in seawater with corrosion protection.

Table 7.5: Parameters for S-N-curve

m1	3
m2	5
loga1	11.764
loga2	15.606
k	0.2
stress limit	52.63 [MPa]

Since short crested waves are applied in some of the analysis, it is interesting to observe the distribution of the fatigue damage around the circumference of the monopile. The fatigue damage will therefore be calculated at seven evenly distributed points along one half of the cross-section. A sketch of the seven points where the fatigue damage will be calculated is shown in figure 7.3. The stress on the opposite side of the cross-section will have equal value but with op-

positive sign, which is why the fatigue damage is only calculated for one half of the cross-section. The moments about x and y are needed when calculating the stresses around the circumference.

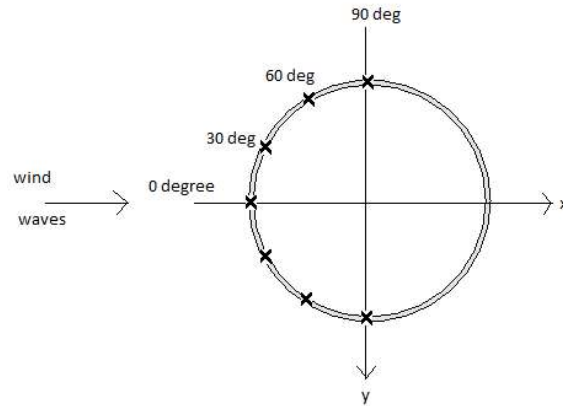


Figure 7.3: A sketch of the cross-section of the monopile with points where the fatigue damage is calculated

The predeveloped function SPEGEN\_T has been used to perform the Fourier Transform of the time history of the moments to plot them as response spectra in frequency domain.

# Chapter 8

## Results

Results from the different simulations are presented in this chapter. The main results are the total fatigue damages.

First, the two natural periods for fore-aft and side-side motion are presented. Then the total fatigue damage from all six methods are presented. The fatigue damage accumulated from every load case for each of the six methods are then presented in bar graphs.

Remember that the diffraction effect included in Morison's equation is referred to as long wave diffraction, while the added effect of diffraction which is included in MacCamy and Fuchs in addition to the long wave diffraction, is referred to as short wave diffraction.

The response spectra of the moments at the baseline of the monopile are then reviewed. The first natural period are indicated on these graphs. One graph is presented her, while the rest is in appendix C. This presentation in frequency domain makes it easy to see which frequencies are important for the response.

Results from the damping and availability sensitivity studies are presented last.

### 8.1 Eigenvalue Analysis

An eigenvalue analysis was performed by FEDEM, and the first two natural periods, along with their corresponding mode, are presented here.

These values look reasonable for an offshore wind turbine. The natural period for the 5MW reference wind turbine is 3.1 and 3.2 seconds(Jonkman, J., Butterfield, S., Musial, W. & Scott, G.

Table 8.1: Natural period for the Offshore Wind Turbine

Mode	Description	Natural Period [s]
1	1st Tower Fore-Aft	4.24
2	1st Tower Side-Side	4.20

(2009)), which is lower than the ones obtained here. This is because the natural periods in table 8.1 are for an offshore wind turbine with tower and monopile, while the natural periods for the 5MW reference wind turbine are only for the wind turbine without monopile. The monopile adds mass and length, which increases the mass and decreases the stiffness of the system. Both of these increases the natural period of the system.

## 8.2 Dynamic Analysis

Results from the dynamic analysis of the six different methods are examined below.

Before looking at the results, it is important to remember that the damping level was set very low. This means the fatigue damages obtained here are not representative of the fatigue damages that would be obtained for a real offshore wind turbine. However, the results are good for comparing, since the same damping level has been applied to the model for every simulation method.

The total fatigue damage may be considered in relation to DNV GL requirement. A design fatigue factor of three should be used(DNV GL (2014)). This implies that the total fatigue damage during the fatigue life cannot surpass  $\frac{1}{3}$ . However, there is only a point in doing this check when more realistic total fatigue damages have been obtained.

The total fatigue damage accumulated from these load cases over a lifetime of 20 years is presented for all six methods. Both the total fatigue damage from the 10 minutes and the 1 hour simulations are presented. The confidence in the results is greater from the 1 hour simulations than the 10 minutes simulations, because of the increased simulation time.

The fatigue damage accumulated in every load case for each of the six methods are presented in bar graphs. This presentation enables a comparison of the accumulated fatigue damage from the different load cases for each method.

### 8.2.1 Total Fatigue Damage

For each analysis method the total fatigue damage is calculated. The probability of occurrence for the different load cases are included in this, along with the design life.

The total fatigue damage accumulated over 20 years from the 10 minutes simulations are presented in table 8.2. The total fatigue damage was calculated for the seven points around the circumference as illustrated in figure 7.3.

Table 8.2: Total fatigue damage over 20 years for each method, from the 10 minutes simulations.

Calculation Method	Fatigue Damage accumulated over 20 years						
	[-]						
	-90 °	-60 °	-30 °	0 °	30 °	60 °	90 °
Morison	4.78E-11	0.0124	0.2208	0.4120	0.2210	0.0124	4.78E-11
MacCamy	4.71E-11	0.0086	0.1528	0.2928	0.1527	0.0086	4.71E-11
Short-crested Morison	4.97E-11	0.0186	0.2094	0.3885	0.2096	0.0187	4.97E-11
Short-crested MacCamy	4.91E-11	0.0045	0.0777	0.1645	0.0777	0.0044	4.91E-11
Torsethaugen	4.91E-11	0.0126	0.2155	0.4460	0.2157	0.0125	4.91E-11
Torsethaugen MacCamy	5.13E-11	0.0085	0.1395	0.2806	0.1395	0.0085	5.13E-11

From table 8.2, the short MacCamy method results in the lowest calculated total fatigue damage.

The 0 ° point, which is at the x-axis, is as expected the point that always accumulates the most fatigue damage. This is because the main propagation of the applied waves are along the x-axis. The 0 ° point is therefore the most critical point for fatigue damage. The point at the y-axis, the -90 and 90 ° points, are the points that accumulates the least damage, this is also as expected.

The total fatigue damage at the 0 ° point is investigated. The Torsethaugen method results in the largest total fatigue damage. This shows that to separate the wind and swell sea by employing Torsethaugen, long crested waves and Morison's equation, does not reduce the calculated total fatigue damage. The Morison method results in the second largest fatigue damage, while the short Morison method results in the third largest. This shows that the three methods that calculated the wave load according to Morison's equation, results in the largest total fatigue damages.

The three methods that calculated the wave load according to MacCamy and Fuchs equation resulted in the lowest fatigue damages. The MacCamy method resulted in the fourth largest total fatigue damage, the Torsethaugen MacCamy method resulted in the fifth largest, and as said, the short MacCamy method resulted in the lowest total fatigue damage out of these six different methods. This shows that when doing a fatigue analysis on a large diameter offshore wind turbine with monopile foundation, the effect of short wave diffraction should be included so that the wave loads are not over-estimated.

Now to look at the effect of applying short crested waves. The short Morison method has larger fatigue damage at the 60 and 90 ° points, and smaller in the 0 and 30 ° points, in comparison with the Morison method. This is caused by the use of the short crested waves. The short crested waves spread the wave energy over multiple wave directions, which results in a decrease of the wave load in the main wave propagation direction and an increase in the wave load perpendicular to this. The short crested waves reduced the fatigue damage in line with the main propagation more than it increased the fatigue damage across the main propagation of the waves. The point that accumulates the most damage around the circumference is still at the 0 ° point. The same result can be seen between the short MacCamy method and the MacCamy method. An increase in the fatigue damage perpendicular to the main wave propagation, and a decrease in the fatigue damage in line. The reduction of the fatigue damage due to the short crested waves, was greater when the effect of short waves diffraction was included as well.

The Torsethaugen MacCamy method reduced the calculated total fatigue damage for every point around the circumference, except at the 90 ° point, when compared with both the Torsethaugen method and the MacCamy method. This implies that by applying Torsethaugen, while the effect of short wave diffraction is included, the calculated total fatigue damage is reduced, and that by including the effect of short wave diffraction, while applying the Torsethaugen spectrum, reduces the calculated fatigue damage. This means that to apply Torsethaugen spectrum, instead of JONSWAP spectrum, only reduces the calculated total fatigue damage when the wave load is calculated according to MacCamy and Fuchs. The differences in the JONSWAP and Torsethaugen spectra will be discussed later, in chapter 9.3. The reason why the calculated fatigue damage was so large for the 90 ° point is not known, however, it has to do with the moment about x and how the Torsethaugen spectrum apparently excites the moment about

x more than the other methods. More analysis is needed to explain this.

### 1 hour simulations

1 hour simulations were run for the Morison method, the MacCamy method and the short MacCamy method. The results from this is seen in table 8.3.

Table 8.3: Total fatigue damage for each method, from the 1 hour simulations.

Calculation Method	Fatigue Damage accumulated over 20 years						
	[-]						
	-90 °	-60 °	-30 °	0 °	30 °	60 °	90 °
Morison	1.00E-11	0.0095	0.1530	0.2797	0.1531	0.0095	1.00E-11
MacCamy	7.16E-12	0.0065	0.1040	0.1898	0.1040	0.0065	7.16E-12
Short-crested MacCamy	1.00e-11	0.0014	0.0241	0.0524	0.0240	0.0014	1.00e-11

The short MacCamy method results in the lowest calculated total fatigue damage from the 1 hour simulations as well.

The large differences in the total fatigue damage in table 8.2 and 8.3 are present because they are based on a different number of load cases, and different simulation length. Table 8.3 is only based on five load cases and table 8.2 is based on 15, and therefore the total fatigue damage in table 8.3 is significantly smaller.

Based on both the 1 hour simulations and the 10 minutes simulations, the short MacCamy method have significantly reduced the calculated fatigue damage compared with the MacCamy method. This means that the application of short crested waves significantly reduced the calculated fatigue damage, compared with long crested waves. This observation is based on both simulations, which means there is an acceptable level of confidence connected with the results.

The MacCamy method have significantly reduced the calculated total fatigue damage compared with the Morison method. This was as expected.

In appendix B, the accumulated fatigue damage from every load case are presented in tables. The results from both the 10 minutes and 1 hour simulations from the Morison method, MacCamy method and short MacCamy method are presented. From these it is clear that the accumulated fatigue damage is not linearly dependent on time. This is reasonable since the time history of the forces and moments are stochastic variables with random phase, and so no

random time history is perfectly equal to the next, unless same seed number have been used.

### **8.2.2 Comparison of Fatigue Damage**

The fatigue damage accumulated from each of the load cases for the six methods, and at different points around the circumference are investigated.

As stated, tables containing the fatigue damage accumulated from every load case at the seven points around the circumference, for all six methods is presented in appendix B. For better visualization the fatigue damage is presented in bar graphs here. One bar graph is made for each of the four points around the circumference, from 0 to 90°. Only a quarter of the circumference is chosen because, as might have been observed, the fatigue damage in the other quarters of the circumference will be equal to this one.

The fatigue damage in the points is due to the stress ranges caused by the moment about y and x. Accumulated fatigue damage in the point at 0°, is due to the stress ranges caused by the responding moment about y. The fatigue damage in the point at 90° angle, is due to the stress ranges caused by the responding moment about x. The fatigue damage in the two other points are caused by a combination.



### 0° point

Figure 8.2 shows a bar graph of the accumulated fatigue damage from the 10 minutes simulations of each of the load cases, in the 0° point. Take notice that the y-axis are of different magnitude for each individual plot. The 0° point have been circled in figure 8.1. This point

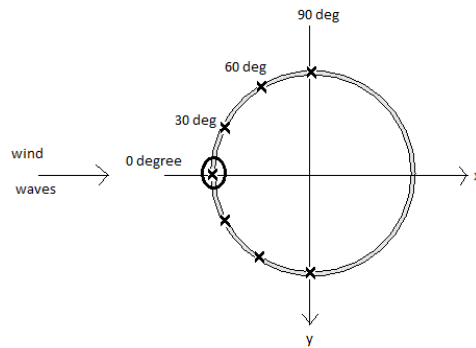


Figure 8.1: The circumference of the monopile, with the 0° point circled

accumulated the most damage for all six methods and from all load cases, because it is in-line with the main propagation of the waves and wind. It is therefore the worst point around the circumference.

As can be seen in figure 8.2 there are large variations in the fatigue damage between the different load cases and different methods. It is difficult to draw a conclusion on which method is the best one for the total fatigue damage based on this figure. However, it is obvious that load cases 2-1 to 2-4, which have wind speed below cut-in and small sea states, leads to low fatigue damage. Load cases 3-1 and 3-2, which have wind speed above cut-out and large sea states, leads to larger fatigue damage. Remember that wind speed above cut-out is rare, while wind speed below cut-in is more common, and they will therefore contribute differently to the total fatigue damage. Load cases 1-1 to 1-9 have increasing wind speeds and increasingly larger sea states, and these load cases therefore results in increasingly larger fatigue damages. In general, as the wind speed and sea state increase in strength and size the more fatigue damage is accumulated from the load case. This is as expected, since with larger loads there will be larger responses and therefore, more fatigue damage.

The yellow bar in the bar graph, which is the fatigue damage from the short MacCamy method, is the lowest bar in almost every load case. This shows that the short MacCamy method

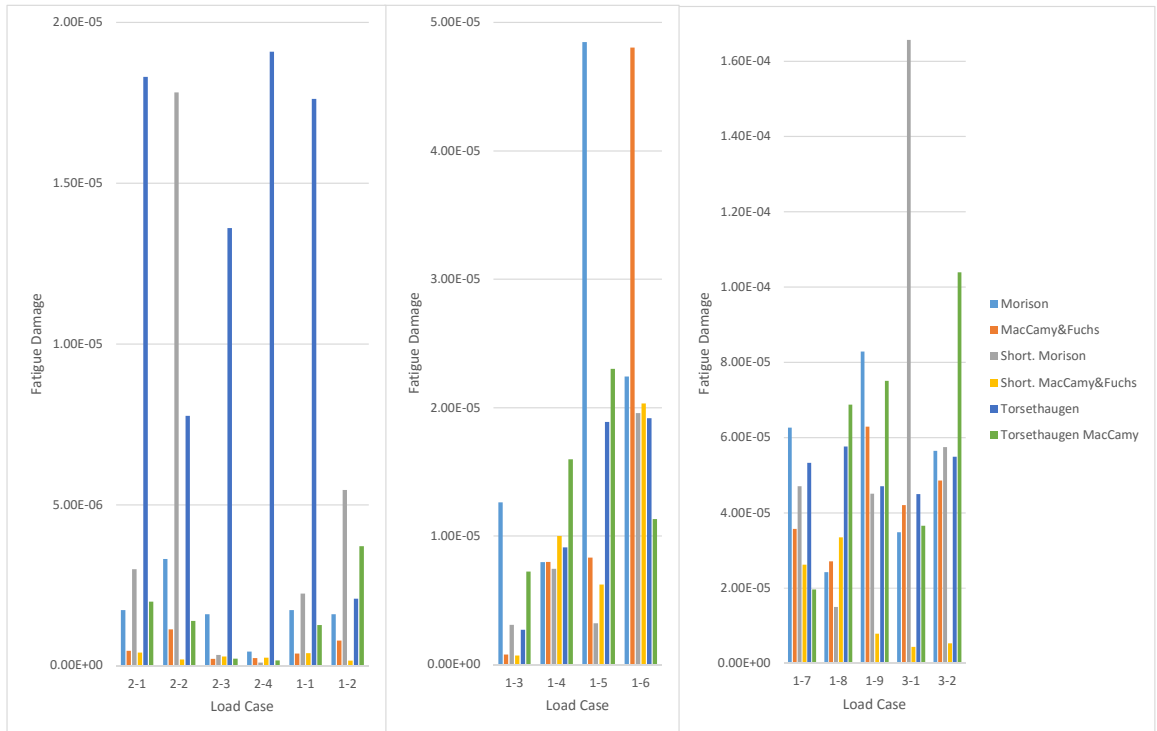


Figure 8.2: The fatigue damage from the 10 minutes simulations of each of the load case for the six methods, at the  $0^\circ$  point

probably will result in the lowest total fatigue damage.

The MacCamy method accumulates less damage than the Morison method in most load cases. This shows that according to the damage accumulated in every load case, it looks like including the effect of short wave diffraction does reduce the total fatigue damage on the structure. This short wave diffraction has the most significant effect on the accumulated damage in the small sea states, low  $T_p$ . This is as expected, since short wave diffraction is important when the waves are small compared with the structure diameter,  $\lambda \leq 5D$ . In chapter 9.2, there will be a further discussion and look into the effect short wave diffraction has on the wave load in two different sea states and at two different water depths.

In the load cases with the small peak period sea states, load cases 2-1 to 2-4 and 1-1, the

Torsethaugen method bar is significantly larger than the Morison method bar. These small sea states are where including the effect of short wave diffraction can have a large impact on the calculated wave load, and therefore fatigue damage.

In the Torsethaugen MacCamy method, the effect of the short wave diffraction is clearly seen. By including the effect of short wave diffraction the accumulated damage in the small peak period sea states have reduced significantly, compared with Torsethaugen method. A further discussion on the difference between the Torsethaugen spectrum and JONSWAP spectrum is in chapter 9.3, and this will explain why the Torsethaugen method accumulates that much more damage in the small peak period sea states, compared with the Morison method.

In the larger load cases with larger sea states, like load case 1-5, 1-6 and 3-1, there is one method that accumulates significantly more damage than the others. This is expected to be due to the wave realization applied in that load case for that method. The response spectra of the moments, in appendix C, show that these methods also have the largest spectral peak for the moment about  $y$  at the first natural frequency. The reason for these large accumulated damages is probably due to the uncertainties and randomness of the wave realizations applied.

### 30 ° point

Figure 8.4 shows a bar graph of the accumulated damage from the 10 minutes simulations of each of the load cases, for the 30 ° point. Take notice that the y-axis are of different magnitude for each individual plot. The point have been circled in figure 8.3. This point accumulates less damage from every load case and every method, than at the 0 ° point.

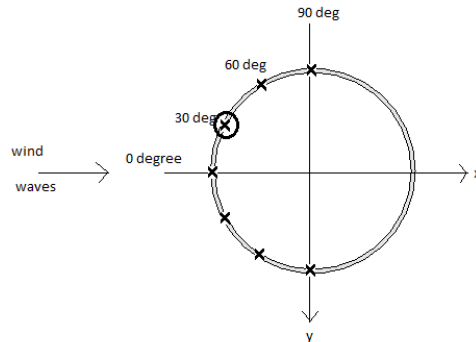


Figure 8.3: The circumference of the monopile, with the 30° point circled

Accumulated fatigue damage is dependent on the load case, the larger the wind speeds and sea states the more accumulated fatigue damage.

The short MacCamy method accumulates the least damage in almost every load case at the 30 ° point. The MacCamy method accumulates less damage than the Morison method, especially in the load cases with the smaller sea states, low  $T_p$ , and in some of the larger sea states as well. This is as expected since the short wave diffraction will reduce the calculated wave load from waves with wavelength shorter than five times the diameter of the monopile.

Torsethaugen is among the methods that accumulates the most fatigue damage, especially in the load cases with small peak period sea states. The results from the Torsethaugen MacCamy method shows that the included short wave diffraction have a significant effect on the fatigue damage in the load cases with small peak period sea states, and some effect in the load cases with larger peak period. This is the same as was observed between the Morison method and the MacCamy method.

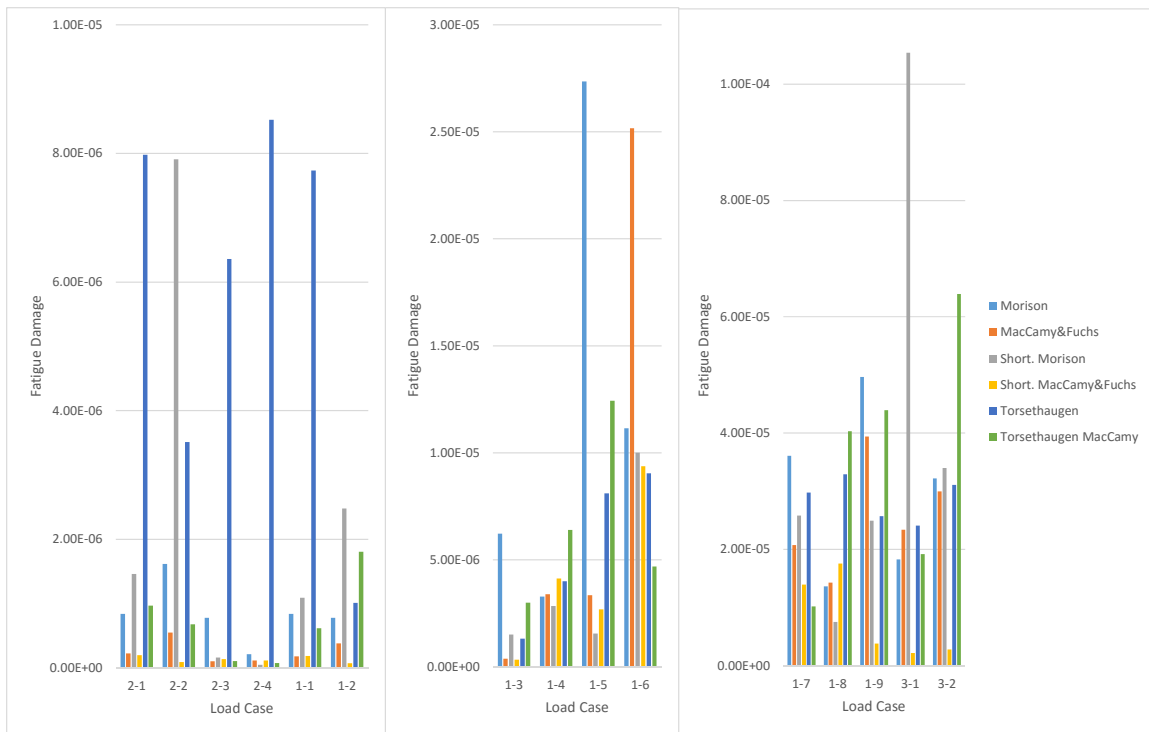


Figure 8.4: The fatigue damage from the 10 minutes simulations of each of the load case for the six methods, at the 30 ° point

**60° point**

Figure 8.6 shows a bar graph of the accumulated damage for the six methods from every load case, for the 60° point. Take notice that the y-axis are of different magnitude for each individual plot. Figure 8.5 shows this point.

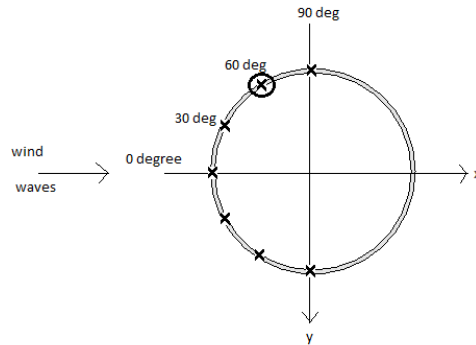


Figure 8.5: The circumference of the monopile, with the 60° point circled

The effect of the short crested waves can be viewed to some extent here. The fatigue damage accumulated for the methods that applied short crested waves have decreased less than for the other methods, compared with the fatigue damage in the previous two points, for most of the load cases. The short crested waves have increased the responding moment about x and decreased the responding moment about y, this can be seen in the response spectra of the moments shown in appendix C.

Other than that the same trends are seen for the different methods as before. As the wind and sea states increase in size and strength so does the accumulated fatigue damage. The short MacCamy method accumulates the least damage in most of the load cases. The fatigue damage for the MacCamy method is generally lower than the fatigue damage for the Morison method, especially for the small peak period sea states. The same observation is seen for the Torsethaugen MacCamy method in comparison with the Torsethaugen method.

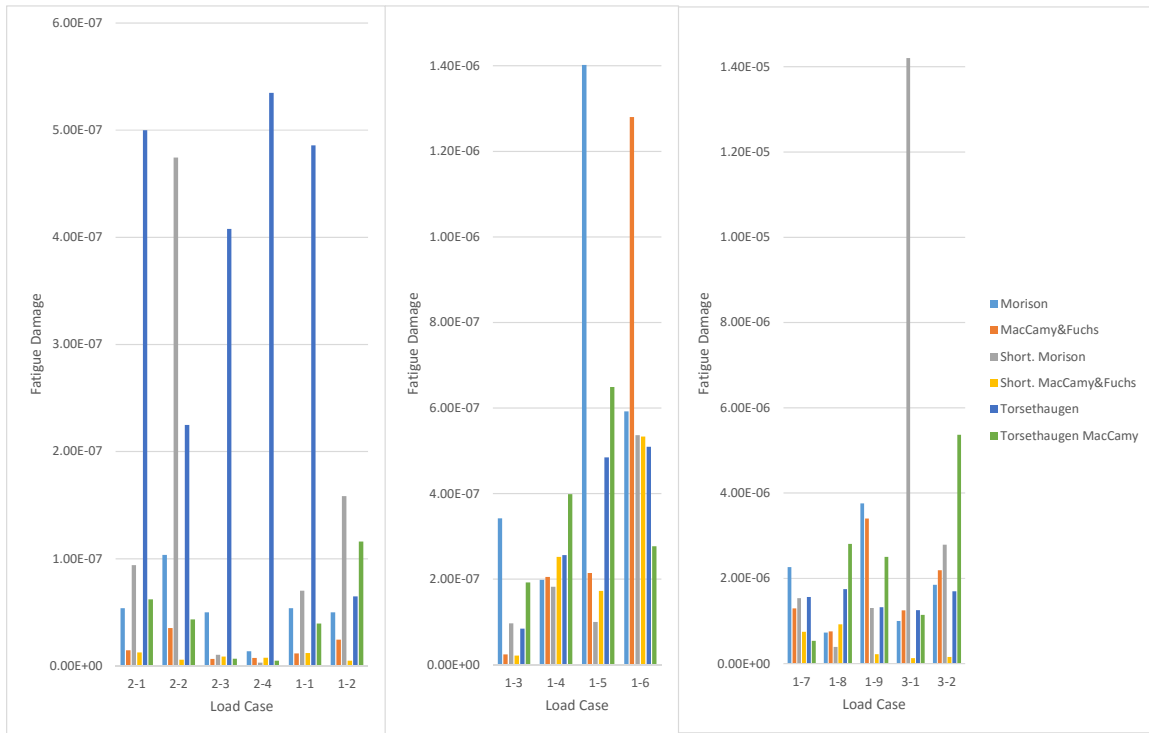


Figure 8.6: The fatigue damage from the 10 minutes simulations of each of the load case for the six methods, at the 60° point

### 90 ° point

Figure 8.8 shows a bar graph of the accumulated damage for the six methods from every load case, for the 90 ° point. In figure 8.8 take notice that the y-axis are of different magnitude for each individual plot. As stated before, the fatigue damage in this point is caused by the responding moment about x. Figure 8.7 shows this point.

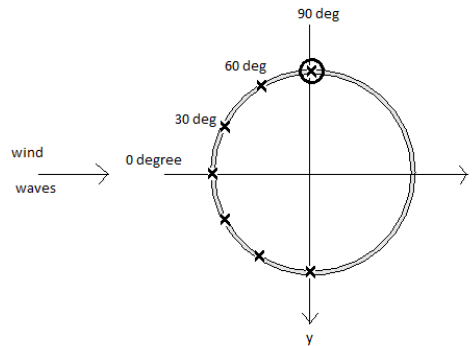


Figure 8.7: The circumference of the monopile, with the 90° point circled

The accumulated fatigue damage in this point is very small, this is due to the small responding moment about x. The responding moment about x does increase when short crested waves are applied, although it is still small. This can be observed in the response spectra of the moments in appendix C.

Here the effect of the short crested waves is seen, since the two methods that applied short crested waves accumulates the most damage in most of the load cases at this point. The difference in accumulated fatigue damage between the methods where long crested and short crested waves was applied, is the largest in the small load cases (load case 2-1 to 2-4 and 1-1 to 1-2). This means that the effect of the short crested waves is largest for the small peak period sea states. As the wind and sea state increase, the accumulated fatigue damage increase and the difference between using short or long crested waves decrease.

From the table for the total fatigue damage, the Torsethaugen MacCamy method has the largest total fatigue damage in the 90 ° point. This bar graph does not support this. It does not look like the Torsethaugen MacCamy method will result in the largest total fatigue damage. However, the fatigue damage in this point is very small, and is therefore very sensitive, and besides this, and both Torsethaugen methods, are only based on the 10 minutes simulations which



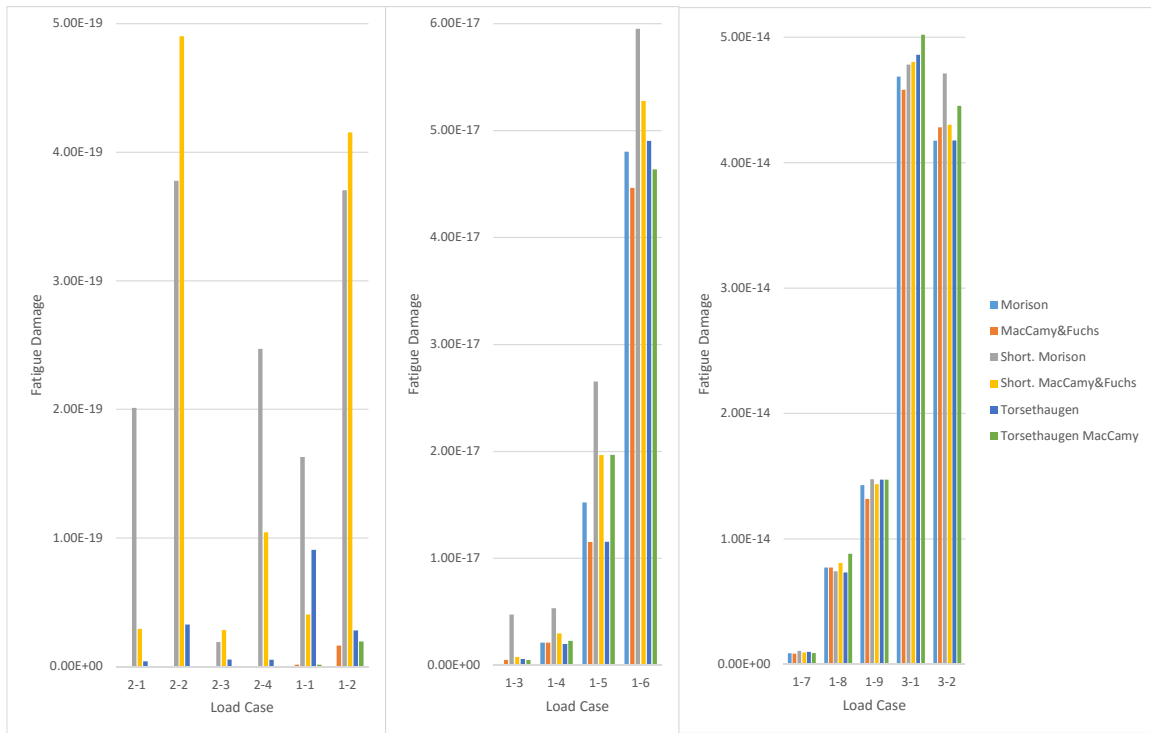


Figure 8.8: The fatigue damage from the 10 minutes simulations of each of the load case for the six methods, at the 90 ° point

means there are large uncertainties.

## 8.3 Response Spectra

The response spectra of the moments both in x- and y-direction for all six simulation methods are examined. The response spectra of both moments for each load case is presented in six graphs, one for each of the methods. The spectral values of the moment about x have been scaled up so that it may be viewed in the graphs. The natural frequency of the motion in x-direction is represented as a black vertical line at  $f=0.236\text{Hz}$ . The natural frequency of the motion in y-direction is,  $f=0.238\text{Hz}$ , which is almost equal to the natural frequency of motion in x-direction, so the one line represents them both. The response spectra for every load case is presented in appendix C, and the response spectra for load case 3-1 is presented in figure 8.9.

A summary of the trends observed from all the load cases is presented below.

### 8.3.1 Summary of Trends

To calculate the wave load according to MacCamy and Fuchs equation does usually reduce the responding moment about y, and as have been seen to apply MacCamy and Fuchs have reduced the fatigue damage in most load cases.

The response spectra of the moments increase their spectral values with increasing wind and sea states.

The highest peaks of both moment spectra are centered around the first and second natural frequency. This means that the natural frequencies, and their corresponding modes, are excited by the loading.

Usually the method that results in the highest spectral peak for the moment about y, also accumulates the most damage for the  $0^\circ$  point.

Short crested waves always increase the spectra for the moment about x, especially around the natural frequency. This means that the short crested waves excite the side-side motion more than long crested waves. The short crested waves, in most of the load cases, reduce the moment about y. This is due to the spreading of the waves for short crested waves. The spreading function decreases the energy of the waves in the main propagation direction, and increases the energy of the waves in other directions.

The Torsethaugen MacCamy method have usually decreased the moment about y, com-

pared with Torsethaugen method.

The response spectra for load case 3-1 is shown in figure 8.9.

Most of the trends listed above can be observed in figure 8.9. This response spectra was chosen because of the large accumulated damage from this load case for the short Morison method. As can be seen, the spectral values of the moment about y is significantly larger for the short Morison method than for any of the other methods.

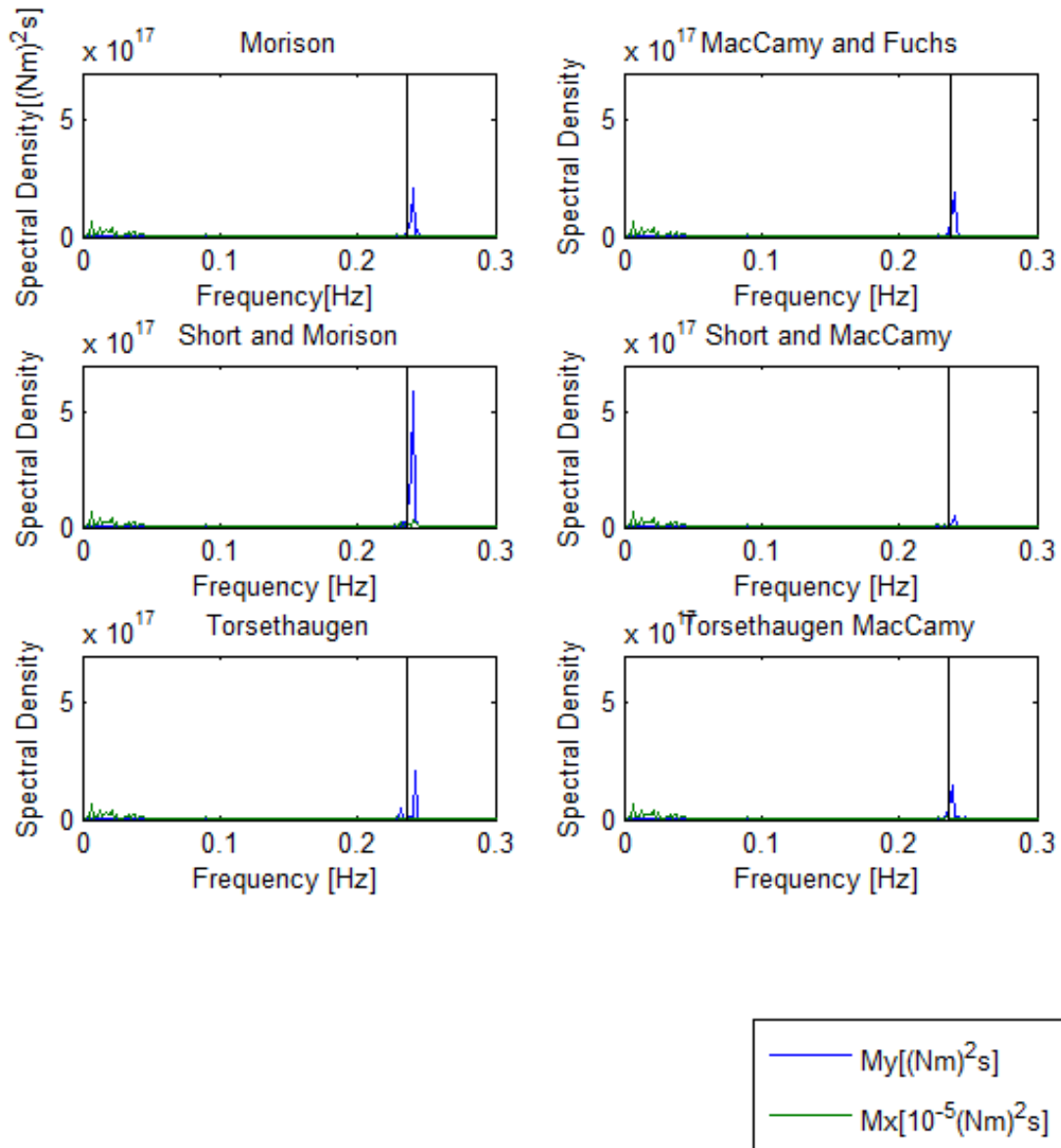


Figure 8.9: Response spectra of the moments from load case 3-1

## 8.4 Damping Sensitivity

The results from the damping sensitivity are now presented. Damping is known to be most efficient close to the natural frequency. The highest peak of the responding moments are located at the natural frequency. Therefore, even a small increase in damping is expected to give a significant reduction in fatigue damage.

The damping sensitivity study was performed on the MacCamy method. The results presented are from the 0 ° point.

Table 8.4: Fatigue damage from the damping sensitivity study for four load cases

Load Case	Fatigue Damage [10 <sup>-5</sup> ]			
	case 1 0.37%	case 2 0.96%	case 3 4.96%	case 4 0.54%
1.3	0.078	0.0147	0.0013	0.0498
1.4	0.799	0.0648	0.0030	0.3606
1.6	4.804	0.2288	0.0100	1.9132
1.7	3.573	0.6322	0.0384	2.3382

The effect of increasing the structural damping is clearly seen. With a small increase in the structural damping, the fatigue damage decreases significantly, as can be seen in table 8.4.

Case 1 is the case that has the damping level as applied for the other analysis in this thesis.

Case 2 has a structural damping of almost 1%, which is the value specified for the NREL reference turbine and in the OC3 project (Jonkman, J., Butterfield, S., Musial, W. & Scott, G. (2009) and Jonkman, J. & Musial, W. (2010)).

The results obtained in the damping sensitivity study is as expected, as the damping level is increased the fatigue damage is reduced. A small increase in the structural damping results in a large decrease of the fatigue damage.

Case 4 is the only case with mass proportional damping. According to the percentage of critical damping the fatigue damage obtained from case 4 should lie between the fatigue results obtained from case 1 and 2, and they do.

For future analysis for a real structure, a structural damping level closer to 1% should probably be applied, unless otherwise specified. Case 2 is 0.96% of critical damping for both tower and monopile, which gives a good indication of the damage achieved with 1 % damping.

## 8.5 Availability Sensitivity

This sensitivity study investigates the sensitivity of the fatigue damage to the availability of the offshore wind turbine. The fatigue analysis is performed on the non-operational situations, which includes the non-availability situations. The non-availability is the largest contribution to the non-operational situations. An increase in non-availability is expected to increase the total fatigue damage. A non-availability of 10 % was assumed for the previous work on this thesis. The results from the short MacCamy method is investigated in this availability sensitivity study. The results from this study is presented in table 8.5.

Table 8.5: Total fatigue damage from the non-availability sensitivity study

non-availability [%]	Total Fatigue Damage over 20 years						
	-90 °	-60 °	-30 °	0 °	30 °	60 °	90 °
5	4.67E-11	0.0023	0.0408	0.0860	0.0407	0.0023	4.67E-11
10	4.91E-11	0.0045	0.0780	0.1645	0.0777	0.0044	4.91E-11
15	5.16E-11	0.0066	0.1152	0.2431	0.1147	0.0066	5.16E-11

These results clearly show that the total fatigue damage is highly dependent on the non-availability of the structure. As the non-availability increases so does the total fatigue damage and vice versa. This is as expected, and are in agreement with the case study on the availability effects on fatigue damage presented in chapter 4.10.4.

# Chapter 9

## Discussion

In this chapter some aspects of the results are further discussed.

### 9.1 Total Fatigue Damage

The thesis investigated different analysis methods to see if any of the methods would reduce the total fatigue damage. The short wave diffraction is known to reduce the calculated wave loads and calculated fatigue damage. Therefore the most interesting part was to look at the effect of short crested waves and the separation of swell and wind driven sea.

The total fatigue damage from the 10 minutes simulations was presented in table 8.2. The table shows the total fatigue damage from each of the different calculation methods and in seven points along half the circumference. The total fatigue damage from the 1 hour simulations was presented in table 8.3. Based on the results presented in those two tables, the short MacCamy method results in the lowest calculated total fatigue damage. The three methods that applied MacCamy and Fuchs equation for the wave load calculation resulted in lower total fatigue damages than the three methods that calculated the wave load according to Morison's equation. Therefore it is these three methods that will be further discussed.

As seen in table 8.2 and 8.3, the different methods alters the total fatigue damage in varying degrees. The percentage change, based on the 10 minutes simulations, for the short MacCamy and the Torsethaugen MacCamy method compared with the MacCamy method, is presented in table 9.1.

Table 9.1: Percentage change for the total fatigue damage for the method compared with the MacCamy method which applied long crested waves based on JONSWAP spectrum, from the 10 minutes simulations

Calculation Method	Change for four points along circumference [%]			
	0 °	30 °	60 °	90 °
MacCamy	0.00	0.00	0.00	0.00
Short-crested MacCamy	-44.84	-50.35	-49.46	4.24
Torsethaugen MacCamy	-3.12	-6.96	-0.26	8.85

The wave load calculations have been performed according to MacCamy and Fuchs equation for all three methods in table 9.1. The effect of applying short crested waves instead of long crested waves and the effect of applying Torsethaugen instead of JONSWAP spectrum is observed.

As can be seen from this table, table 9.1, to use short crested waves have had the best effect by reducing the total fatigue damage by up to 50% compared with long crested waves. The Torsethaugen MacCamy method also reduces the calculated total fatigue damage, compared with applying JONSWAP spectrum in the MacCamy method, with up to 7%.

In the 90 ° point, both of these methods have increased the total fatigue damage compared with the MacCamy method. For the short MacCamy method this increase in the 90 ° point is due to the short crested waves, which increases the response moment about x. The Torsethaugen spectrum have been seen to increase the total fatigue damage in the 90 ° point with the wave load calculated according to MacCamy and Fuchs and according to Morison's equation. The Torsethaugen spectrum assumes that the swell and wind-driven sea is propagating in the same direction, but the separation of the swell and wind driven sea has, based on the results from the 10 minutes simulations, increased the fatigue damage in the direction perpendicular to the wave propagation.

With waves modeled as short crested waves instead of long crested, this reduces the fatigue damage in the 0, 30 and 60 ° points and increases the fatigue damage in the 90 ° points. The increase of the fatigue damage in the 90 ° point is lower than the decrease in any of the other points. As previously found in the literature review, short crested waves reduce the fatigue dam-



age on structures in deep waters, and the same result is observed here for shallower waters. Based on the literature review, if more short crested waves were applied this might further reduce the calculated total fatigue damage. The degree of short crested waves will depend on the site. This means that the effect of increasing or decreasing the short crestedness of the waves should be investigated to observe the effect it has on the total fatigue damage.

The results from both the 10 minutes and the 1 hour simulations, shows that the hypothesis that short crested waves would reduce the fatigue damage for offshore wind turbines, like it have done for structures in deeper waters before, is valid. Since this conclusion is based on results from both the 10 minutes and the 1 hour simulations, the statistical confidence in the results is assumed to be acceptable. Even though, analysis with different wave realizations should be run to increase the confidence in the results.

As seen above to apply Torsethaugen spectrum and calculating the wave load according to MacCamy and Fuchs reduces the calculated total fatigue damage, compared with the MacCamy method, which applied JONSWAP spectrum. However, the Torsethaugen only reduces the calculated total fatigue damage when the effect of short waves diffraction is included as well. The reason for this, is explained by observing the differences in the two spectra in chapter 9.3.

Based on the results obtained from the 10 minutes simulations, the Torsethaugen MacCamy method, which separated the swell and wind driven sea, while calculating the wave load according to MacCamy and Fuchs, did reduce the calculated total fatigue damage, when compared to when the total sea was considered, the MacCamy method. This means that the hypothesis that separating swell and wind driven sea will reduce the calculated total fatigue damage seems valid, with the small modification that the effect of short wave diffraction has to be included. However, the confidence level in these results are low, since it is only based on the 10 minutes simulations, so to ascertain a higher confidence level in the validity of the hypothesis, more simulations should be run, preferably 1 hour simulations. The more wave realizations run, the greater the confidence in the results and less uncertainty connected with the results.

## 9.2 Morison's Force versus MacCamy and Fuchs Force

The wave forces on the monopile, both according to Morison's equation and according to MacCamy and Fuchs, were calculated with MATLAB. Figures are here presented to show that by calculating the wave load according to MacCamy and Fuchs equation, the inertia wave force is reduced, and that the short wave diffraction has largest effect on the sea states with small peak period and close to the surface. The inertia wave force is reduced because MacCamy and Fuchs includes the effect of short wave diffraction. The short wave diffraction has a significantly greater impact close to the sea surface, and in short waves compared with the monopile diameter. Figures 9.1 and 9.3 show graphs of the inertia wave force at the sea surface calculated according to Morison's, and MacCamy and Fuchs equation from two different sea states, while figure 9.2 and 9.4 are from 10 meters below the sea surface. These graphs are shown to observe the effect of short wave diffraction for different sea states and at different depths.

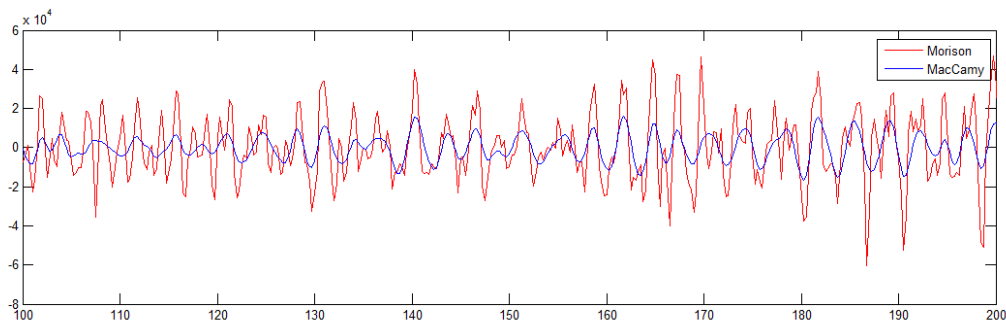


Figure 9.1: Graph comparing the wave load calculated at  $z=0$  according to Morison inertia force and MacCamy & Fuchs, for  $H_s=0.5\text{m}$ , and  $T_p=4\text{s}$

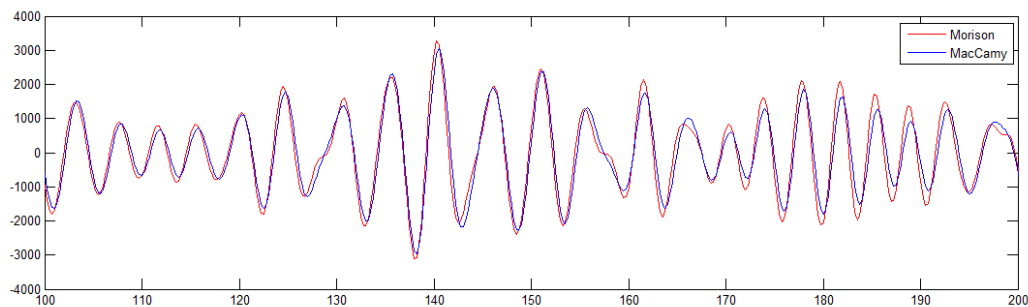


Figure 9.2: Graph comparing the wave load calculated at  $z=-10$  according to Morison inertia force and MacCamy & Fuchs, for  $H_s=0.5\text{m}$ , and  $T_p=4\text{s}$

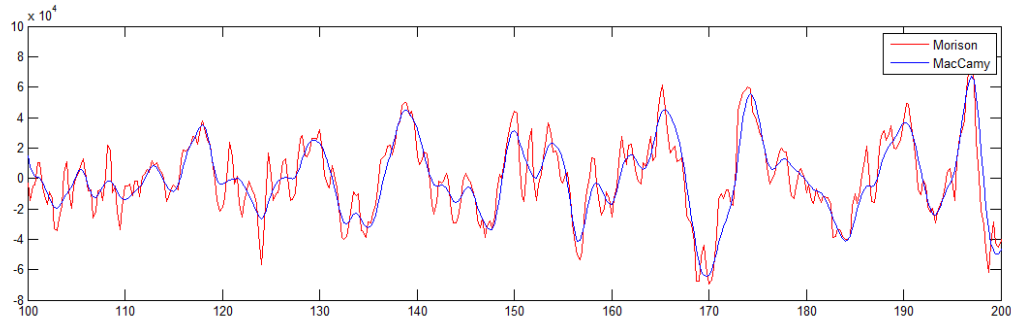


Figure 9.3: Graph comparing the wave load calculated at  $z=0$  according to Morison's inertia force and MacCamy & Fuchs, for  $H_s=6\text{m}$ , and  $T_p=17\text{s}$

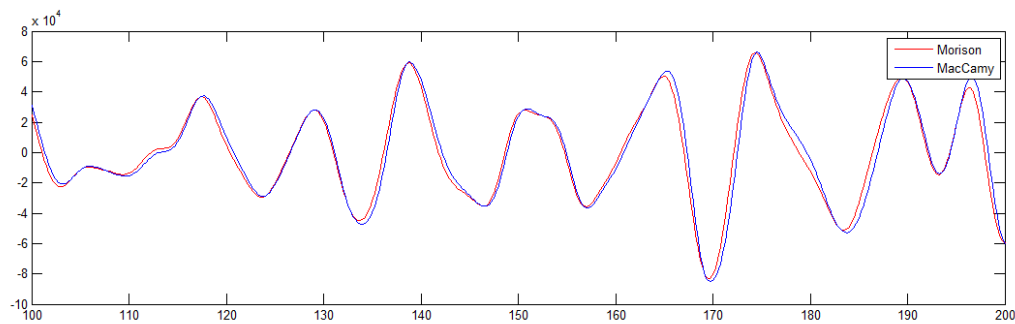


Figure 9.4: Graph comparing the wave load calculated at  $z=10$  according to Morison's inertia force and MacCamy & Fuchs, for  $H_s=6\text{m}$  and  $T_p=17\text{s}$

The first two figures show the inertia wave load from a sea state with a significant wave height of 0.5 meters and a peak period of 4 seconds, while the other two show the wave load in a sea state with significant wave height of 6 meters and a peak period of 17 seconds. The effect of diffraction is greatest for the sea state with low  $T_p$ , and it is greatest close to the surface for both sea states. This is as expected.

Short wave diffraction becomes important when the waves are short compared to the cylinder diameter, therefore the effect of short wave diffraction is significantly greater in the sea state with  $T_p=4$  seconds than in the sea state with  $T_p=17$  seconds.

A method of determining whether short wave diffraction will be important is by looking back at figure 4.6, which showed the classification of wave forces. The figure showed that short wave diffraction is important when  $\frac{\lambda}{D} \leq 5$ . This limit needs to be checked for the waves striking the monopile, to see whether short wave diffraction is important for that wave. This limit check will be performed now to confirm that diffraction is more important for the sea state with small  $T_p$

than for the sea state with large  $T_p$ . Since the sea state is known the check will only be performed for the peak wavelength, and not for every wave length present in the sea state.

If the wind turbine was located in deep water, an approximation can be made for the wavelength,  $\lambda$ , which is  $\lambda = \frac{gT^2}{2\pi}$ . Deep water will now be assumed, so that a quick look at the peak wavelength for the sea states are possible to observe. The diameter of the monopile is 6 meters. The sea states considered here have a  $T_p=4$  seconds and a  $T_p=17$  seconds. For  $T_p=4$  seconds the ratio becomes  $\frac{\lambda_p}{D} = 4.2$  which is smaller than 5. This supports the claim that short wave diffraction will be important for the monopile in this sea state, and MacCamy and Fuchs equation needs to be applied when accurate load predictions are desired. For  $T_p=17$  seconds the ratio becomes  $\frac{\lambda}{D} = 75.2$ . This is larger than five and short wave diffraction is not very important. This is seen in the graphs of the calculated wave loads. However, this is only a consideration of the peak period and there will be waves present in the sea state with lower and higher periods. The slightly reduced wave load according to MacCamy and Fuchs seen in figure 9.3 is due to the short wave diffraction of the short wave components present in that sea state. This consideration of the peak wave length have confirmed that short wave diffraction is more important for the sea state with low  $T_p$  than in the sea state with large  $T_p$ , as seen in the aforementioned graphs.

Now to investigate the depth variation of the wave load. As the  $z$  value decreases, moving down below the sea surface, the difference between the wave load calculated with Morison's and with MacCamy and Fuchs equation decreases, as can be seen in figures 9.2 and 9.4 in comparison with 9.1 and 9.3. The effect of short wave diffraction is looked into to explain this.

Including short wave diffraction will cause the greatest difference between the two load calculations when the waves are short, meaning the wave frequency,  $\omega$ , is high. High  $\omega$  means a large fluid acceleration, and this acceleration decreases with depth. As the acceleration decreases with depth, so does the effect of short wave diffraction. This causes the difference between the wave load calculated according to Morison's and MacCamy and Fuchs equation to decrease with depth, and therefore the effect of short wave diffraction is most important close to the surface where the fluid acceleration has its maximum.

However, even though short wave diffraction will not be important for every sea state, short wave diffraction will be important for some of them. By performing the wave load calculation

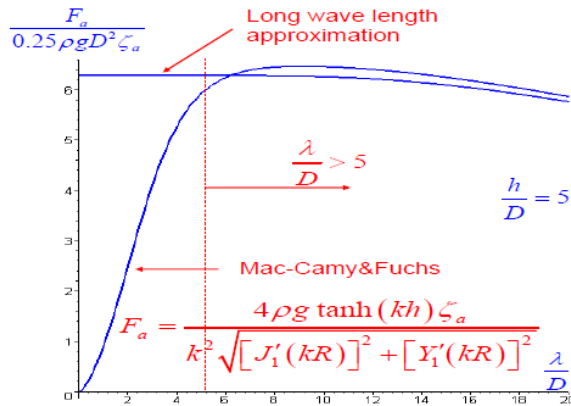


Figure 9.5: Figure showing that the asymptotic value of MacCamy and Fuchs wave load is equal to the wave load according to Morison's with  $C_M = 2$  (Greco, M. (2014))

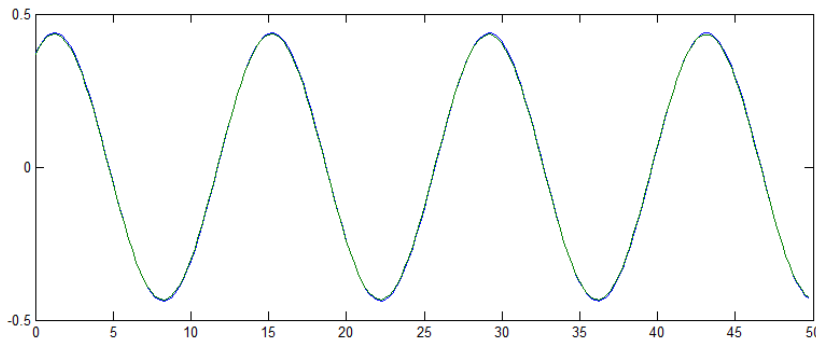


Figure 9.6: Figure showing the wave load of a long wave according to both Morison's and Mac-Camy and Fuchs equation

according to MacCamy and Fuchs for every sea state, the wave load is significantly reduced for sea states with low  $T_p$ , and slightly reduced in the sea states with larger  $T_p$ , due to, as stated, the low period waves present in the sea state. As can be seen on figure 9.5, the wave load calculated according to MacCamy and Fuchs equation will become equal to the wave load calculated according to Morison's equation with  $C_M = 2$  for a long wave. Figure 9.6 shows the wave load calculated according to MacCamy and Fuchs and according to Morison's equation for a long wave, as seen these are equal. This means that when the wave load is calculated according to MacCamy and Fuchs in the larger sea states the calculated wave load approaches the value of the wave load calculated according to Morison's equation, as seen in figure 9.3. Based on this MacCamy and Fuchs equation should be used to calculate the wave load on the monopile in every sea state.

### 9.3 JONSWAP versus Torsethaugen Spectrum

The JONSWAP spectrum describes the total sea for a developing sea state with limited fetch. A real sea state consists of both swell and wind driven sea, often propagating in different directions. The Torsethaugen spectrum is a two-peaked spectrum, which combines the swell and wind driven spectra into one wave spectrum. It assumes that the swell and wind driven sea is propagating in the same direction. This means that Torsethaugen is a conservative way of separating the swell and wind driven sea. The Torsethaugen spectrum distributes the wave energy in the sea state over more periods than the JONSWAP spectrum.

To apply Torsethaugen spectrum alone did not reduce the total fatigue damage on the structure. To explain this the Torsethaugen wave spectra is plotted along with the JONSWAP spectra for four of the load cases, in figure 9.7.

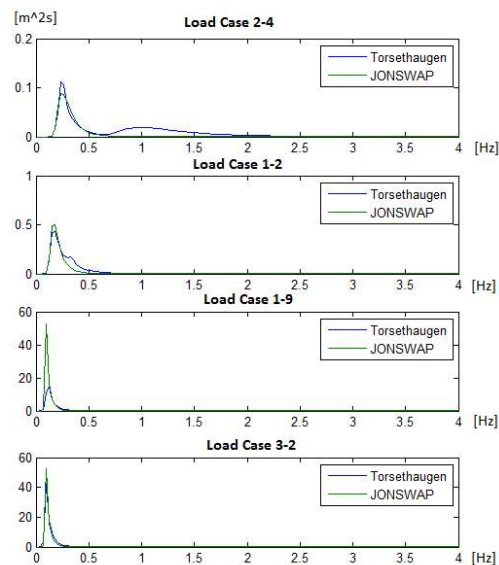


Figure 9.7: Graph comparing the wave spectra defined by Torsethaugen and JONSWAP for four sea states, frequency along x-axis

In figure 9.7, for load case 2-4, the Torsethaugen spectrum clearly contains more wave energy, since the area below the graph is larger for Torsethaugen than for JONSWAP spectrum. Torsethaugen spectrum contains more of the high frequency waves.

When the wave load is calculated according to Morison's equation, the Torsethaugen method accumulates significantly more damage than the Morison method, which applied JONSWAP spectrum. This can be explained by the differences in the wave spectra. Torsethaugen spectrum contains significantly more wave energy in the sea state, than JONSWAP spectrum, which leads to larger calculated wave loads and therefore more fatigue damage when the sea state is based on Torsethaugen instead of JONSWAP spectrum.

MacCamy and Fuchs equation for the wave load includes the effect of diffraction from waves with wavelength shorter than five times the diameter of the monopile, this means high frequency waves. The wave load from the Torsethaugen spectrum calculated according to MacCamy and Fuchs compared with Morison's, is expected to be significantly reduced. This is due to the effect of short wave diffraction.

The wave load calculated according to MacCamy and Fuchs equation based on the Torsethaugen spectrum compared with the JONSWAP spectrum, might be reduced as well, due to the effect of short wave diffraction of the high frequency waves in the Torsethaugen spectrum.

Load case 1-2, in figure 9.7, shows that the Torsethaugen spectrum has lower spectral values than the JONSWAP spectrum at the peak for JONSWAP, but larger spectral values at the higher frequencies. The Torsethaugen spectrum contains more wave energy than the JONSWAP spectrum in this sea state as well.

Morison's equation will calculate a higher wave load based on the Torsethaugen spectrum than based on the JONSWAP spectrum. The Torsethaugen spectrum with wave load according to Morison's equation accumulates more fatigue damage compared with JONSWAP spectrum with wave load according to Morison's.

The MacCamy and Fuchs equation reduces the calculated wave load for both spectra. However, the Torsethaugen spectrum have more energy in the higher frequency waves than JONSWAP spectrum, therefore the effect of applying MacCamy and Fuchs equation for the wave load calculations in this sea state, will be greater for Torsethaugen spectrum than for JONSWAP spectrum. The Torsethaugen spectrum with wave load according to MacCamy and Fuchs equation accumulates less damage in this sea state compared with the JONSWAP spectrum with wave load according to MacCamy and Fuchs equation.

The sea state in load case 1-9 and 3-2 is the same according to the JONSWAP spectrum,

$H_s=6$  meters and  $T_p=10$  seconds, but as can be seen on figure 9.7, not the same according to the Torsethaugen spectrum. The Torsethaugen spectra is smaller than the JONSWAP spectrum in both load cases. This means that the JONSWAP spectrum contains more energy than either of the two Torsethaugen spectra. The Torsethaugen spectrum for load case 1-9 is significantly smaller, and therefore contains less energy, than the Torsethaugen spectrum for load case 3-2. The reason why the two Torsethaugen wave spectra are different is because of the composition of wind and swell sea in the sea states. Load case 3-2 is exposed to a greater wind speed than load case 1-9 and therefore load case 3-2 has a larger wind driven sea. The swell sea is equal for the two load cases.

The differences in the wave frequencies represented in the Torsethaugen spectrum compared with the JONSWAP spectrum for these two load cases are not as distinct as they were for the other two load cases.

The accumulated damage, when the wave load is calculated according to Morison's equation, is larger with the JONSWAP spectrum than Torsethaugen spectrum in both load cases. The accumulated damage from Torsethaugen spectrum with wave load according to Morison's equation is less for load case 1-9 than for load case 3-2, this is as expected since the Torsethaugen wave spectra contains less wave energy for load case 1-9 than for 3-2.

To apply MacCamy and Fuchs equation along with Torsethaugen spectrum in these two load cases does not appear, based on the wave spectra, to reduce the wave load more than it does for when JONSWAP spectrum was applied for load cases 1-9 and 3-2. In both load cases, the accumulated damage from the Torsethaugen spectrum with wave load according to MacCamy and Fuchs equation is larger compared with JONSWAP spectrum with wave load according to MacCamy and Fuchs.

Based on the discussion here, calculating the wave load according to MacCamy and Fuchs equation reduces the wave load and fatigue damage more when the sea state is based on Torsethaugen spectrum than based on JONSWAP spectrum, for the sea states with small  $T_p$ . The total fatigue damage for Torsethaugen spectrum with wave load according to MacCamy and Fuchs was smaller compared with when JONSWAP spectrum was applied with wave load according to MacCamy and Fuchs.

As stated, the Torsethaugen spectrum is a conservative way of separating the swell and wind



driven sea, therefore other methods of separating the swell and wind driven sea should be investigated for further analysis.

## 9.4 The Natural Periods Effect on the Fatigue

As seen in figure 8.9, or in figures C.1 to C.15 in appendix C, the first and second natural frequencies are excited in every load case. This means that the fatigue damage is highly dependent on the natural frequency and the damping level of the structure. If the natural frequency was modified to a larger value, this would reduce the excitation of the natural frequency because less waves would have the same frequency.

The natural frequency of the structure is very close to the peak frequency of the small sea states, low  $T_p$ , but as the sea state increase the peak frequency of the waves is reduced, and the difference between the peak frequency and the natural frequency increases. This means that as the sea state increase, the natural frequency will be equal to a wave frequency further towards the tail of the spectrum.

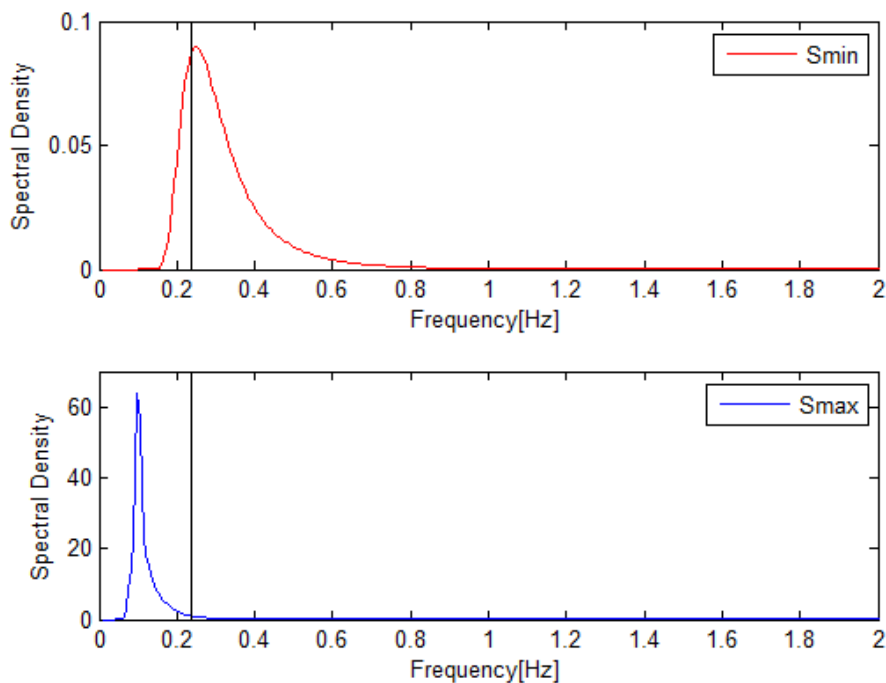


Figure 9.8: Graph of the spectrum of the smallest sea state and of the largest sea state, with the first natural frequency

Figure 9.8 is presented to show this. The top graph is from a small sea state, and the bottom graph is from a larger sea state. The spectral values are directly related to the wave energy. As can be seen on the figure, the smallest sea state has low spectral values, which means the area under the curve is small and therefore low energy content. The larger sea state has significantly larger spectral values, which results in a larger area and significantly higher energy content in the sea state and in the individual wave components. This means that the spectral value of the wave component with wave frequency equal to the natural frequency is different for the two sea states. The smallest sea state has a spectral value at the first natural frequency of approximately  $0.09 \text{ m}^2\text{s}$ , and for the largest sea state of approximately  $1 \text{ m}^2\text{s}$ , which means that the energy in the wave component with this frequency have increased between the smallest and largest sea state, even though it is further towards the tail of the spectrum in the large sea state. All of this along with figure 9.8 shows that a large natural frequency is aimed for, to avoid the high energy wave frequencies. However, it is important to know that 1P and 3P also needs to be avoided for an operational offshore wind turbine.

## 9.5 Statistical Confidence of the Results

The wave and wind data are stochastic variables. Seed numbers are used to obtain different realizations of the data. If the same seed number is used, the same realization is obtained, as long as all the other input parameters are the same.

The uncertainty associated with the result is directly related to the number of seeds and the length of the simulation. This is because with longer simulations and with more seeds, the results are based on more data. A smaller number of seeds are needed for the 1 hour simulation than the 10 minutes simulation to obtain the same level of confidence in the results. The 10 minutes simulation is more sensitive to the selection of seed number than the 1 hour simulation. It is because of the statistical confidence, the sensitivity to chosen seed and the need for less seeds, that makes the 1 hour simulations preferable to the 10 minutes simulations for the analysis.

The simulations, both the 10 minutes and the 1 hour simulations, were run for one seed number per load case and analysis method in this thesis. The statistical confidence connected

with the results are greater for the 1 hour simulations, because of the simulation length. The results and conclusions based on both the 10 minutes and the 1 hour simulations is assumed to have an acceptable level of confidence, because of the 1 hour simulations. The results based only on the 10 minutes simulations have large uncertainties connected with it. To increase the statistical confidence of the results, the load cases should be run for multiple seed numbers, preferably the 1 hour simulations. However, due to limited time this was not done.

A fatigue analysis is less sensitive to seed numbers than an ULS analysis. A fatigue analysis have usually reached an acceptable level of confidence after a few 1 hour simulations while the ULS will need more seeds to reach the same level of confidence.

The statistical confidence and the uncertainties connected with the results influences the conclusion of the thesis. When the results have low confidence it is difficult to draw a conclusion. However, the results based on both the 1 hour and the 10 minutes simulations have an acceptable confidence in the results, and a conclusion can be drawn. The results only based on the 10 minutes simulations at least gives an indication for a conclusion.

# Chapter 10

## Conclusion

The total fatigue damage over the design life of 20 years was calculated, as well as the fatigue damage accumulated in every load case, for six analysis methods.

The wave load calculated according to MacCamy and Fuchs equation was lower than the wave load calculated according to Morison's equation. The reduction was most significant close to the sea surface and for the sea states with low peak period. This was as expected, and is because MacCamy and Fuchs equation for the wave load includes the effect of diffraction of waves with wavelength less than five times the diameter of the monopile, as opposed to Morison's equation.

The calculated total fatigue damage over the design life was reduced when the wave load was calculated according to MacCamy and Fuchs compared with according to Morison's equation. This observation is based on both 10 minutes and 1 hour simulations. This gives acceptable confidence in the results and conclusion. MacCamy and Fuchs equation should be used to calculate the wave loads on a large diameter offshore wind turbine with monopile foundation.

The effect on the total fatigue damage of modeling the waves as short crested or long crested waves was investigated. Based on the previous conclusion, there have been a larger focus on the results from when the wave load was calculated according to MacCamy and Fuchs equation. The short crested waves reduced the calculated fatigue damage compared with long crested waves, with both equations for calculation of the wave load. The reduction of the calculated total fatigue damage due to the change from long crested to short crested waves, was greater when the wave load was calculated according to MacCamy and Fuchs equation instead of Morison's

equation. The method that applied short crested waves with wave load according to MacCamy and Fuchs, resulted in the lowest calculated total fatigue damage. The results from when the wave load was calculated according to MacCamy and Fuchs is based on both the 10 minutes and 1 hour simulations. This means that the confidence in the results is acceptable. The results implies that the hypothesis that short crested waves will reduce the calculated total fatigue damage on a large diameter offshore wind turbine with monopile foundation, is valid.

The effect of separating the swell and wind driven sea on the calculated total fatigue damage was then investigated. Torsethaugen spectrum was used to model the separated swell and wind driven sea. With the wave load calculated according to Morison's equation, the calculated total fatigue damage was increased when the waves was based on Torsethaugen compared with JONSWAP spectrum. When the wave load was calculated according to MacCamy and Fuchs, the calculated total fatigue damage was reduced when the waves was based on Torsethaugen compared with JONSWAP spectrum. The results here are only based on 10 minute simulations, which means the confidence in the results is low. However, the results observed here indicates that the hypothesis, that the total fatigue damage is reduced when the swell and wind driven sea is separated, is valid. More simulations, preferably 1 hour, should be run to ascertain a higher confidence.

The goal of the thesis was to reduce the calculated total fatigue damage by performing more accurate wave load calculation and by modeling the sea more accurately. To calculate the wave load according to MacCamy and Fuchs, instead of Morison's equation, will yield more realistic estimation of the wave loads, as expected. For a moderate sea state, as present for fatigue analysis for offshore wind turbines, short crested waves are a more accurate way of modeling the sea state than long crested waves. The results showed that the short crested waves did reduce the total fatigue damage. In a moderate sea state, the swell and wind driven sea is separated, so to model them as such is more accurate than to model the total sea. However, Torsethaugen is a conservative method of modeling the separated swell and wind driven sea. The results showed that by applying Torsethaugen instead of JONSWAP, while doing wave load calculation according to MacCamy and Fuchs, the calculated total fatigue damage was reduced. However, not by as much as when short crested waves was applied. The goal of the thesis have been reached, because the calculated total fatigue damage was reduced by performing more accurate wave

load calculations and more accurate modeling of the sea state. The analysis recommended for use based on this thesis, is to use short crested waves with wave load calculation according to MacCamy and Fuchs equation.

The damping sensitivity study showed that the calculated fatigue damage is highly dependent on the damping level. As the damping level is increased the calculated total fatigue damage is reduced. The availability sensitivity study showed that the calculated total fatigue damage is increased when the availability of the wind turbine was decreased.

# Chapter 11

## Further Work

Here are some suggestions for further work presented.

First of all the statistical confidence in the results should be improved. This may be done by running more simulations of the different analysis methods with multiple different seeds for both the wind and waves. These simulations should preferably be run as 1 hour simulations. The results will then achieve the confidence level aimed for with fewer seeds.

Simulations with different parameters used to describe the short crested waves should be run. This is to investigate different effects different parameters for the short crested waves may have on the calculated total fatigue damage.

A suggestion for a new analysis method to be run for simulations, is to model the sea state as short crested waves based on Torsethaugen spectrum with the wave load calculated according to MacCamy and Fuchs equation. This should result in the lowest calculated fatigue damage out of all the methods tested here.

The separated swell and wind driven sea may be modeled in a different way than with Torsethaugen spectrum. Simulations should be run for this as well. This new method of modeling the separated swell and wind driven sea should include that the swell and wind driven sea may propagate in different directions.

The offshore wind industry calculates the wave load according to Morison's equation with a diffraction corrected mass coefficient. Simulations should be run with this, and the results be compared with the results from when the wave load is calculated according to MacCamy and Fuchs equation. This is to investigate if the offshore wind industry is conservative with the wave

load model used.

An investigation of the damping present from the wind while in non-operation is also possible to perform. The damping may be investigated with decay tests. The decay tests are run for one load case with the wind present and without, the damping contribution from the wind can then be found.



# Bibliography

Arshad, M. & O’Kelly, B.C. (2016). Analysis and design of monopile foundations for offshore wind-turbine structures. *Marine Georesources & Geotechnology*, 34(6):503–525.

Boehn, A. (2015). Fatigue loads on large diameter offshore wind monopile foundations in confused seas.

Carswell, W., Johansson, J., Løvholt, E., Arwade, S.R., Madshus, C., DeGroot, D.J. & Myers, A.T. (2015). Foundation damping and the dynamics of offshore wind turbine monopiles. *Renewable Energy*, 80:724–736.

Corbetta, G. & Mbistrova, A. (2014). The european offshore wind industry-key trends and statistics 2014. 2015. Fuente: <http://www.ewea.org/fileadmin/files/library/publications/statistics/EWEA-European-Offshore-Statistics-2014.pdf>.

DNV GL (2007). Environmental conditions and environmental loads. No. DNV-RP-C205.

DNV GL (2010). Fatigue design of offshore steel structures. No. DNV-RP-C203.

DNV GL (2014). Design of offshore wind turbine structures. No. DNV-OS-J101.

Eliassen, L. (2016). Conversation with lene eliassen.

Eurocode (2001). Eurocode - basis of structural design.

Faltinsen, O.M. (1990). *Sea Loads on Ships and Offshore Structures*. Cambridge University Press.

- Fichaux, N., Beurskens, J., Jensen, P.H., Wilkes, J., Frandsen, S., Sorensen, J.D. & Eecen, P. (2011). Upwind: Design limits and solutions for very large wind turbines. *Sixth Framework Programme*.
- Fischer, T. & Kühn, M. (2010). Importance and mitigation of loading on offshore wind turbines on monopiles support structures in cases of non-availability. In *The Twentieth International Offshore and Polar Engineering Conference*. International Society of Offshore and Polar Engineers.
- Fischer, T., Vries, W., Rainey, P., Schmidt, B., Argyriadis, K. & Kühn, M. (2012). Offshore support structure optimization by means of integrated design and controls. *Wind Energy*, 15(1):99–117.
- Gao, Z. (2015). Lecture - introduction to offshore wind power and technology.
- Greco, M. (2014). *Sealloads - Lecture Notes*.
- Hansen, M. O. L. (2008). *Aerodynamics of Wind Turbines*. Earthscan, 2. edition.
- Haver, S. (2016). Lecture material - ocean structures.
- Horn, J.T.H. (2015). Stochastic dynamic analysis of offshore bottom-fixed structures.
- Jonkman, J. & Musial, W. (2010). Offshore code comparison collaboration (oc3) for IEA task 23 offshore wind technology and deployment. *Contract*, 303:275–3000.
- Jonkman, J., Butterfield, S., Musial, W. & Scott, G. (2009). Definition of a 5-mw reference wind turbine for offshore system development - nrel.
- Kühn, M. (2001). Dynamics and design optimisation of offshore wind energy conversion systems.
- Krokstad, J. R. (2014). Requirements for performing optimised design of a large offshore wind turbine with tower and supporting foundation as an integrated unit - 4th annual future offshore wind foundations statkraft final.

- Krokstad, J. R. (2015). Relative contribution from wind and waves to loads on offshore wind turbines - with focus on support structures.
- Krokstad, J. R. (2016). Conversation with jørgen krokstad.
- Langen, I. & Sigbjørnsson, R. (1979). *Dynamic Analysis of Structures*. Tapir.
- Leira, B.J. & Olufsen, A. (1987). Short-crested sea and riser estimation. In *Offshore Technology Conference*. Offshore Technology Conference, Offshore Technology Conference.
- MacCamy, R.C. & Fuchs, R.A. (1954). Wave forces on piles: a diffraction theory. Technical report, DTIC Document.
- Myrhaug, D. & Lian, W. (2014). *TMR4182 - Marine Dynamics, Irregular Waves*. Kompendieforlaget, Akademika forlag.
- Neelamani, S., Sundar, V. & Vendhan, C.P. (1989). Dynamic pressure distribution on a cylinder due to wave diffraction. *Ocean engineering*, 16(4):343–353.
- Newland, D.E. (1993). *An introduction to random vibrations, spectral and wavelet analysis*. Longman Scientific and Technical, 3. edition edition.
- Salzmann, D. & Van der Tempel, J. (2005). Aerodynamic damping in the design of support structures for offshore wind turbines. In *Paper of the Copenhagen offshore conference*. Citeseer.
- Sarkar, A. (2013). Design basis for offshore wind turbines for shallow and deep water.
- Schløer, S. (2014). *Fatigue and Extreme Wave Loads on Bottom Fixed Offshore Wind Turbines: Effects from Fully Nonlinear Wave Forcing on the Structural Dynamics*. DTU Vindenergi.
- Semedo, A., Sušelj, K., Rutgersson, A. & Sterl, A. (2011). A global view on the wind sea and swell climate and variability from era-40. *Journal of Climate*, 24(5):1461–1479.
- Tavner, P. (2012). Offshore wind turbine reliability.
- Trøen, T. L. (2014). Fatigue loads on large diameter monopile foundations of offshore wind turbines.

- Van Bussel, G.J.W. & Zaayer, M.B. (2001). Reliability, availability and maintenance aspects of large-scale offshore wind farms, a concepts study. In *MAREC 2011: Proceedings of the 2-day International Conference on Marine Renewable Energies, Newcastle, UK, 27-28 March 2001*. Institute of marine engineers.
- Van Der Meulen, M. B., Ashuri, T., Van Bussel, G. J.W. & Molenaar, D. P. (2012). Influence of nonlinear irregular waves on the fatigue loads of an offshore wind turbine. In *The Science of Making Torque from Wind; 4th scientific conference, Oldenburg (Germany), 9-12 Oct, 2012*.
- Van der Tempel, J. (2006). *Design of Support Structures for Offshore Wind Turbines*. TU Delft, Delft University of Technology.
- Veldkamp, HF & Van Der Tempel, J. (2005). Influence of wave modelling on the prediction of fatigue for offshore wind turbines. *Wind Energy*, 8(1):49–65.
- Zhu, S. (1993). Diffraction of short-crested waves around a circular cylinder. *Ocean Engineering*, 20(4):389–407.
- Zhu, S. & Moule, G. (1994). Numerical calculation of forces induced by short-crested waves on a vertical cylinder of arbitrary cross-section. *Ocean Engineering*, 21(7):645–662.

# Appendix A

## Appendix A - MATLAB CODE

A description of the MATLAB codes will be presented here. The MATLAB codes have been handed in as a electronic zip-file.

### A.1 head.m

This is the head file for the wave load calculation. This script calls on all the functions to calculate the wave load according to MacCamy and Fuchs equation, and writes the resulting wave loads into one file for each sea state.

The inertia force and the drag force is calculated in this script, after the velocity and acceleration of the wave have been calculated.

#### A.1.1 spekter.m

This function is called upon by the head file. It calculates the JONSWAP wave spectrum. The  $H_s$  and  $T_p$  values have been read in the head file and taken into the spekter function. The JONSWAP spectrum is calculated according to DNV GL.

#### A.1.2 kinematics1.m

This function calculates the wave amplitude, along with the random phase from the wave spectrum.

### **A.1.3 kinematics.m**

This function calculates the kinematics of the waves from the spectrum. The velocity and acceleration of the wave is calculated from the still water surface and down to the sea bottom.

### **A.1.4 McF.m**

This function calculates the wave load according to MacCamy and Fuchs. The Bessel functions are applied here.

### **A.1.5 tot\_F.m**

The total wave load is calculated in this function. The wave load at specific z-values are calculated, because that is what is needed as input to FEDEM. The wave load at specific z-values have been integrated so that, when added, the total wave load is obtained.

## **A.2 head\_postproc2.m**

This is the head file for the post-processing of the results from the simulations.

The WAFO Toolbox is applied in these calculations.

dat2tp is applied to find the turning points of the stress time series, then the tp2rfc is used to do the rainflow count. The damage is then calculated with cc2dam. All these three functions are part of WAFO.

### **A.2.1 readresults.m**

This function reads in the results file from the simulation. The location and name of the file need to be changed when examining different simulation results.

### **A.2.2 calc\_stress.m**

This function calculates the stress along the circumference from the resulting moments at the mudline.

# **Appendix B**

## **Appendix B - Fatigue Damage**

Tables containing the fatigue damage accumulated from the different load cases at the seven points around the circumference, for all five methods.

### **B.1 Morison Method**

Results from the 10 minutes simulations:

Table B.1: Fatigue damage for each load case after 10 minute simulation. Load calculations done with Morison,  $C_m=2.0$   $C_d=1.0$

Load Case	Fatigue Damage 10 min analysis [10 <sup>-5</sup> ]						
	-90°	-60°	-30°	0°	30°	60°	90°
1-1	3.59E-18	0.0054	0.0842	0.1729	0.0842	0.0054	3.59E-18
1-2	5.10E-18	0.0050	0.0780	0.1601	0.0780	0.0050	5.10E-18
1-3	2.23E-18	0.0342	0.6220	1.2626	0.6220	0.0342	2.23E-18
1-4	2.12E-13	0.0199	0.3288	0.7966	0.3284	0.0199	2.12E-13
1-5	1.52E-12	0.1396	2.7328	4.8480	2.7355	0.1402	1.52E-12
1-6	4.80E-12	0.0593	1.1157	2.2420	1.1153	0.0592	4.80E-12
1-7	8.79E-11	0.2264	3.6066	6.2641	3.6084	0.2267	8.79E-11
1-8	7.72E-10	0.0727	1.3615	2.4241	1.3627	0.0728	7.72E-10
1-9	1.43E-09	0.3744	4.9602	8.2884	4.9637	0.3759	1.43E-09
2-1	3.59E-18	0.0054	0.0842	0.1729	0.0842	0.0054	3.59E-18
2-2	1.49E-17	0.0104	0.1616	0.3317	0.1616	0.0104	1.49E-17
2-3	5.10E-18	0.0050	0.0780	0.1601	0.0780	0.0050	5.10E-18
2-4	2.36E-18	0.0014	0.0214	0.0439	0.0214	0.0014	2.36E-18
3-1	4.69E-09	0.1006	1.8136	3.4850	1.8298	0.1001	4.69E-09
3-2	4.18E-09	0.1843	3.2132	5.6481	3.2189	0.1849	4.18E-09

Results from the 1 hour simulations:

Table B.2: Fatigue damage for each load case after 1 hour simulation. Load calculations done with Morison,  $C_m=2.0$   $C_d=1.0$

Load Case	Fatigue Damage 1 hour analysis [10 <sup>-5</sup> ]						
	-90°	-60°	-30°	0°	30°	60°	90°
1-4	2.65e-12	0.5030	9.1180	17.3336	9.1169	0.5026	2.65e-12
1-5	8.98e-12	0.5020	9.0956	18.0981	9.0950	0.5019	8.98e-12
1-7	6.10e-10	1.6328	22.8517	37.8430	22.8988	1.6559	6.10e-10
2-1	9.17e-16	0.0206	0.3213	0.6597	0.3214	0.0206	9.17e-16
3-2	3.02e-08	1.3980	19.1943	32.4669	19.2034	1.3996	3.02e-08



## B.2 MacCamy Method

Results from the 10 minutes simulations:

Table B.3: Fatigue damage for each load case for 10 minute simulation. Wave load according to MacCamy and Fuchs

Load Case	Fatigue Damage 10 min analysis [10 <sup>-5</sup> ]						
	-90°	-60°	-30°	0°	30°	60°	90°
1-1	1.48E-16	0.0012	0.0181	0.0372	0.0181	0.0012	1.48E-16
1-2	1.64E-15	0.0024	0.0381	0.0782	0.0381	0.0024	1.64E-15
1-3	5.08E-14	0.0024	0.0378	0.0776	0.0378	0.0024	5.08E-14
1-4	2.13E-13	0.0206	0.3394	0.7988	0.3390	0.0205	2.13E-13
1-5	1.15E-12	0.0215	0.3350	0.8333	0.3347	0.0215	1.15E-12
1-6	4.47E-12	0.1281	2.5170	4.8039	2.5168	0.1280	4.47E-12
1-7	8.48E-11	0.1295	2.0713	3.5729	2.0716	0.1297	8.48E-11
1-8	7.72E-10	0.0756	1.4463	2.7134	1.4278	0.0755	7.72E-10
1-9	1.32E-09	0.3392	3.9337	6.2925	3.9383	0.3407	1.32E-09
2-1	8.56E-19	0.0015	0.0226	0.0465	0.0226	0.0015	8.56E-19
2-2	9.95E-19	0.0035	0.0549	0.1128	0.0549	0.0035	9.95E-19
2-3	2.59E-18	0.0007	0.0103	0.0211	0.0103	0.0007	2.59E-18
2-4	1.20E-18	0.0007	0.0115	0.0235	0.0114	0.0007	1.20E-18
3-1	4.58E-09	0.1242	2.3361	4.2087	2.3375	0.1249	4.58E-09
3-2	4.28E-09	0.2194	3.0204	4.8553	2.9984	0.2194	4.28E-09

Results from the 1 hour simulations:

Table B.4: Fatigue damage for each load case after 1 hour simulation. Load calculations done with MacCamy and Fuchs

Load Case	Fatigue Damage 1 hour analysis [10 <sup>-5</sup> ]						
	-90°	-60°	-30°	0°	30°	60°	90°
1-4	2.65E-12	0.3816	6.6861	12.1810	6.6856	0.3816	2.65E-12
1-5	8.94E-12	0.3814	6.6340	12.8994	6.63746	0.3819	8.94E-12
1-7	6.26E-10	1.0439	14.3605	24.5486	14.3595	1.0434	6.26E-10
2-1	1.53E-16	0.0270	0.4211	0.8646	0.4213	0.0270	1.53E-16
3-2	1.98E-08	0.1556	2.7068	5.1969	2.7154	0.1578	1.98E-08

### B.3 Short Morison Method

Results from the 10 minutes simulations:

Table B.5: Fatigue damage for each load case for short crested 10 min analysis. Wave load calculated according to Morison equation

Load Case	Fatigue Damage 10 min analysis [10 <sup>-5</sup> ]						
	-90°	-60°	-30°	0°	30°	60°	90°
1-1	1.63E-14	0.0070	0.1090	0.2239	0.1091	0.0070	1.63E-14
1-2	3.70E-14	0.0160	0.2485	0.5465	0.2478	0.0158	3.70E-14
1-3	4.76E-13	0.0097	0.1510	0.3098	0.1508	0.0097	4.76E-13
1-4	5.34E-13	0.0183	0.2846	0.7457	0.2843	0.0182	5.34E-13
1-5	2.65E-12	0.0100	0.1561	0.3204	0.1561	0.0100	2.65E-12
1-6	5.95E-12	0.0536	1.0002	1.9576	1.0007	0.0537	5.95E-12
1-7	1.07E-10	0.1530	2.5801	4.7072	2.5806	0.1535	1.07E-10
1-8	7.42E-10	0.0392	0.7535	1.5006	0.7532	0.0391	7.42E-10
1-9	1.48E-09	0.1320	2.4983	4.5102	2.4935	0.1307	1.48E-09
2-1	2.01E-14	0.0094	0.1460	0.3001	0.1463	0.0094	2.01E-14
2-2	3.78E-14	0.0467	0.7873	1.7827	0.7910	0.0474	3.78E-14
2-3	1.91E-15	0.0010	0.0162	0.0333	0.0162	0.0010	1.91E-15
2-4	2.47E-14	0.0003	0.0047	0.0096	0.0047	0.0003	2.47E-14
3-1	4.78E-09	1.4151	10.5275	16.5639	10.5377	1.4206	4.78E-09
3-2	4.71E-09	0.2997	3.4055	5.7467	3.3986	0.2794	4.71E-09

## B.4 Short MacCamy Method

Results from the 10 minutes simulations:

Table B.6: Fatigue damage for each load case for short crested 10 min analysis. Wave load according to MacCamy and Fuchs equation

Load Case	Fatigue Damage 10 min analysis [10 <sup>-5</sup> ]						
	-90°	-60°	-30°	0°	30°	60°	90°
1-1	4.04E-15	0.0012	0.0188	0.0386	0.0188	0.0012	4.04E-15
1-2	4.15E-14	0.0005	0.0076	0.0155	0.0075	0.0005	4.15E-14
1-3	7.80E-14	0.0022	0.0335	0.0688	0.0335	0.0021	7.80E-14
1-4	2.99E-13	0.0254	0.4137	1.0015	0.4126	0.0252	2.99E-13
1-5	1.97E-12	0.0171	0.2676	0.6234	0.2682	0.0173	1.97E-12
1-6	5.28E-12	0.0533	0.9370	2.0333	0.9374	0.0534	5.28E-12
1-7	9.33E-11	0.0749	1.3976	2.6254	1.3966	0.0746	9.33E-11
1-8	8.07E-10	0.0922	1.7387	3.3465	1.7564	0.0921	8.07E-10
1-9	1.44E-09	0.0221	0.3780	0.7883	0.3791	0.0223	1.44E-09
2-1	2.93E-15	0.0013	0.0198	0.0406	0.0198	0.0013	2.93E-15
2-2	4.90E-14	0.0006	0.0093	0.0190	0.0092	0.0006	4.90E-14
2-3	2.83E-15	0.0009	0.0138	0.0282	0.0137	0.0009	2.83E-15
2-4	1.04E-14	0.0008	0.0119	0.0244	0.0119	0.0008	1.04E-14
3-1	4.80E-09	0.0128	0.2164	0.4398	0.2163	0.0128	4.80E-09
3-2	4.30E-09	0.0156	0.2772	0.5340	0.2770	0.0155	4.30E-09

Results from the 1 hour simulations:

Table B.7: Fatigue damage for each load case after 1 hour simulation. Load calculations according to MacCamy and Fuchs

Load Case	Fatigue Damage 1 hour analysis [10 <sup>-5</sup> ]						
	-90°	-60°	-30°	0°	30°	60°	90°
1-4	4.57E-12	0.0808	1.2934	2.8956	1.2910	0.0803	4.57E-12
1-5	1.42E-11	0.0795	1.3303	3.0799	1.3304	0.0795	1.42E-11
1-7	6.34E-10	0.2142	3.6769	7.6634	3.6545	0.2132	6.34E-10
2-1	1.11E-13	0.0040	0.0616	0.1263	0.0615	0.0039	1.11E-13
3-2	2.97E-08	0.3410	6.2267	12.2283	6.2725	0.3428	2.97E-08

## B.5 Torsethaugen Method

Results from the 10 minutes simulations:

Table B.8: Fatigue damage for each load case from the 10 minute simulation. Torsethaugen applied as wave spectrum

Load Case	Fatigue Damage 10 min analysis [10 <sup>-5</sup> ]						
	-90°	-60°	-30°	0°	30°	60°	90°
1-1	9.08E-15	0.0482	0.7717	1.7619	0.7737	0.0486	9.08E-15
1-2	2.80E-15	0.0065	0.1015	0.2082	0.1013	0.0065	2.80E-15
1-3	6.14E-14	0.0085	0.1317	0.2703	0.1316	0.0084	6.14E-14
1-4	2.02E-13	0.0257	0.4001	0.9115	0.3999	0.0256	2.02E-13
1-5	1.16E-12	0.0484	0.8098	1.8897	0.8103	0.0485	1.16E-12
1-6	4.90E-12	0.0512	0.9054	1.9177	0.9046	0.0510	4.90E-12
1-7	9.83E-11	0.1575	2.9792	5.3287	2.9761	0.1568	9.83E-11
1-8	7.33E-10	0.1757	3.2938	5.7604	3.2890	0.1748	7.33E-10
1-9	1.47E-09	0.1323	2.5692	4.7060	2.5719	0.1325	1.47E-09
2-1	4.03E-16	0.0501	0.7985	1.8309	0.7980	0.0500	4.03E-16
2-2	3.27E-15	0.0226	0.3518	0.7771	0.3513	0.0225	3.27E-15
2-3	5.44E-16	0.0408	0.6363	1.3610	0.6360	0.0408	5.44E-16
2-4	5.30E-16	0.0535	0.8527	1.9092	0.8523	0.0535	5.30E-16
3-1	4.86E-09	0.1271	2.3804	4.5017	2.4110	0.1254	4.86E-09
3-2	4.18E-09	0.1699	3.1087	5.4919	3.1074	0.1698	4.18E-09

## B.6 Torsethaugen MacCamy Method

Results from the 10 minutes simulations:

Table B.9: Fatigue damage for each load case from the 10 minute simulation. Torsethaugen applied as wave spectrum and wave load calculation according to MacCamy and Fuchs

Load Case	Fatigue Damage 10 min analysis [10 <sup>-5</sup> ]						
	-90°	-60°	-30°	0°	30°	60°	90°
1-1	1.48E-16	0.0040	0.0616	0.1265	0.0617	0.0040	1.48E-16
1-2	1.95E-15	0.0116	0.1809	0.3713	0.1809	0.0116	1.95E-15
1-3	5.16E-14	0.0192	0.2996	0.7240	0.2995	0.0192	5.16E-14
1-4	2.29E-13	0.0398	0.6393	1.5974	0.6397	0.0399	2.29E-13
1-5	1.97E-12	0.0648	1.2428	2.3021	1.2433	0.0649	1.97E-12
1-6	4.64E-12	0.0278	0.4701	1.1319	0.4694	0.0277	4.64E-12
1-7	8.99E-11	0.0540	1.0207	1.9607	1.0184	0.0535	8.99E-11
1-8	8.81E-10	0.2796	4.0285	6.8781	4.0316	0.2812	8.81E-10
1-9	1.47E-09	0.2509	4.4145	7.5061	4.3950	0.2504	1.47E-09
2-1	2.15E-18	0.0062	0.0969	0.1989	0.0969	0.0062	2.15E-18
2-2	2.82E-18	0.0044	0.0678	0.1392	0.0678	0.0043	2.82E-18
2-3	1.22E-18	0.0007	0.0105	0.0216	0.0105	0.0007	1.22E-18
2-4	1.04E-18	0.0005	0.0077	0.0158	0.0077	0.0005	1.04E-18
3-1	5.02E-09	0.1143	1.9186	3.6570	1.9200	0.1145	5.02E-09
3-2	4.45E-09	0.5358	6.3943	10.3915	6.3944	0.5368	4.45E-09

# **Appendix C**

## **Appendix C - Response Spectrum**

### C.1 Load Case 1-1

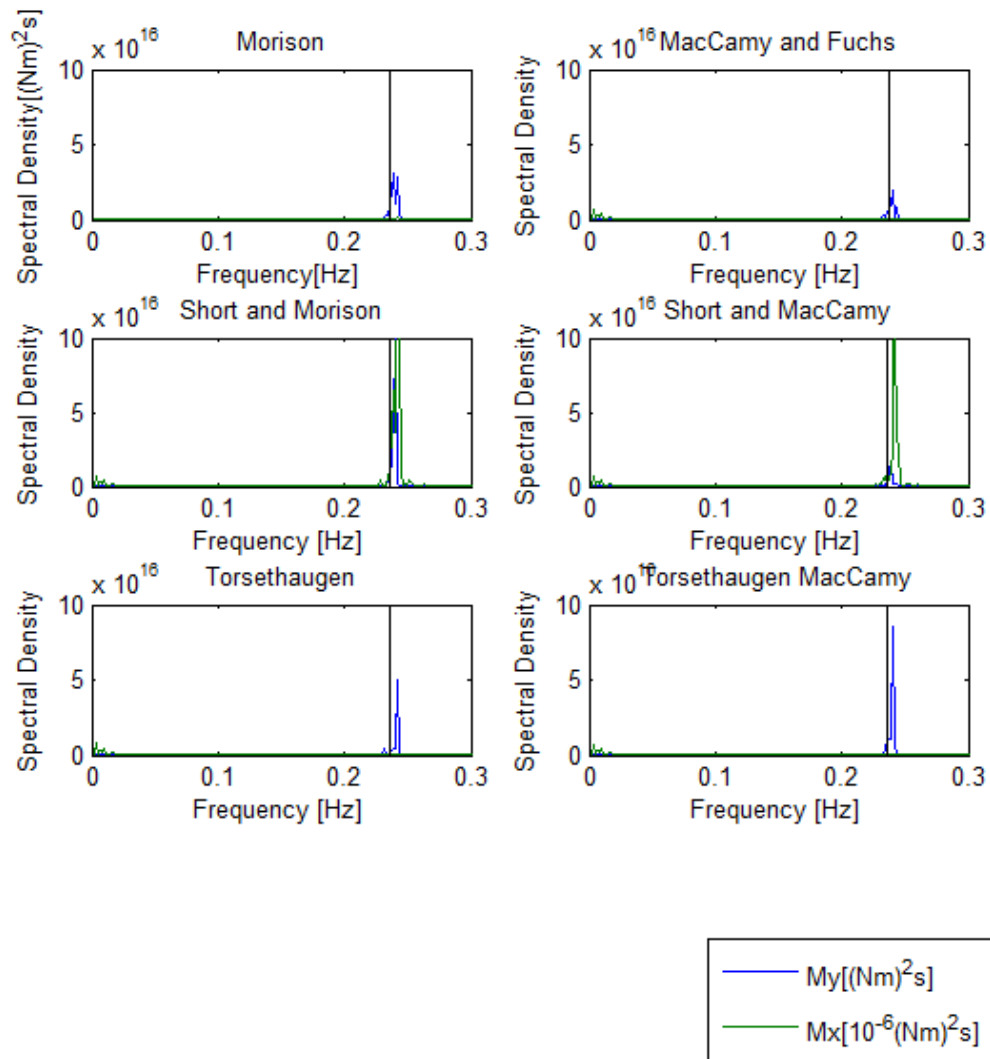


Figure C.1: Graph of responding moments from load case 1-1, in frequency domain

## C.2 Load Case 1-2

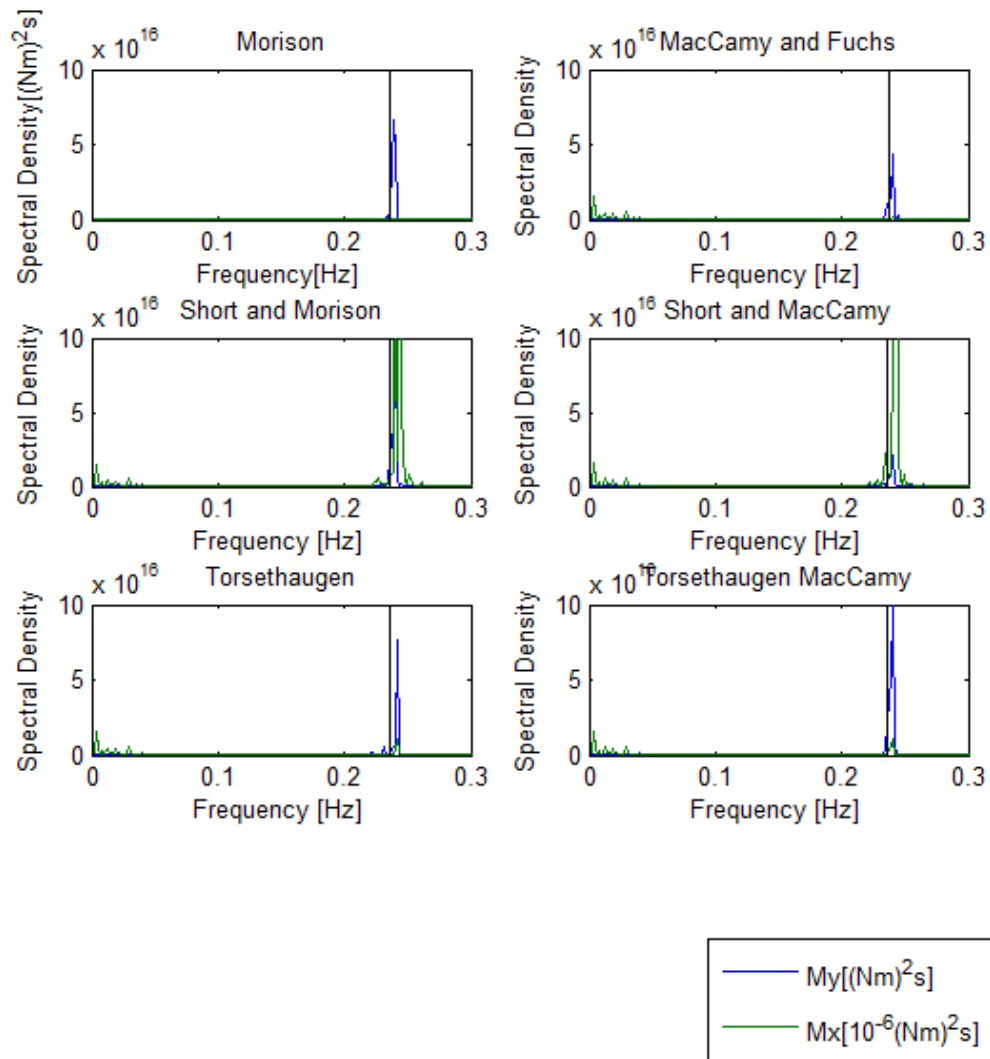


Figure C.2: Graph of responding moments from load case 1-2, in frequency domain



### C.3 Load Case 1-3

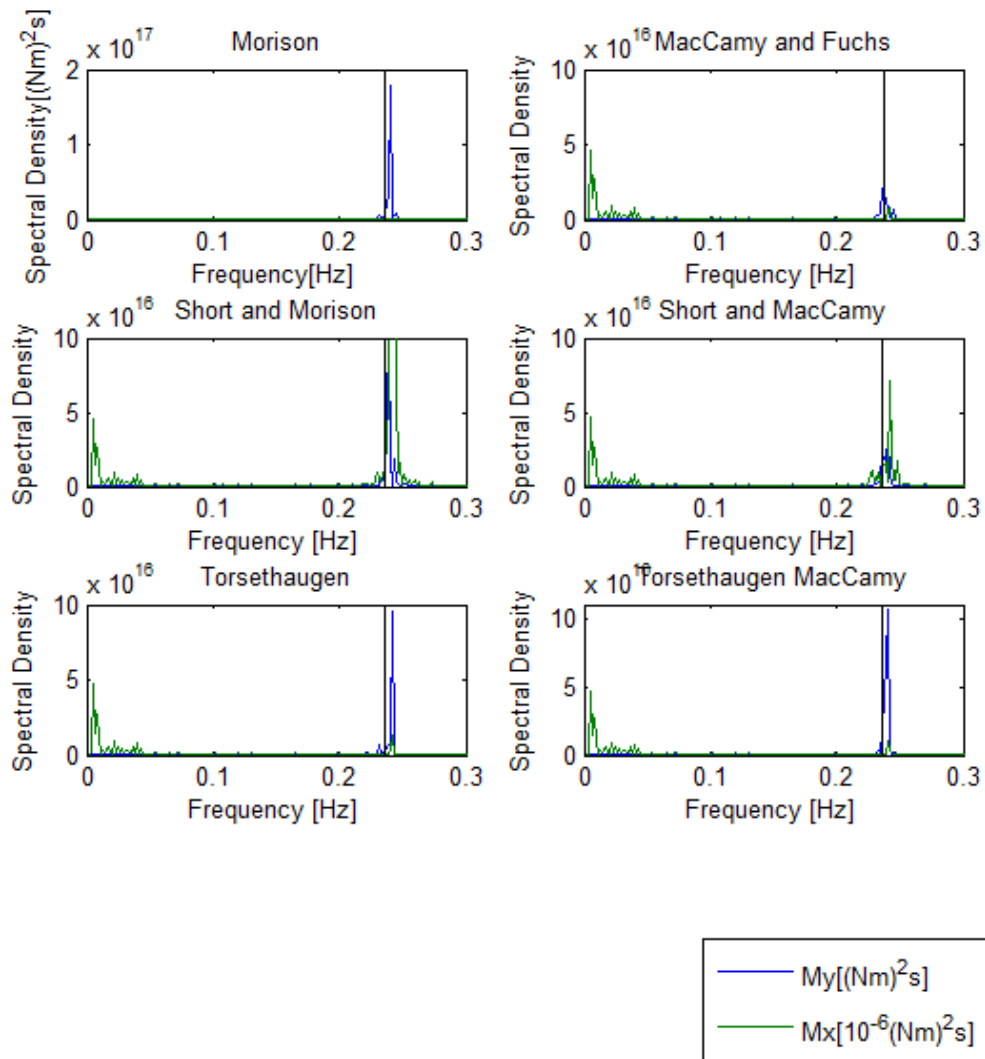


Figure C.3: Graph of responding moments from load case 1-3, in frequency domain

### C.4 Load Case 1-4

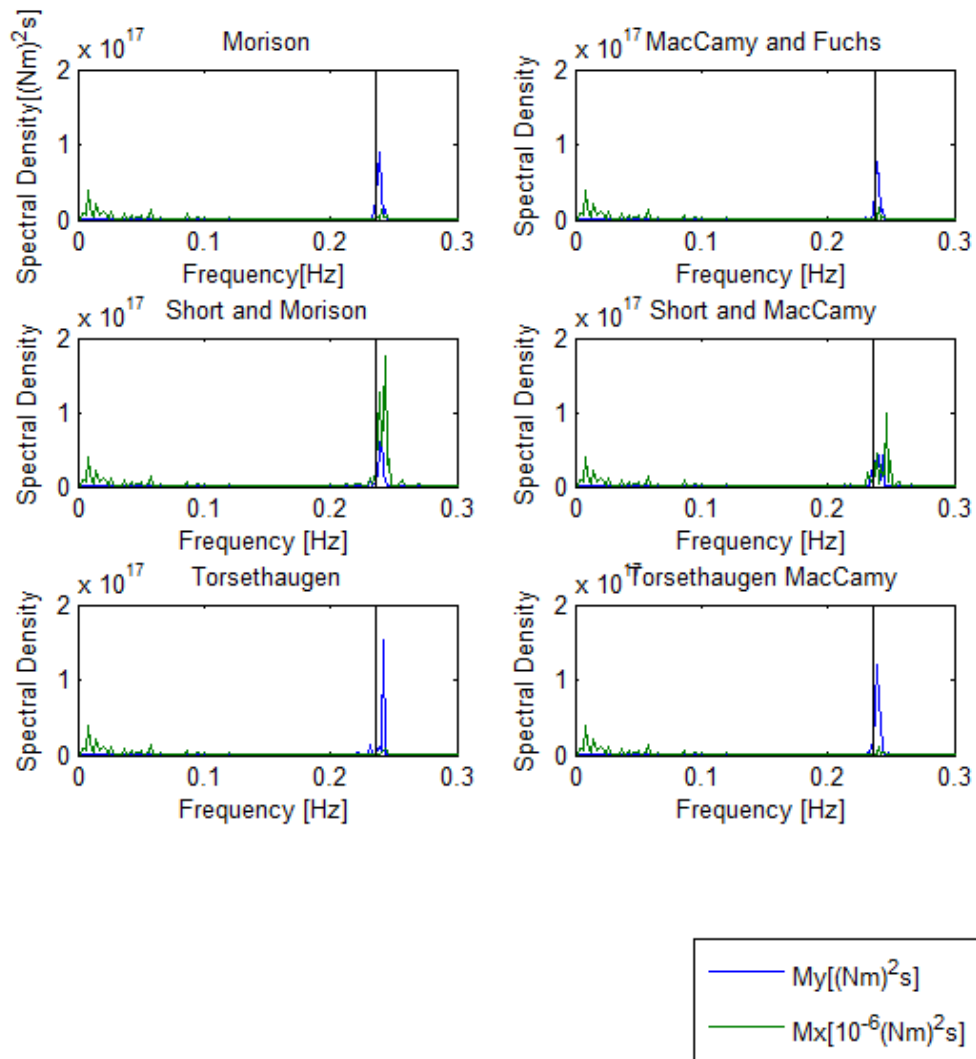


Figure C.4: Graph of responding moments from load case 1-4, in frequency domain

### C.5 Load Case 1-5

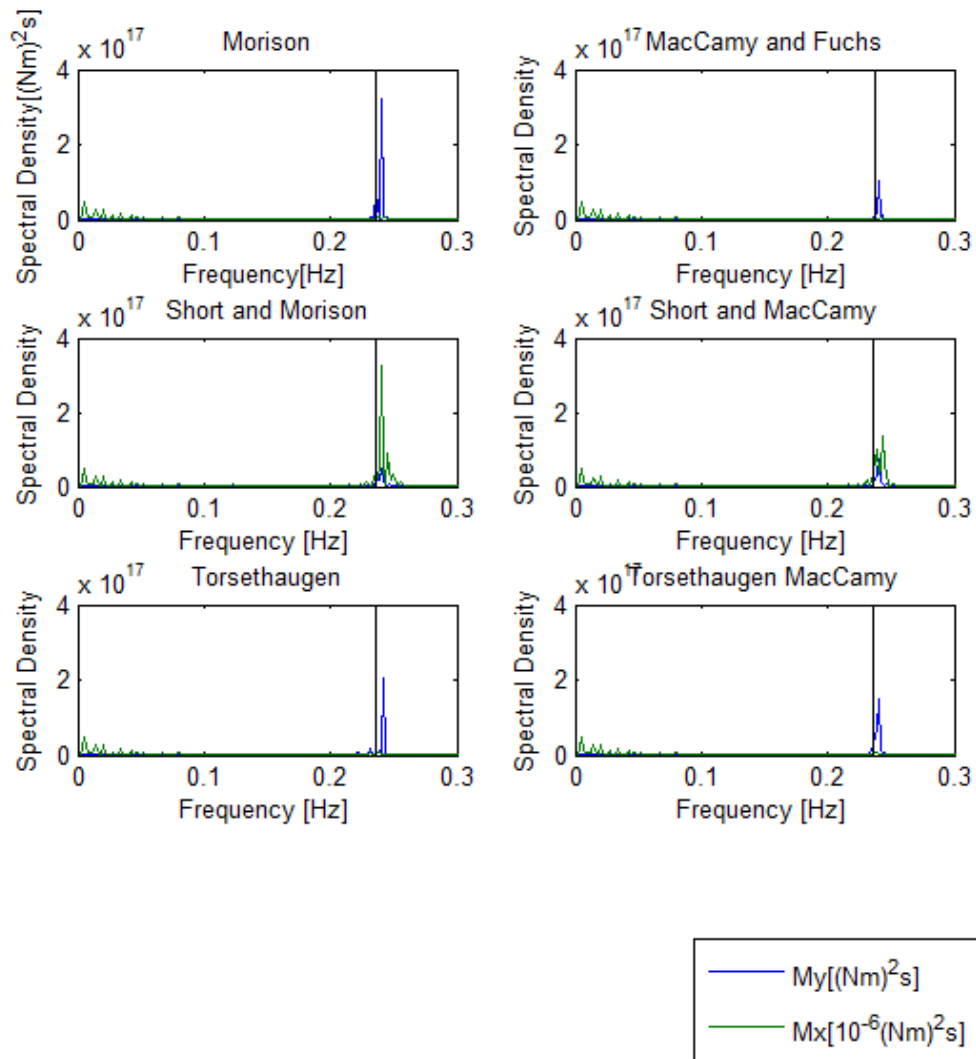


Figure C.5: Graph of responding moments from load case 1-5, in frequency domain

### C.6 Load Case 1-6

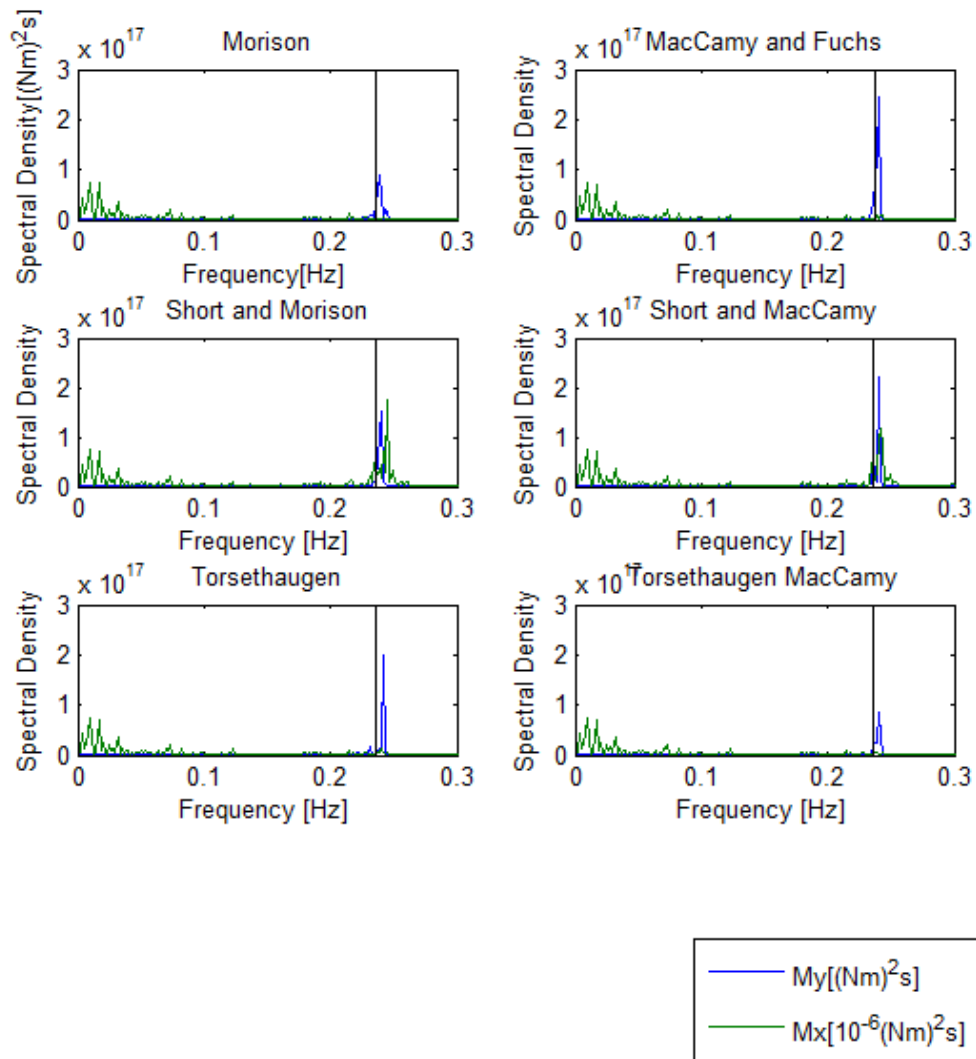


Figure C.6: Graph of responding moments from load case 1-6, in frequency domain

### C.7 Load Case 1-7

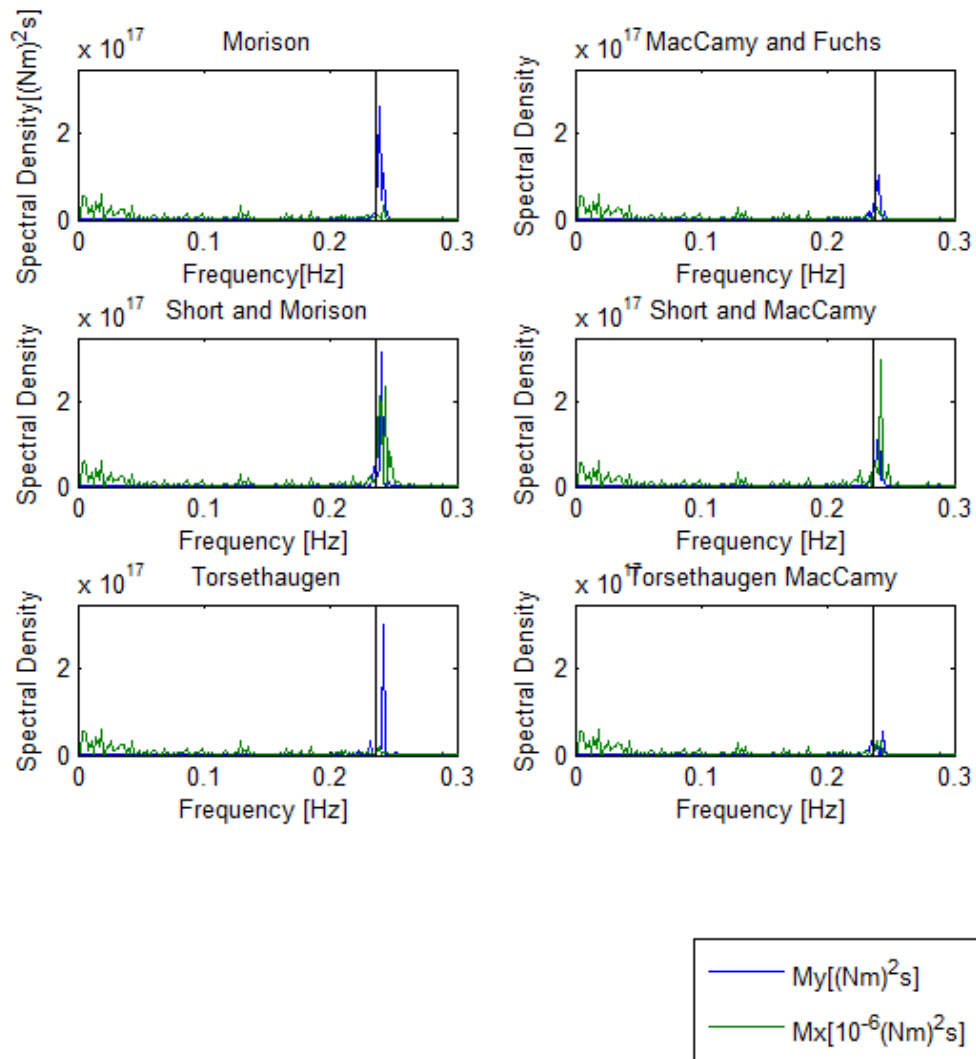


Figure C.7: Graph of responding moments from load case 1-7, in frequency domain

### C.8 Load Case 1-8

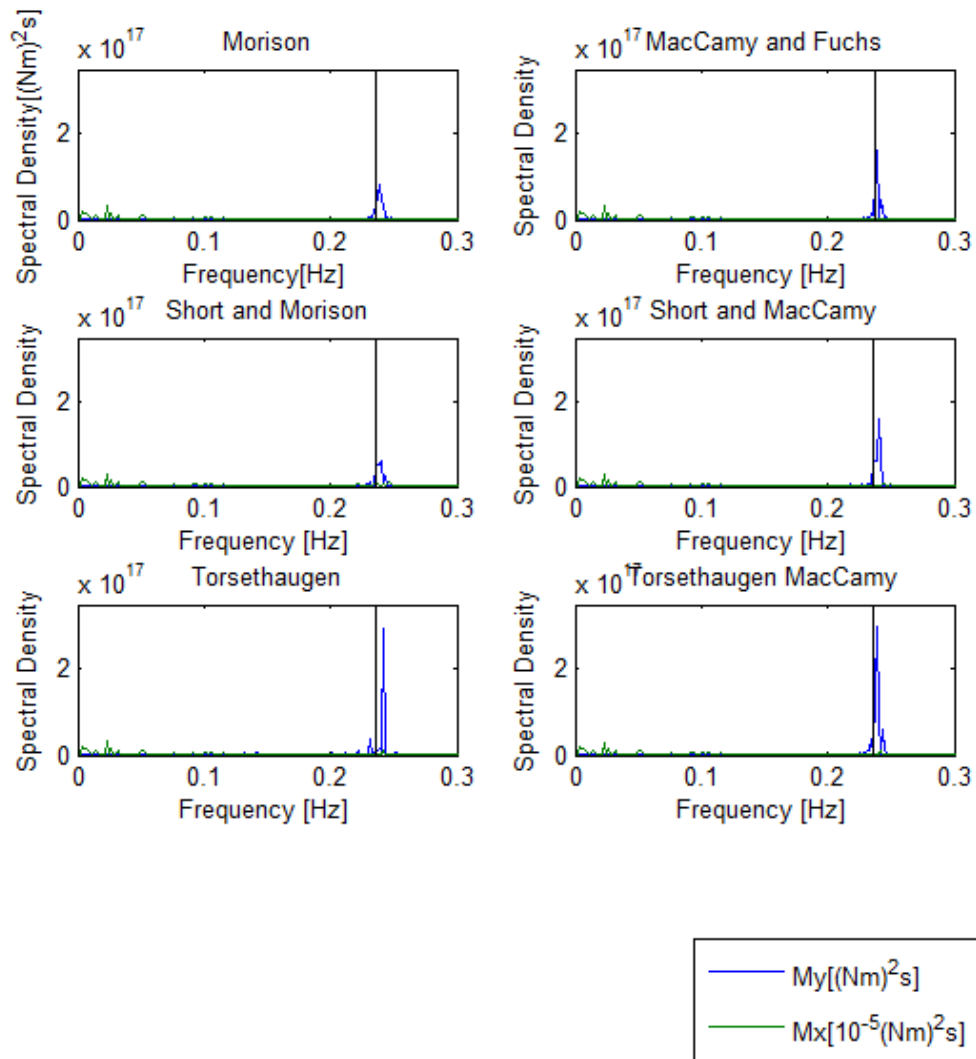


Figure C.8: Graph of responding moments from load case 1-8, in frequency domain

### C.9 Load Case 1-9

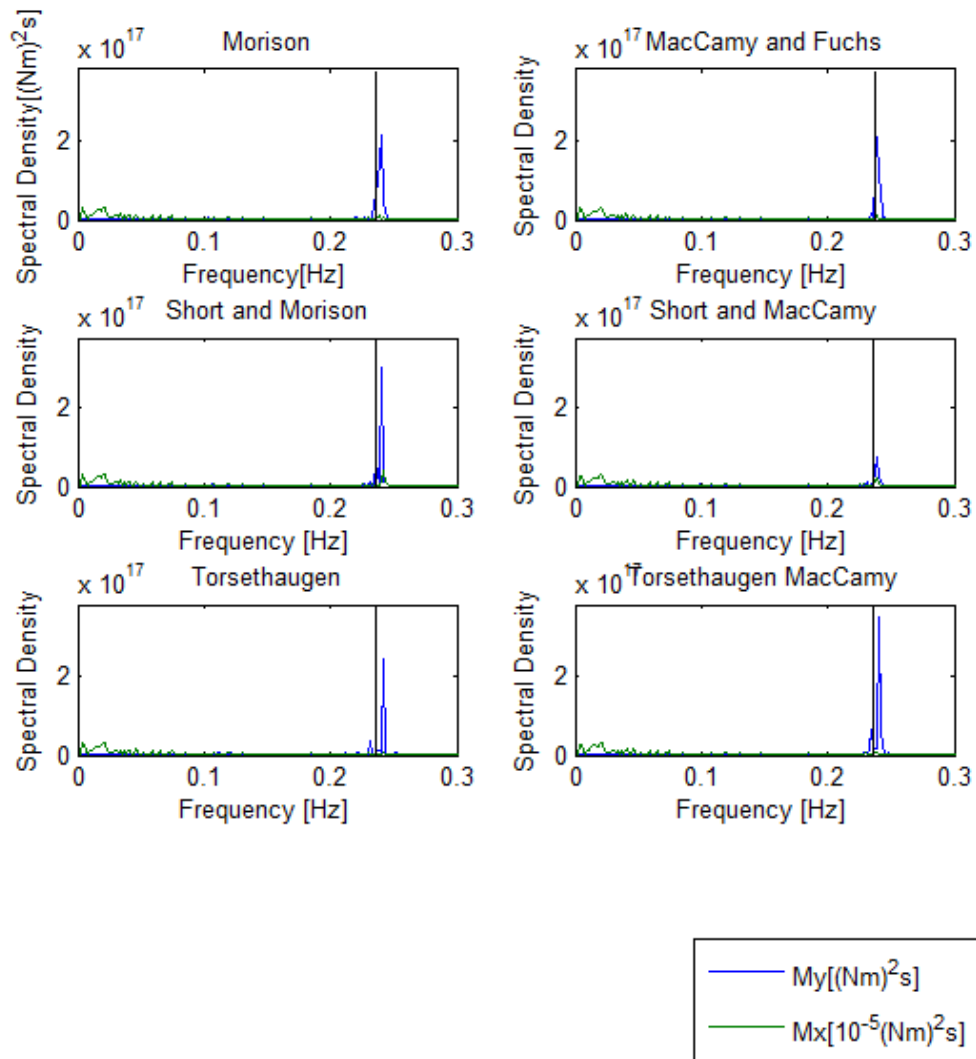


Figure C.9: Graph of responding moments from load case 1-9, in frequency domain

### C.10 Load Case 2-1

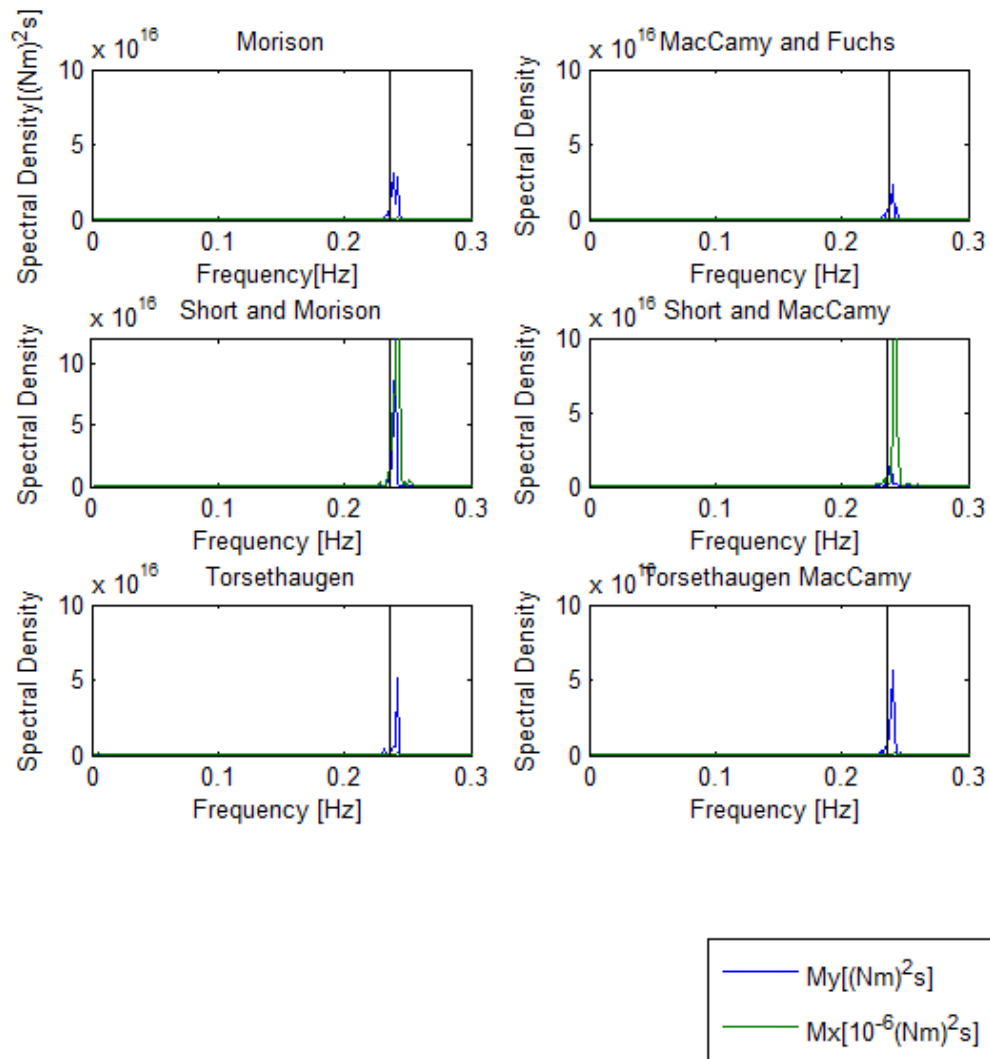


Figure C.10: Graph of responding moments from load case 2-1, in frequency domain



### C.11 Load Case 2-2

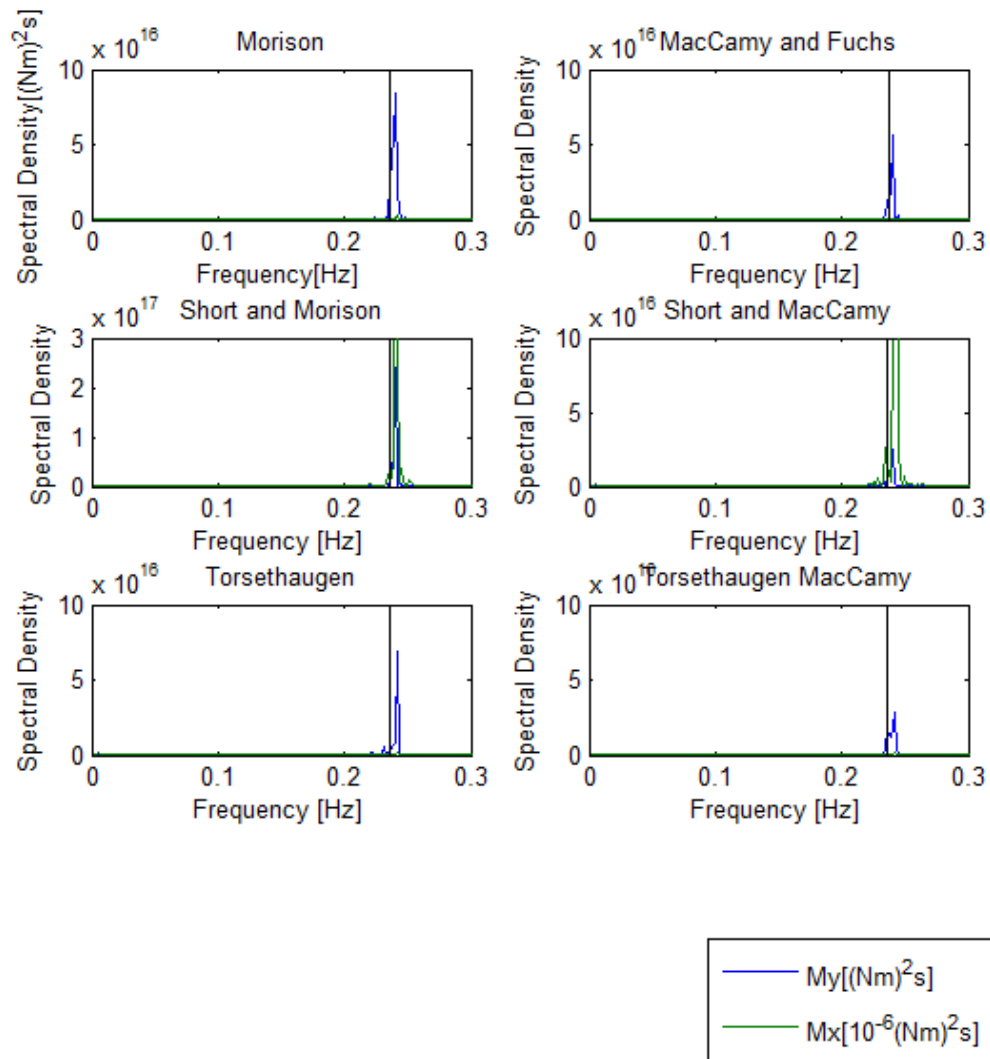


Figure C.11: Graph of responding moments from load case 2-2, in frequency domain

### C.12 Load Case 2-3

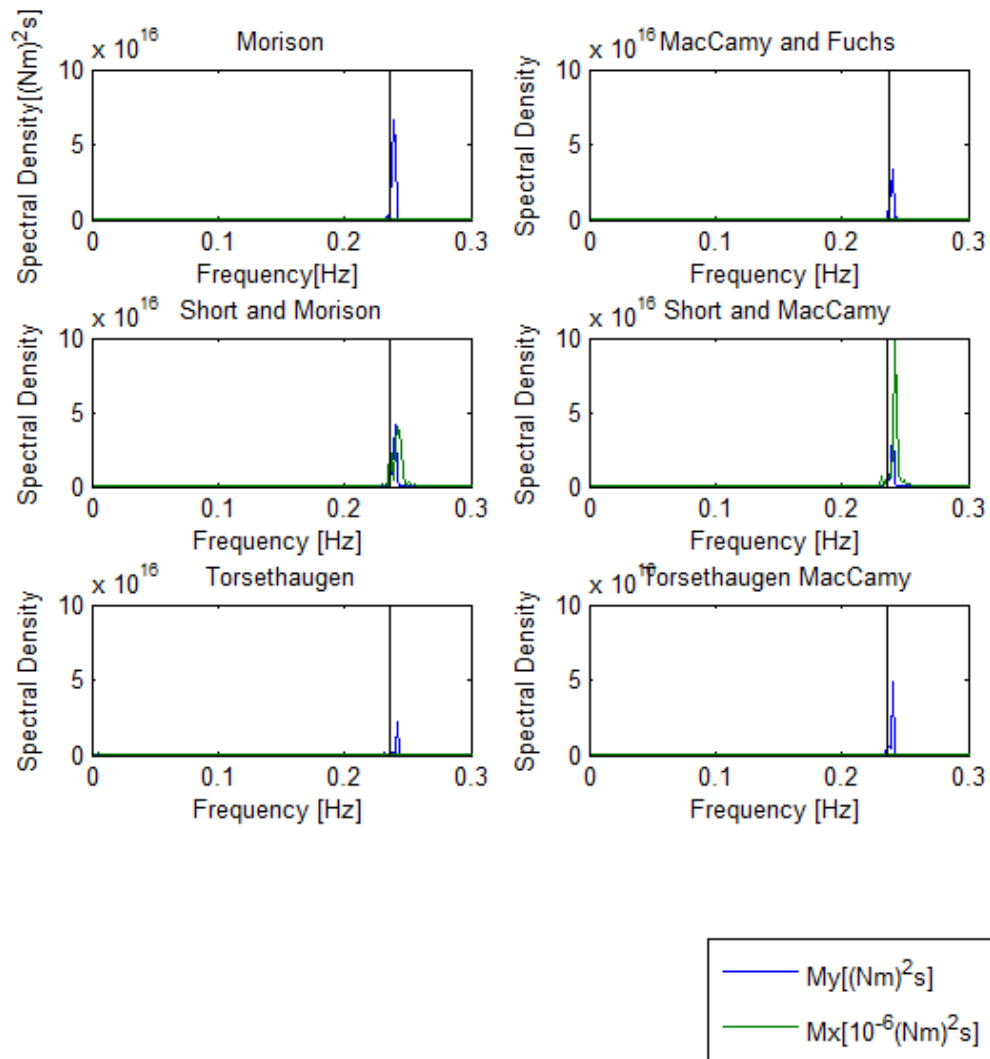


Figure C.12: Graph of responding moments from load case 2-3, in frequency domain

### C.13 Load Case 2-4

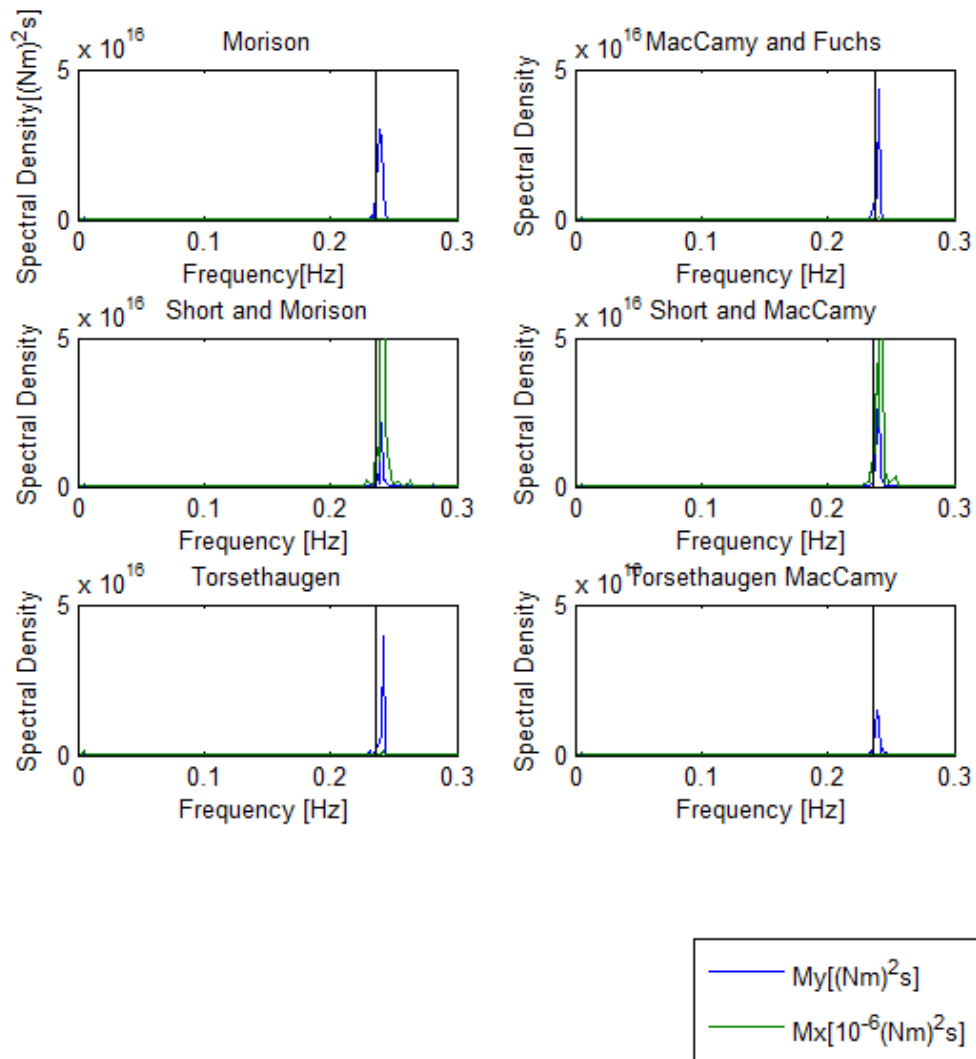


Figure C.13: Graph of responding moments from load case 2-4, in frequency domain

### C.14 Load Case 3-1

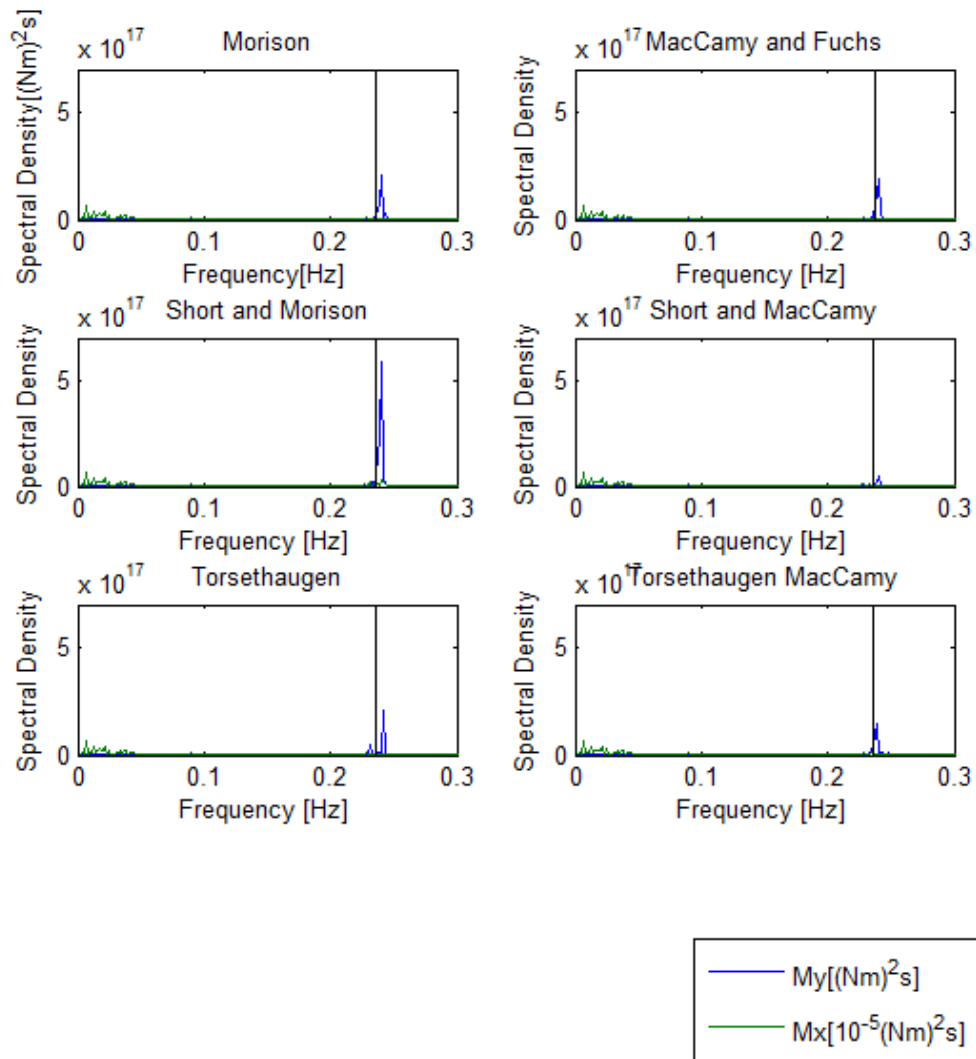


Figure C.14: Graph of responding moments from load case 3-1, in frequency domain

### C.15 Load Case 3-2

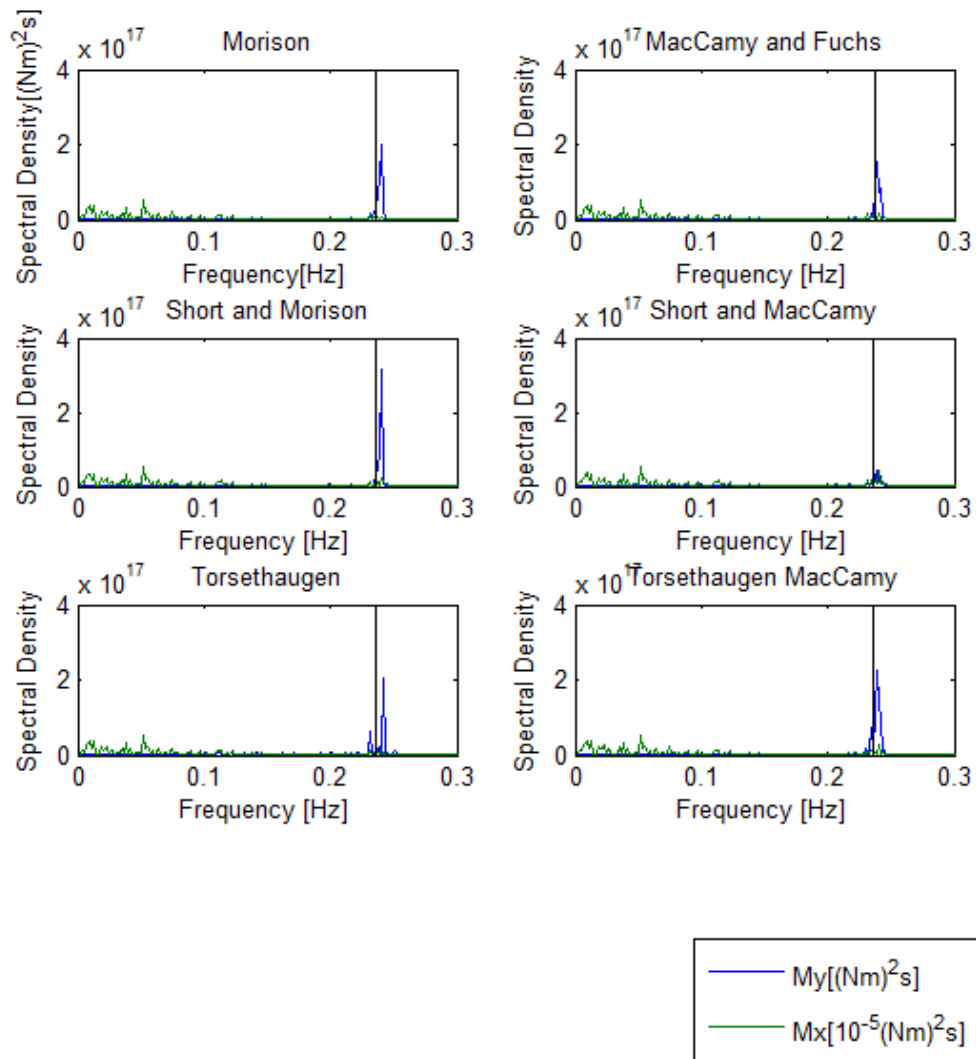


Figure C.15: Graph of responding moments from load case 3-2, in frequency domain